REVERSE ENGINEERING
OF A
CENTRIFUGAL TURBINE HOUSING

Marius Christiaan Rossouw
B.Eng. (Mechanical)

Dissertation submitted in partial fulfilment of the requirements for the degree

MASTER OF ENGINEERING

in the
School for Mechanical and Materials Engineering,
Faculty of Engineering,
at the
Potchefstroom University for Christian Higher Education

Promoter: Prof. J. Markgraaff
Potchefstroom
2003

ABSTRACT

Title	***:***	Reverse engineering of a centrifugal turbine housing.
Author	***:***	Marius Christiaan Rossouw
Promoter	***:***	Prof. J. Markgraaff
School	***:***	Mechanical and Materials Engineering
Degree	***:***	Master of Engineering

The Garrett GT 42 turbine housing is a spheroidal ductile cast iron casting, which according to the ASME B31.3 (1996) Code for Pressure Piping, does not satisfy the Pebble Bed Micro Model (PBMM) design requirements. By using Geometrical Reverse Engineering (GRE) methods, a 3-D virtual model, and if required, a mould of the existing design can be created to recast a turbine housing in a suitable material.

The aim of this research was to study, evaluate, identify and implement the most promising method(s) to reverse engineer the Garrett GT 42 turbine housing without destroying it in the process.

GRE advantages and limitations influenced by practical contact (tactile) and non-contact data acquisition problem areas provided evaluation guidelines that assisted in the allocation of **Computed Tomography (CT)** as the most promising method to reverse engineer the turbine housing. X-ray and neutron CT were implemented. Neutron Computed Tomography (NCT) using *CADKEY® V21* CAD modelling software at the SAFARI-1 nuclear reactor, NECSA, produced the most favourable 3-D NURBs model, which had a geometrical external accuracy of 95% and a volumetric internal accuracy of 94%. It was verified by comparing the results with an 87% geometrical external- and 85% volumetric internal accurate 3-D NURBs model created by the implementation of an alternative contact GRE method, i.e. geometrical inspection and measurements.

UITTREKSEL

Titel	***:***	Truwaartse ontwerp van ‘n sentrifugale turbine omhulsel.
Outeur	***:***	Marius Christiaan Rossouw
Promotor	***:***	Prof. J. Markgraaff
Skool	***:***	Meganiese en Materiaal Ingenieurswese
Graad	***:***	Meestersgraad in Ingenieurswese

Die Garrett GT 42 turbine omhulsel is ‘n sferoïdaal smeebare gietyster gietstuk wat, volgens die ASME B31.3 (1996) Kode vir Druk Silinders, nie aan die Korrel Bed Mikro Model (KBMM) se ontwerp vereistes voldoen nie. Deur Geometriese Truwaartse Ontwerp (GTO) metodes toe te pas, kan ‘n 3-D virtuele model en ‘n gietvorm, indien dit benodig word, van die bestaande ontwerp geskep word om ‘n turbine omhulsel in die geskikte materiaal te hergiet.

Die doel van hierdie navorsing was om die mees geskikte metode(s) te bestudeer, evalueer, identifiseer en te implementeer ten einde die Garrett GT 42 turbine omhulsel truwaarts te ontwerp, sonder om dit in die proses te vernietig.

GTO voordele en beperkings wat deur praktiese kontak asook nie-kontak data verkryging probleem areas beinvloed is, het ‘n evaluasie riglyn verskaf wat bygedra het tot die aanwysing van **Rekenaar Tomografie (RT)** as die mees geskikte metode om die turbine omhulsel truwaarts te ontwerp. X-straal en neutron RT is geimplementeer. Deur gebruik te maak van Neutron Rekenaar Tomografie (NRT) en *CADKEY® V21* modellering sagteware te SAFARI-1 kernreaktor, NECSA, is die mees gunstige 3-D NURBs model geskep, wat ‘n geometriese eksterne akkuraatheid van 95%, en ‘n volumetriese interne akkuraatheid van 94% gehad het. Dit is bevestig deur die resultate te vergelyk met ‘n 87% geometries ekstern- en 85% volumetries interne akkurate 3-D NURBs model wat verkry is deur ‘n alternatiewe kontak GTO metode nl. geometriese inspeksie en meetings, toe te pas.

ACKNOWLEDGEMENTS

Special thanks to my family and friends for their loving support.

Sincere gratitude towards Prof. J. Markgraaff for his guidance and professionalism. Thank you for your help, advice and constant support. It was a great honour to be your student.

I would like to thank the School for Mechanical and Materials Engineering at the Potchefstroom University for Christian Higher Education for giving me the opportunity in contributing towards the engineering and manufacturing industry.

Credit to the following institutions and personnel in the engineering and manufacturing industry for their input resulting in the successful completion of this research:

- Millpark Hospital - Miss. C. Gibbs;

- South African Nuclear Energy Corporation (NECSA) - Mr. F. de Beer.

Last but not the least I thank God for providing me with the opportunities and talents to complete this study. For the guidance, strength and courage He has given me over the past two years. His greatness cannot be expressed in words.

TABLE OF CONTENTS

ABSTRACT**……p. i**

UITTREKSEL**……p. ii**

ACKNOWLEDGEMENTS**…… p.iii**

LIST OF FIGURES**……p.vii**

LIST OF TABLES**……p. x**

CHAPTER 1: INTRODUCTION**……p. 1**

1.1. Background……p. 1

1.2. Problem Definition……..p. 6

1.3. Purpose of this Research……p. 8

1.4. Structure of Dissertation……..…p. 8

CHAPTER 2: THE GEOMETRICAL REVERSE ENGINEERING (GRE) PROCESS……p. 10

2.1 Background - Reverse Engineering……p. 10

2.2 Geometrical Reverse Engineering (GRE)……...p. 11

2.3 The GRE Process……..……p. 11

2.3.1 Phase One - Contact (Tactile) and Non-Contact Data Acquisition……p. 12

2.3.2 Phase Two - Data Manipulation with 3-D, GRE and/or CAD Modelling Software……..…… p. 15

CHAPTER 3: EVALUATION OF GRE METHODS……p. 18

3.1 Introduction……p. 18

3.2 Data Acquisition Problem Areas……..……... p. 18

3.3 Advantages of Contact (Tactile) and Non-Contact Methods…...……...p. 21

3.3.1 Contact (Tactile) Methods…….……...……..p. 21

3.3.2 Non-Contact Methods…….……..…….……p. 22

3.4 Limitations of Contact (Tactile) and Non-Contact Methods……..……... p. 23

3.4.1 Contact (Tactile) Methods……..……..……...p. 23

3.4.2 Non-Contact Methods……..…….……..p. 24

3.5 Evaluation of Contact (Tactile) and Non-Contact GRE Methods…….. p. 25

3.6 Garrett GT 42 Turbine Housing Attributes……p. 27
3.7 Discussion and Conclusions……p. 30
3.7.1 X-ray Computed Tomography (X-ray CT)……..p. 31
3.7.2 Neutron Computed Tomography (NCT)…….p. 34

CHAPTER 4: IMPLEMENTATION OF COMPUTED TOMOGRAPHY (CT)……p. 38
4.1 Introduction…….p. 38
4.2 X-ray Computed Tomography (X-ray CT)……..p. 38
4.2.1 System Set-up and Characteristics…….....p. 39
4.2.2 Implementation……...…… p. 39
4.2.3 3-D NURBs Model Generation……p. 42
4.2.4 Discussion and Conclusions…..…….…p. 44
4.3 Neutron Computed Tomography (NCT)……p. 45
4.3.1 System Set-up and Characteristics……...……...p. 45
4.3.2 Implementation……...…… p. 48
4.3.3 3-D NURBs Model Generation……...p. 58
4.3.4 Discussion and Conclusions…..…….…p. 61

CHAPTER 5: VERIFICATION OF RESULTS……p. 62
5.1 Introduction…….p. 62
5.2 Geometrical Inspection and Measurements…….……...p. 62
5.2.1 External 3-D NURBs Model…….……...p. 63
5.2.2 Internal 3-D NURBs Model……..…….. p. 65
5.2.3 Complete 3-D NURBs Model……..p. 68
5.3 Discussion and Conclusions……... p. 69

CHAPTER 6: CONCLUSION……..p. 70
6.1 Introduction…….p. 70
6.2 Summary…….……...……. p. 70
6.3 Conclusions…….p. 73

REFERENCES……..…p. 74

APPENDIX A: CONTACT (TACTILE) GRE METHODS AND TECHNIQUES……...……p. 85

APPENDIX B: NON-CONTACT GRE METHODS AND TECHNIQUES…….……..p. 89

APPENDIX C: NURBs SOLIDS……...…….….. p. 99

APPENDIX D: INSTRUCTIONS FOR VIEWING X-RAY CT AND NCT ANIMATION VIDEO CLIPS…….p.102

APPENDIX E: 3-D NURBs MODEL GENERATION WITHIN CADKEY® V21……p.104

LIST OF FIGURES

Figure 1.1: *Three-dimensional (3-D) Computer-Aided Design (CAD) illustration of the PBMM plant……p. 1*

Figure 1.2: *Schematic layout of the PBMM cycle……p. 2*

Figure 1.3: *A 3-D CAD illustration of the PBMM plant subsystems……p. 4*

Figure 1.4: *A 3-D CAD illustration of the high and low-pressure turbocharger units' locations and interfaces within the PBMM plant……...p. 4*

Figure 1.5: *A photographic image of the Garrett GT 42 turbocharger unit……p. 5*

Figure 1.6: *An illustration of the Garrett GT 42 HPC and HPT assemblies……p. 6*

Figure 1.7: *External photographic image of the Garrett GT 42 turbine housing p. 7*

Figure 2.1: *Flowchart depicting the two basic phases of the GRE process…….p. 12*

Figure 2.2: *Flowchart summarising the different contact (tactile) GRE methods and techniques……...p. 13*

Figure 2.3: *Flowchart summarising the different non-contact GRE methods and techniques……...p. 14*

Figure 3.1*: External photographic view of the Garrett GT 42 turbine housing's sub-components……p. 28*

Figure 3.2: *Photographic views of Garrett GT 42 turbine housing's physical exterior dimensions……..p. 29*

Figure 3.3*: CFD model illustration of the exhaust gas flow through a centrifugal turbine housing volute……..……..p. 29*

Figure 3.4: *Neutron and X-ray mass attenuation coefficients for the elements [Byrne (1994)]……... p. 35*

Figure 3.5: *Set-up of the typical NCT system……... p. 36*

Figure 4.1: *2-D X-ray radiographs of the Garrett GT 42 turbine housing in three different orientations……..p. 39*

Figure 4.2: *2-D images of the first X-ray CT orientation as displayed by Osiris 4™ ……....p. 40*

Figure 4.3: *2-D images of the second X-ray CT orientation as displayed by Osiris 4™ ……....p. 40*

Figure 4.4: *2-D images of the third X-ray CT orientation as displayed by Osiris 4™ ……p. 41*

Figure 4.5: *Screenshot images of the 3-D polygonal model in different orientations within the Slice-O-Matic™ software……...p. 42*

Figure 4.6: *Top (a) and isometric (b) views of the Garrett GT 42 turbine housing's 3-D polygonal model within the Slice-O-Matic™ software……p. 43*

Figure 4.7*: Example of the 2-D X-ray CT image conversion process into a 2-D line drawing with Adobe® software……...p. 44*

Figure 4.8*: A simplified layout of the NCT set-up for the SAFARI-1 reactor…..p. 46*

Figure 4.9: *Photographic image of the NCT system's beam-stop at SAFARI-1...p. 47*

Figure 4.10: *Photographic image of the NCT system control room at SAFARI-1.p. 47*

Figure 4.11: *External photographic image of the Garrett GT 40 turbine housing p. 49*

Figure 4.12: *2-D neutron radiographs of the Garrett GT 42 turbine housing's perpendicular (a) and parallel (b) orientations…….p. 49*

Figure 4.13: *2-D neutron radiographic projections at a 1º rotation angle……p. 50*

Figure 4.14: *The Garrett GT 40 turbine housing's 3-D polygonal model as visualised by VG-Studio® 1.1 at 1º rotation angle……..p. 51*

Figure 4.15: *2-D neutron radiographic projections at a 0.6º rotation angle…….p. 52*

Figure 4.16: *The Garrett GT 40 turbine housing's 3-D polygonal model as visualised by VG-Studio® 1.1 at 0.6º rotation angle……...p. 53*

Figure 4.17: *The Garret GT 40 turbine housing at a minimum material orientation ……....p. 54*

Figure 4.18: *2-D neutron radiographic projections at a 0.6º rotation angle and a minimum material orientation……....p. 55*

Figure 4.19: *The Garrett GT 40 turbine housing's 3-D polygonal model as visualised by VG-Studio® 1.1 at a minimum material orientation and a longer exposure time…….p. 55*

Figure 4.20: *2-D line drawings with CorelTRACE 9™ imported into CAD modelling software, in different display orientations……..p. 58*

Figure 4.21: *Examples of 2-D bitmap images converted into 2-D line drawings with the tracing by hand approach……p. 58*

Figure 4.22: *Stacking of the hand traced NURBs contours within CADKEY® V21, in different display orientations…….p. 59*

Figure 4.23: *The Garrett GT 40 turbine housing's 3-D NURBs model, generated from the NCT slices, in different display orientations……p. 60*

***Figure 5.1**: Photographic images of the Garrett GT 40 turbine housing's exterior surface, segmented and marked at 15º intervals……...p. 63*

***Figure 5.2:** NURBs at 15º segments in CADKEY® V21 in different display orientations…… p. 64*

***Figure 5.3:** The Garrett GT 40 turbine housing's exterior 3-D NURBs model, displayed at different orientations……..p. 64*

***Figure 5.4:** Photographic image of the Silastic J™ internal polymer casting…...p. 66*

***Figure 5.5:** Respective views of the volute profile's extrapolated NURBs……...p. 67*

***Figure 5.6:** Respective views of the volute profile's 3-D NURBs model within CADKEY® V21……...p. 67*

***Figure 5.7:** Respective views of the complete Garrett GT 40 turbine housing's 3-D NURBs model…….p. 68*

LIST OF TABLES

Table 2.1: *GRE and possible compatible CAD modelling software packages... p. 16*

Table 3.1: *Evaluation of contact (tactile) GRE methods with regard to general equipment factors……...p. 25*

Table 3.2: *Evaluation of non-contact GRE methods with regard to general equipment factors……...p. 26*

Table 3.3: *Evaluation of contact (tactile) GRE methods with regard to component attributes…… p. 26*

Table 3.4: *Evaluation of non-contact GRE methods with regard to component attributes…… p. 27*

Table 4.1: *NCT system component descriptions and characteristics……..p. 46*

CHAPTER 1: INTRODUCTION

1.1. Background……p. 1
1.2. Problem Definition……..p. 6
1.3. Purpose of this Research……p. 8
1.4. Structure of Dissertation……p. 8

1.1 Background

M-Tech Industrial (Pty) Ltd., a company based within the School for Mechanical and Materials Engineering at the Potchefstroom University for Christian Higher Education, in conjunction with PBMR (Pty) Ltd., developed the Pebble Bed Micro Model (PBMM) [*Figure 1.1*]. The PBMM serves as a simulation model for the revolutionary nuclear power plant commonly referred to as the Pebble Bed Modular Reactor (PBMR).

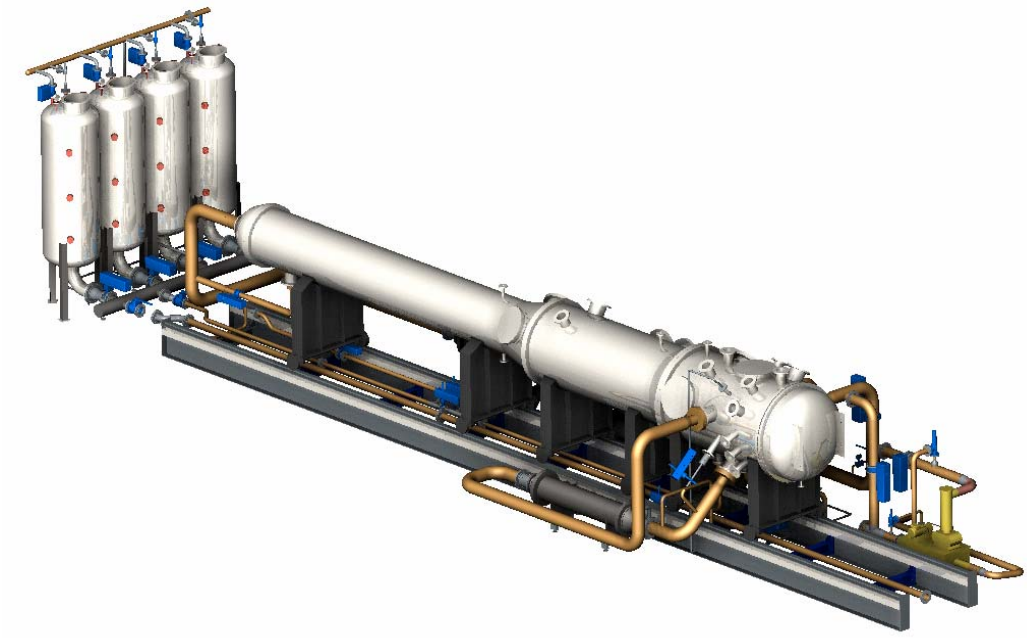

Figure 1.1: *Three-dimensional (3-D) Computer-Aided Design (CAD) illustration of the PBMM plant.*

According to Rousseau and Greyvenstein (2001), the main purpose of the PBMM is to illustrate the envisaged PBMR control methodologies and operational procedures, and to allow experiments and measurements of cycle parameters and process variables to aid in the validation and verification of the software (*Flownex*™) used to perform thermo-hydraulic analyses of the PBMR.

Rousseau and Greyvenstein (2001) also stated that the PBMM plant is not an exact scaled-down version of the actual PBMR plant, however, it is similar in that it contains all the main components of the PBMR layout in the same cycle configuration [*Figure 1.2*]. Furthermore, the representative main components are not exact scaled-down versions of the actual PBMR plant components but are able to mimic the same qualitative behaviour with regard to power and heat input and output, frictional and other pressure losses as well as thermal inertia during transients.

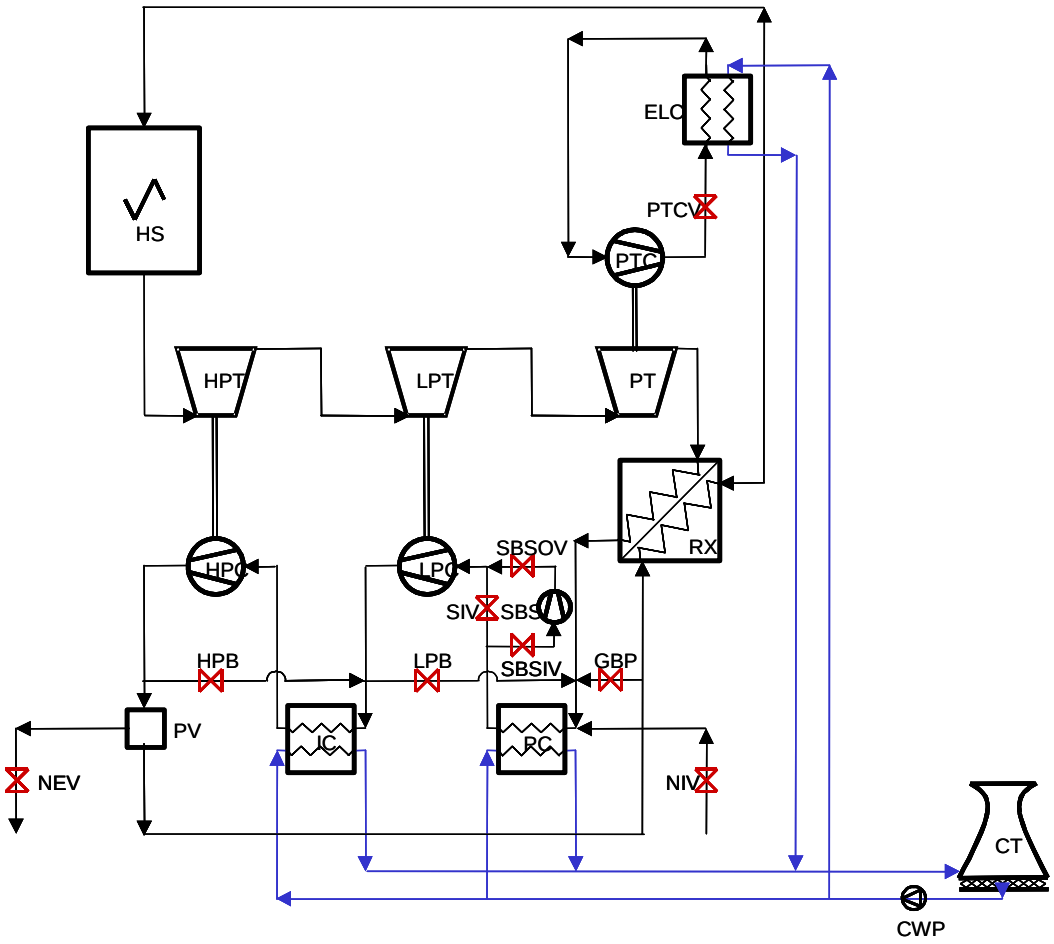

Figure 1.2: *Schematic layout of the PBMM cycle.*

The main components of the PBMM cycle as illustrated in *Figure 1.2*, are as follows:

CT : Cooling tower;
ELC : External load compressor;
HPC : High-pressure compressor;
HPT : High-pressure turbine;
HS : Heat source;
IC : Inter-cooler;
LPC : Low-pressure compressor;
LPT : Low-pressure turbine;
PC : Pre-cooler;
PT : Power turbine;
PTC : Power turbine compressor;
PV : Pressure volume containing a filter and oil separator;
RX : Recuperator with high-pressure and low-pressure sides;
SBS : Start-up blower system.

Labuschagne (2002) calculated the overall cycle parameters and process variables at crucial positions within the PBMM cycle layout at 100% Maximum Continuous Rating (MCR)[*]. These cycle parameters and process variables gave an indication of the PBMM plant's operational requirements at the respective component locations, indicating which of the aforementioned components could be implemented "off-the-shelf", required modifications, or had to be redesigned and built from basics. It was crucial that the performances of the PBMM and PBMR's components correspond accurately to ensure that reliable, accurate thermo-hydraulic analyses of the PBMR were performed.

Various subsystems illustrating the locations of some of the main components within the PBMM plant's design are displayed in *Figure 1.3*.

[*] *MCR is the operating condition within the cycle where all the applicable components are running at full operating capacity.*

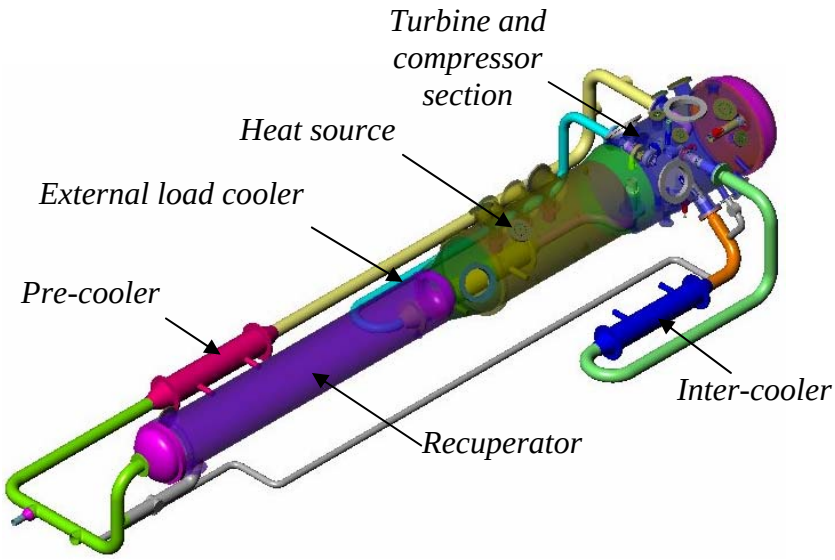

Figure 1.3: *A 3-D CAD illustration of the PBMM plant subsystems.*

By utilising the calculated cycle parameters and process variables, Rousseau and Greyvenstein (2001) concluded that the respective high- and low-pressure turbines and compressors could be integrated, resulting in the implementation of high- and low-pressure turbocharger units into the PBMM plant, making it smaller and more cost-effective. They also concluded that although the actual PBMR plant runs on an axial flow design, small "off-the-shelf" centrifugal-flow turbocharger units could be employed in the PBMM plant. *Figure 1.4* shows the high and low-pressure turbocharger units' locations and interfaces within the PBMM plant.

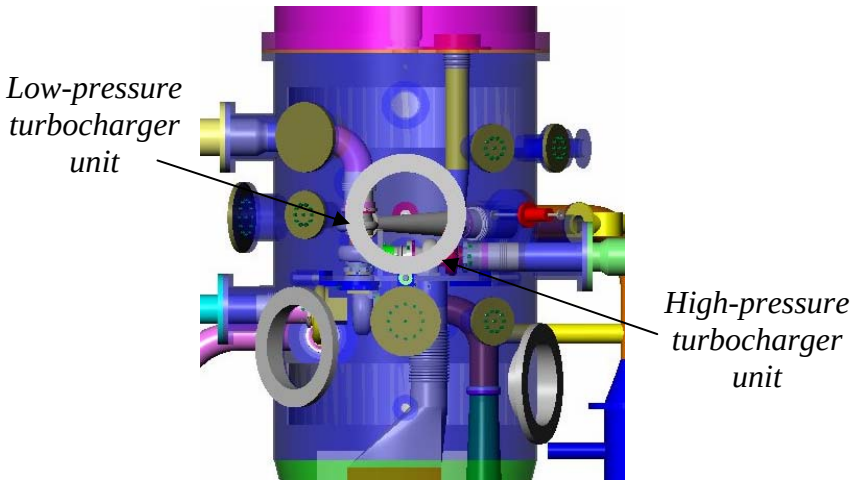

Figure 1.4: *A 3-D CAD illustration of the high- and low-pressure turbocharger units' locations and interfaces within the PBMM plant.*

It was crucial that the correct high- and low-pressure turbocharger units were selected to ensure that the internal gas pressure required by the Power Turbine (PT) to generate electricity was achieved.

Centrifugal-flow turbocharger units that are used on large diesel engines were reviewed. The Garret GT 42 turbocharger unit, consisting of a High-Pressure Turbine (HPT) and a High-Pressure Compressor (HPC) section, was selected as the high-pressure turbocharger unit [*Figure 1.5*].

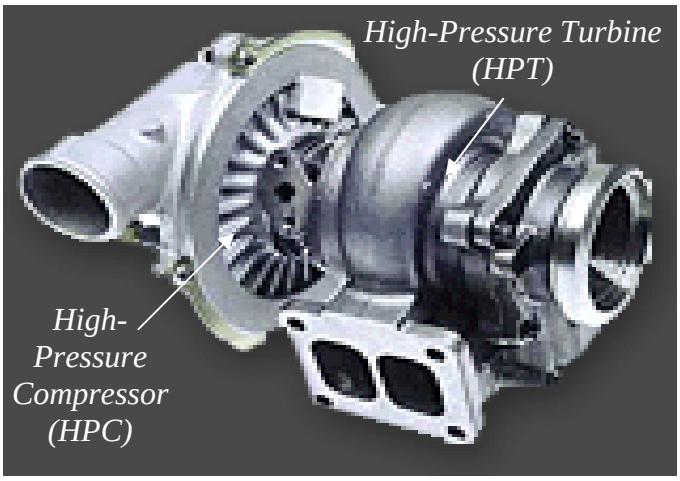

Figure 1.5: *A photographic image of the Garrett GT 42 turbocharger unit.*

The cycle parameter calculations at 100% MCR requires that the Garrett GT 42 HPT withstands a maximum pressure of 896 kPa at a maximum temperature of 700 ºC within the PBMM plant's cycle operation. Important characteristics regarding the operating capabilities of the Garrett GT 42 turbocharger unit, including a brief analysis of the HPT assembly follows to determine if these requirements are met.

Model	*:*	Garrett GT 42 turbocharger unit
Power	*:*	85.2 kW
Mass flow rate	*:*	1.148 kg /s
Inlet pressure	*:*	799.2 kPa
Inlet temperature	*:*	700 ºC
Outlet pressure	*:*	544.7 kPa
Outlet temperature	*:*	635.9 ºC
Pressure ratio	*:*	1 : 1.47

Maximum pressure	:	1000 kPa
Rotational speed	:	65363 rpm
Inlet pipe diameter	:	200 mm nominal
Outlet pipe diameter	:	200 mm nominal

The Garrett GT 42 HPT's assembly can be sub-divided into two basic pieces: *(i)* a turbine impeller and *(ii)* a turbine housing, as displayed in *Figure 1.6*.

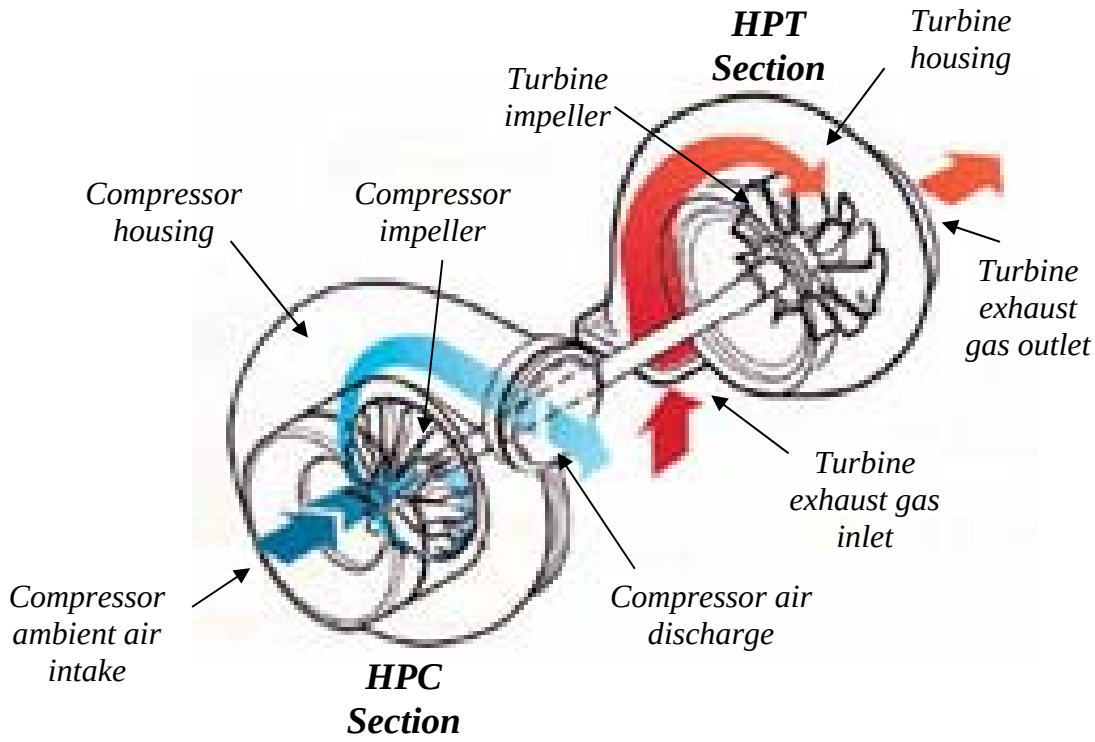

Figure 1.6: *An illustration of the Garrett GT 42 HPC and HPT assemblies.*

The turbine housing provides a flanged exhaust gas inlet and an axially located exhaust gas outlet, which means that the turbine housing is designed to endure a maximum pressure of 799.2 kPa at a maximum temperature of 700 ºC.

1.2 Problem Definition

A material composition study revealed that the Garrett GT 42 turbine housing in question [*Figure 1.7*] is a spheroidal ductile cast iron casting. Rounded iron carbides (cementite) characterise spheroidised steels, with a diameter of about 1 mm in a ferritic matrix.

Figure 1.7: *External photographic image of the Garrett GT 42 turbine housing.*

According to the ASME B31.3 (1996) Code for Pressure Piping, which the PBMM plant design had to comply with, spheroidal ductile cast iron cannot withstand a pressure of 896 kPa at a temperature of 700 ºC, which means that the Garrett GT 42 turbine housing did not satisfy the PBMM plant's design requirements. The material compositions of the turbocharger units were not taken into account in the initial selection process and with the Garrett GT 42 turbocharger unit already purchased and playing such an intricate role in the design of the PBMM, a solution had to be found.

One solution to solve this problem would have been to acquire an alternative turbine housing from the original suppliers, cast in a suitable material that could withstand the PBMM plant's design pressures at high temperatures. However, a turbine housing from a suitable material was not available and the manufacturers argued that casting a single turbine housing was not economically feasible.

Another solution could have been to place the turbocharger unit inside a pressure vessel in order to decrease the pressure gradient across the turbine housing's walls. The artificial pressure environment around the housing would place the pressures endured within the allowable ASME B31.1 Code for Pressure Piping range.

As an alternative, it was considered to have the turbine housing recast in an acceptable material that could withstand the PBMM plant's design pressures at high temperatures. For this purpose, a mould produced through Computer Aided

Manufacturing (CAM) technologies, using a 3-D virtual model obtained by reverse engineering methods, was required.

1.3 Purpose of this Research

The purpose of this research is:

- To study and evaluate reverse engineering methods and techniques in order to identify the most promising method(s) to reverse engineer the existing Garrett GT 42 turbine housing;

- To implement the most promising reverse engineering method(s) identified to recreate an accurate 3-D virtual model of the existing turbine housing that may later be used for mould production purposes.

Furthermore, it was required that non-destructive reverse engineering methods and techniques are implemented to produce a 3-D virtual model, as the housing was required for future use.

1.4 Structure of Dissertation

In *Chapter 2*, reverse engineering as a whole is briefly defined with the emphasis placed on the most applicable approach to create a 3-D virtual model of the Garrett GT 42 turbine housing (Geometrical Reverse Engineering (GRE)). The two major phases of the GRE process, data acquisition and data manipulation are introduced and discussed. Different contact (tactile) and non-contact GRE methods and techniques are presented and studied. Discussions on different data manipulation software are presented as well.

Data acquisition problem areas that influence the advantages and limitations of the different GRE methods, as indicated by the literature, are presented in *Chapter 3*. These advantages and limitations are used to evaluate the contact (tactile) and non-contact GRE methods and techniques, ultimately identifying the most promising

method(s) to reverse engineer the existing turbine housing without destroying it in the process.

In *Chapter 4* the most promising GRE method(s) identified in *Chapter 3* is implemented with the results presented, evaluated and discussed. *Chapter 5* presents the implementation of an alternative GRE method, discussing and comparing the results thereof with the results obtained in *Chapter 4*.

A summary followed by the appropriate conclusions is presented in *Chapter 6*. *A* complete reference list that will help the readers to find the most relevant research contributions is presented at the end of this dissertation.

CHAPTER 2: THE GEOMETRICAL REVERSE ENGINEERING (GRE) PROCESS

2.1 Background - Reverse Engineering…….……p. 10
2.2 Geometrical Reverse Engineering (GRE)……...p. 11
2.3 The GRE Process……...…….p. 11
2.3.1 Phase One - Contact (Tactile) and Non-Contact Data Acquisition……p. 12
2.3.2 Phase Two - Data Manipulation with 3-D, GRE and/or CAD Modelling Software….……..….p. 15

2.1 Background - Reverse Engineering

To many the term reverse engineering conjures up visions of engineers huddled in back rooms painstakingly disassembling products in order to steal their trade secrets. Although this may happen, reverse engineering is nowadays defined by the following:

Reverse engineering is a process of duplicating an existing component, subassembly or product functionally and dimensionally without the aid of drawings, documentation or a 3-D virtual model by means of physical examination and measurements, to develop the technical data (physical and material characteristics) required for competitive procurement [Modified after Varady et al. (1997)].

Literature cited shows that reverse engineering is very common in such diverse fields as e.g., chemical development and production, software engineering, consumer product manufacturing, automotive and mechanical design, which makes it impossible to study as a whole within the scope of this project. However, the most applicable approach to create a 3-D virtual model of the Garrett GT 42 turbine housing for mould production purposes (Geometrical Reverse Engineering (GRE)), is presented and discussed further.

2.2 Geometrical Reverse Engineering (GRE)

According to research by Stanley *et al.* (1995), designing sculptured surfaces in the engineering and manufacturing industry often involves the use of 3-D virtual models for initial conceptual and aesthetic design, finite element analysis, performance experiments, product prototyping and component modifications, enabling several beneficial Computer Aided Manufacturing (CAM) technologies. In this iterative product design process, GRE has played a key-linking role between various steps.

When software was originally created for 3-D modelling in the late 1960's and early 1970's, more thought was given to defining the geometry of a desired product from basics on a computer than was given to reversing the design process. Thirty years later this philosophy still seems to be predominant, however, the literature shows that the necessity to follow a reverse approach is as great or even bigger than before. Ma *et al.* (1997) stated that growing global competition requires designers and manufacturers to deliver more competitive products with better quality and lower prices, and with the traditional methods for creating 3-D virtual models inefficient and error-prone, GRE has received much needed attention over the last few years.

With the GRE approach in contrast to a normal design process, 3-D virtual models of entire existing systems can be achieved in reasonably short time, using the appropriate methods, techniques and computer software.

The creation of a 3-D virtual model of an existing component with any GRE method can better be described and understood by following a guideline better known as the GRE process.

2.3 The GRE Process

According to the literature, the creation of a 3-D virtual model using the GRE process consists of two basic phases, *(i)* data acquisition using some data input method or technique and *(ii)* data manipulation with computer software, as depicted by the flowchart in *Figure 2.1*.

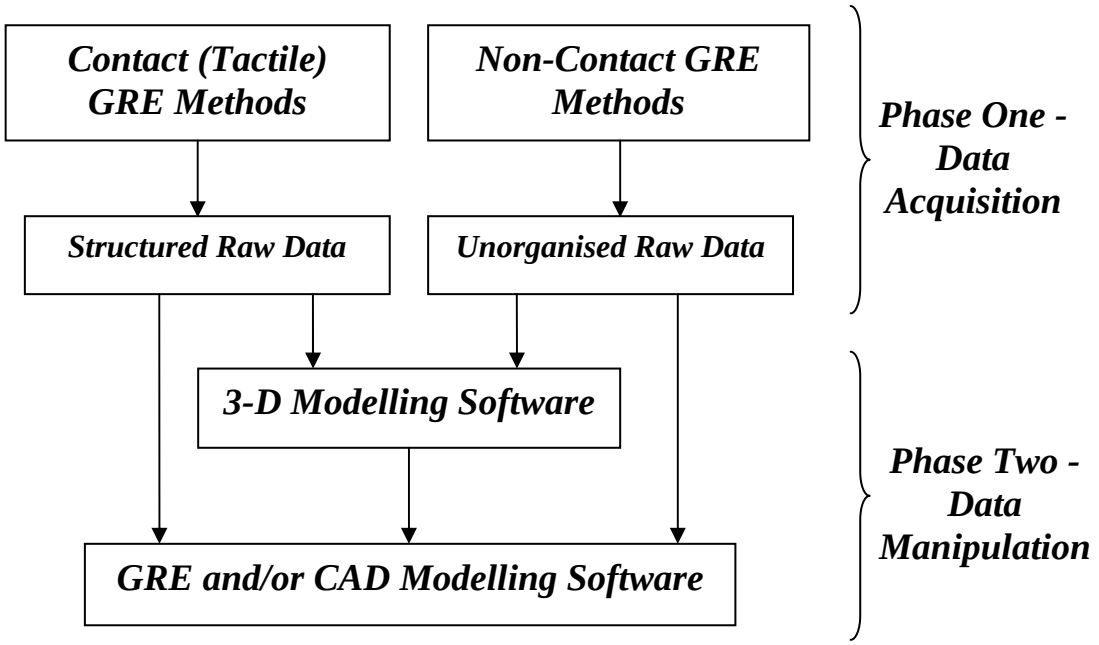

Figure 2.1: *Flowchart depicting the two basic phases of the GRE process.*

2.3.1 Phase One - Contact (Tactile) and Non-Contact Data Acquisition

Data acquisition requires the use of some mechanism or phenomenon interacting with the surface or volume of a component to collect 3-D positional geometric data describing the component's external and/or internal profiles. The 3-D positional geometric data can be represented by an ordered triple of real numbers *(x, y, z)*, known as the Cartesian co-ordinates of a point. Any 3-D curved surface or volume can be represented by an array of points with known Cartesian co-ordinates. From the Cartesian co-ordinates other quantities such as displacement, curvature and ultimately size can be calculated.

According to the literature, a large variety of manipulators capable of measuring these Cartesian co-ordinates of desired points are currently available on the market. The most popular uses non-contact techniques where light, sound, radiation or magnetic fields interacts with the surface or volume of interest to acquire data, while others touches the surface of interest with a selection of probes at the end of mechanical arms or are measured with hand-held measuring equipment (tactile methods). In each case, the operator must perform important tasks to assist with the determination of the

Cartesian co-ordinates of the points, describing the surface or volume profiles of interest.

2.3.1.1 Contact (Tactile) GRE Methods

According to the literature, contact (tactile) data acquisition can be divided into four basic methods: *(i)* geometrical inspection and measurements, *(ii)* point triangulation, *(iii)* electro-mechanical point scanning and *(iv)* co-ordinate measuring. In all of the aforementioned methods the technician must physically touch the component in question with the measuring equipment or probe manually or automatically, to record the Cartesian co-ordinate location of each point. This action generates structured reference points or profile contours in a 3-D environment, which is later entered into the 3-D, GRE and/or CAD modelling software to generate the desired 3-D virtual model (phase two). A flowchart summarising the different contact (tactile) GRE methods including their respective data acquisition techniques is presented in *Figure 2.2*.

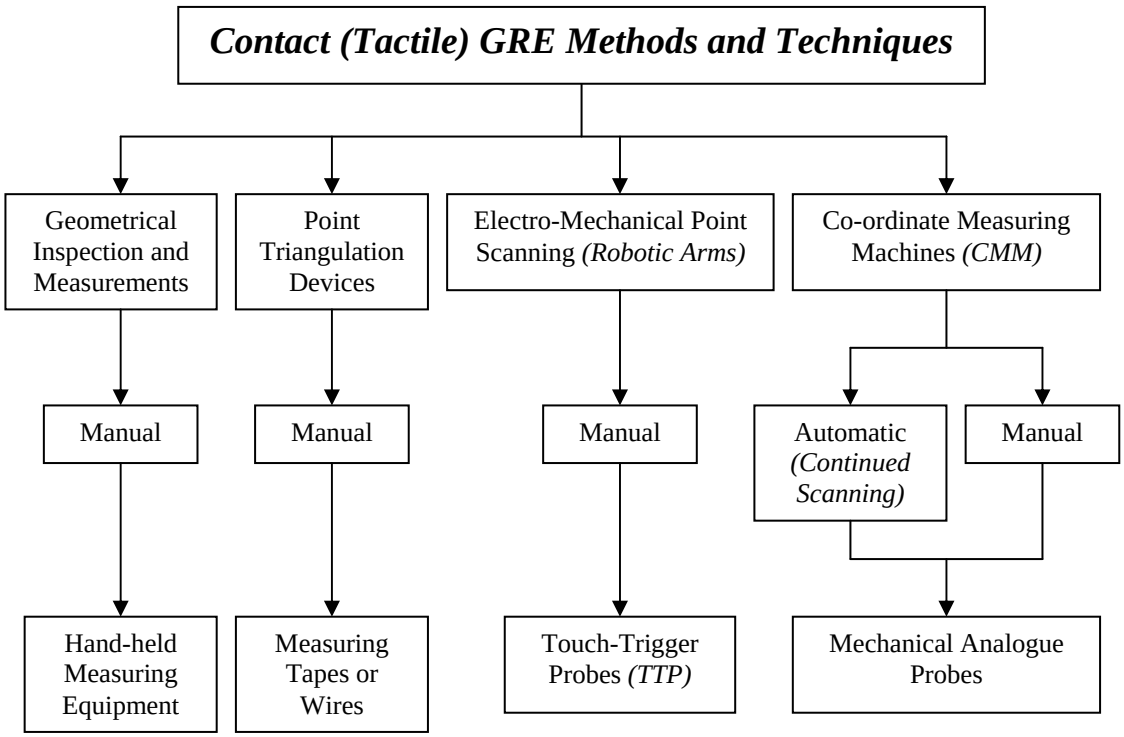

Figure 2.2: *Flowchart summarising the different contact (tactile) GRE methods and techniques.*

Details of the different contact (tactile) GRE methods and techniques are presented in *APPENDIX A.*

2.3.1.2 Non-Contact GRE Methods

The literature also shows that non-contact data acquisition can be divided into three basic methods: *(i)* Magnetic Resonance Imaging (MRI), *(ii)* optical methods and *(iii)* ultrasonic sound waves. In all of the aforementioned methods, the Cartesian co-ordinate location of each point is measured and recorded without any physical contact with the component of interest's surface or volume. This action generates unorganised reference point clouds or profile contours in a 3-D environment, which is later entered into the 3-D, GRE and/or CAD modelling software to generate the desired 3-D virtual model (phase two). A flowchart summarising the different non-contact GRE methods including their respective data acquisition techniques is presented in *Figure 2.3*.

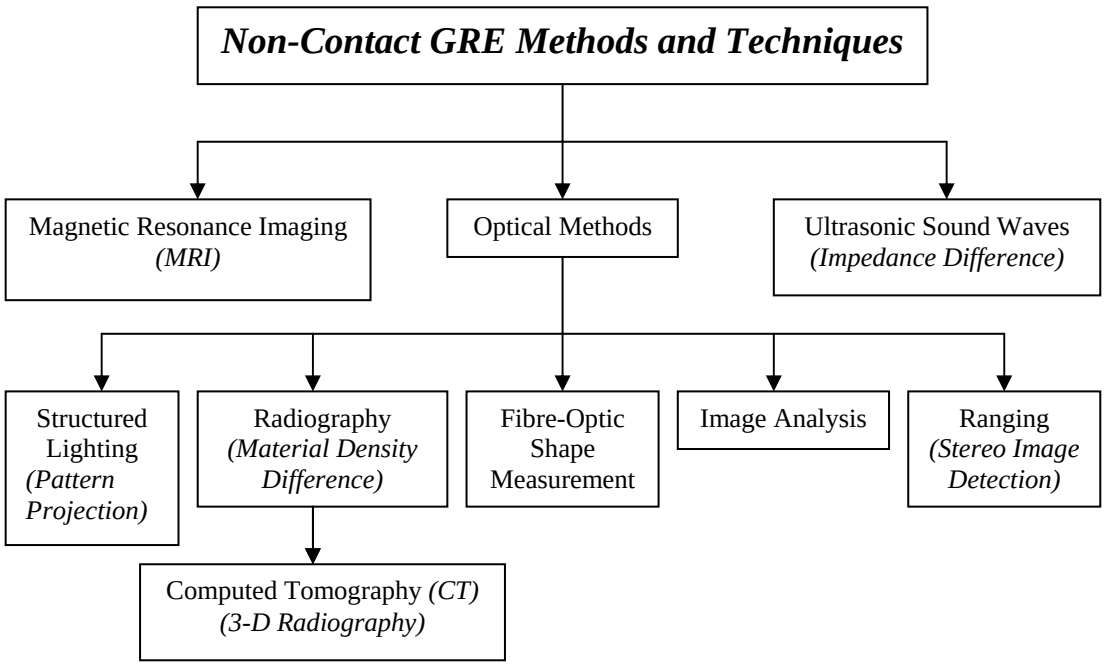

Figure 2.3: *Flowchart summarising the different non-contact GRE methods and techniques.*

Details of the different non-contact GRE methods and techniques are presented in *APPENDIX B.*

2.3.2 Phase Two - Data Manipulation with 3-D, GRE and/or CAD Modelling Software

Modern 3-D, GRE and CAD modelling software can greatly simplify the adequate manipulation of the 3-D positional geometric data acquired in phase one of the GRE process. The main purpose of these software packages is to manipulate and convert the raw 3-D positional geometric data into usable 3-D virtual models and perform desired tasks with the least loss of accuracy.

If the ultimate task of the GRE process is simply to display or render the model, then a 3-D polygonal model is required and the ultimate application would be rendering 3-D modelling software. If other tasks like geometry alteration, CAM operations or construction of templates for repairs are required, then 3-D Non-Uniform Rational B-spline (NURBs) models are required, and general-purpose GRE and/or CAD modelling software packages are necessary. Other possible secondary tasks are applications like Finite Element Analysis (FEA) or Computational Fluid Dynamics (CFD) analysis. These analyses might require only a 3-D polygonal model but the polygons might have to be radically adjusted to meet the requirements of the analysis program. Depending on the amount of data and performance of the software, processing can take from hours to days on a UNIX-based workstation and even longer on a Personal Computer (PC).

The raw 3-D positional geometric data input order and format obtained from the different GRE methods primarily determines which software packages can be used and how easy it is to convert the raw 3-D positional geometric data into a useable and accurate 3-D virtual model. The data input devices are more concerned with the accurate input of 3-D point positions on the component than they are with the order or sequence of the points stored in the data file. It is the job of the 3-D, GRE and/or CAD modelling software to construct usable geometry based on the various stored raw 3-D positional geometric data formats.

Since the ultimate task of this reverse engineering application is to utilise CAD/CAM technologies for mould production purposes, the focus is shifted towards GRE and CAD modelling software. A broader discussion on NURBs solids, which GRE and

CAD modelling software uses to define 3-D NURBs models, is presented in *APPENDIX C.*

Some GRE and possible compatible CAD modelling software packages that provide the user with an interface to interactively create 3-D NURBs models from the raw 3-D positional geometric data have been found and are summarised in *Table 2.1*.

Table 2.1: *GRE and possible compatible CAD modelling software packages.*

GRE Software	***Applications***	***Compatible CAD***
Alias Wavefront: Autostudio Surfacestudio Evalviewer	Free-form conceptual modelling. Technical surfacing. Point cloud processing. Surface quality inspection.	CATIA, IDEAS, Pro-Engineer
AnthroCAM	FARO, Demo (a), Demo (b)	AutoCAD
Anvil Express	Surface/solid modelling, 2.5/3 axis NC, G-post, rendering, animation.	SolidWorks, CADKEY
CIMATRON	Tool-making.	SolidWorks, AutoCAD
DELCAM CopyCAD	Complex surfaces from digitised data. Demo	–
EUCLID Styler	Stand alone industrial design built in. SLA interface.	–
Imageware Surfacer	Point cloud manipulation. Rapid surfacing, Class A surfacing.	CATIA, Pro-Engineer, Unigraphics, CADDS 5, IDEAS
INTIsurf	INTIcad, INTIpoint, and INTIcheck.	Pro-Engineer, Auto CAD, IDEAS
Metris Surfacer / Base / Solid	Solid from point cloud. Surface continuity.	Auto CAD, CADKEY Mechanical Desktop
Pro-Engineer scantools	Real-time manipulation of curves and surfaces using control polygons. Reflection curves.	Pro-Engineer
Raindrop Geomagic	Studio, Wrap, Shape, Decimate.	–

Bradly (1998) presents basic guidelines to follow in the importation and manipulation of the raw 3-D positional geometric data within the software packages during the GRE process. A sequence of steps is given for the manipulation of raw 3-D positional geometric data sequentially organised along key paths on the component, associated with contact (tactile) GRE methods. A second sequence of steps is discussed for the

manipulation of raw 3-D positional geometric point cloud data associated with non-contact GRE methods.

A study by Brocha and Young (1995) discusses some available software vendors. Hoppe *et al.* (1993), (1994) and Lounsbery *et al.* (1992) provide a background for research in this area. Their work is motivated by the need for faster 3-D NURBs model generation with reduced data, and specialises in geometric modelling requirements. Studies by Eck and Hoppe (1996), Greiner and Hormann (1997), Hoschek *et al.* (1998) and Sapidis and Besl (1995) illustrate the generation of 3-D NURBs models of conventional engineering components, using NURBs.

CHAPTER 3: EVALUATION OF GRE METHODS

3.1 Introduction…….p. 18
3.2 Data Acquisition Problem Areas……..……...p. 18
3.3 Advantages of Contact (Tactile) and Non-Contact Methods…...……...p. 21
3.3.1 Contact (Tactile) Methods…….……...……..p. 21
3.3.2 Non-Contact Methods…….……..…….……p. 22
3.4 Limitations of Contact (Tactile) and Non-Contact Methods……..…..…... p. 23
3.4.1 Contact (Tactile) Methods……..……..……...p. 23
3.4.2 Non-Contact Methods……..…….……..p. 24
3.5 Evaluation of Contact (Tactile) and Non-Contact GRE Methods……..p. 25
3.6 Garrett GT 42 Turbine Housing Attributes…….p. 27
3.7 Discussion and Conclusions……...p. 30
3.7.1 X-ray Computed Tomography (X-ray CT)……..p. 31
3.7.2 Neutron Computed Tomography (NCT)…….p. 34

3.1 Introduction

The GRE process discussed in *Chapter 2* clearly illustrates that the first step to create an accurate 3-D NURBs model of an existing component is to acquire sufficient and accurate 3-D positional geometric data. If the selection process of a data acquisition method is neglected or incorrectly approached, data manipulation with computer software becomes unreliable and the GRE process is unsuccessful. This scenario strongly suggests that the different GRE methods and techniques studied in *Chapter 2* be properly evaluated to identify a suitable method to acquire sufficient and accurate 3-D positional geometric data for any project, and consequently for this study.

3.2 Data Acquisition Problem Areas

While studying the literature on the different GRE methods in *Chapter 2*, it was noted that different GRE methods are prone to different irregularities during data acquisition, which needs to be considered when selecting a suitable GRE method. These data acquisition problem areas influence the advantages and limitations of both

contact (tactile) and non-contact methods, providing a guideline to assists in the evaluation and identification of a suitable method(s) to acquire sufficient and accurate 3-D positional geometric data.

According to the literature, the most commonly encountered problem areas to consider can be summarised as follows:

- Calibration;
- Accuracy;
- Accessibility;
- Component size;
- Material composition;
- Occlusion;
- Fixturing;
- Multiple views;
- Surface finish;
- Elimination of unwanted data (noise);
- Restoration of missing data;
- Statistical distribution.

Calibration is an essential part of setting up and operating all GRE methods. Any method must be calibrated to *(i)* accurately determine parameters of the respective method, and *(ii)* to model and allow for as accurately as possible systematic sources of error.

Accuracy should not be assumed by default. Although the method being used may be very accurate, only data at discrete points might have been collected. These disjointed points must then be curve-fitted or surface-fitted to create a useable 3-D NURBs model. This fitting process is where most of the accuracy errors are introduced. Even if thousands of data points are collected, some accuracy will still be lost when the points are converted into a usable form. It should be noted that the accuracy of the data acquisition device might not be the achievable accuracy for the usable 3-D NURBs model.

Accessibility is the issue of gathering 3-D positional geometric data that is not easily obtainable due to the configuration of a component. This usually requires multiple attempts but can also make some data impossible to acquire with certain methods. This aspect will determine if the method being considered can acquire data from complex external or internal profiles, or both. Component size greatly affects the accessibility of a component as well. In some instances lager components can be repositioned and adjusted, however, the potential loss of accuracy in such cases has to be considered. In other cases, the components may be too big for the data acquisition device. Related to this aspect is the amount of space available around the component to work with and the environmental conditions. Data acquisition with some methods are only possible if the capabilities of the techniques used are not influenced by the material composition of the component in question as e.g., magnetic resonance's interaction with metallic components.

Occlusion is the blocking of the data acquisition medium due to obstructions such as e.g., shadowing. This is primarily a problem with optical methods. However, acoustic and magnetic methods may also have this problem. Acquiring data with multiple devices is one approach to obviate this problem. Rious (1984) and Koivunen (1992) have presented detailed discussions on methods to eliminate occlusion in optical systems. Occlusion may also arise due to fixturing of components. Typically, components must be clamped before data is acquired to make sure that the 3-D positional geometric data matches in the same co-ordinate set-up. The geometry of the fixtures becomes a part of the acquired data leading to a loss of accuracy. Elimination of fixture data is difficult and often requires the use of multiple views. A large potential for error and a loss of accuracy can occur because of realigning multiple view data sets.

Smoothness and material coatings can dramatically affect the data acquisition process as well. Contact (tactile) as well as non-contact methods will produce more unwanted data (noise) with a rough surface than a smooth one. Reflective coatings can also affect non-contact methods e.g., reflective surfaces cause inaccurate data acquisition when light reflects off an object. In retrospect, a rough surface may present a very difficult data acquisition process with multiple complications.

Noise elimination in data samples is a difficult issue. The literature showed that noise could be introduced in a multitude of ways, such as extraneous vibrations, specular reflections, etc. Many different filtering approaches can be used to minimise the noise generated. An important aspect to consider is whether to eliminate the noise before, after, or during the 3-D NURBs model building stage. There are cases where the noise should not be eliminated at all. Noise filtering, though, is often an unavoidable step in the GRE process. This may however destroy the sharpness of the data i.e. typically sharp edges disappear and are replaced by smooth blends, which in some cases may be desirable, but in other cases may lead to serious problems in identifying features. An example of noise elimination is presented in Koivunen (1992).

Restoration of missing data is partly necessary due to the above-mentioned inaccessibility and occlusion problems. Moreover, because of the nature of non-contact and even contact (tactile) methods, the data close to sharp edges is fairly unreliable. There might also be situations where data can only be acquired from parts of a certain subsystem. This may lead to missing components or components obscured by other elements while the reconstruction of the whole subsystem from just the visible component is still required.

Statistical distribution of components is the final issue to be addressed. This aspect deals with the fact that any given component being reverse engineered only represents one sample in a distributed population. When GRE methods attempt to reproduce a given shape, the tolerance distribution of the data acquired from the component must be considered. This gives rise to multiple component data acquisition attempts and the averaging of the resulting data. However, it may be somewhat impractical to attempt to sample many components from a population when often only one is available.

3.3 Advantages of Contact (Tactile) and Non-Contact Methods

3.3.1 Contact (Tactile) Methods

The aforementioned data acquisition problem areas contribute to several fundamental advantages of contact (tactile) methods, making them more popular than the majority of available non-contact methods. Some of the major advantages being:

- Data density;
- Noise elimination is not required;
- Treatment of surfaces is not required;
- Vertical and oblique surfaces are accessible.

With contact (tactile) GRE methods, the number of 3-D positional geometric data points required to reproduce an accurate 3-D NURBs model of an existing component can be predicted before data acquisition starts. The density of the data relies on the geometry and complexity of the component in question. Because the path of the data acquisition is pre-determined, a minimum level of unwanted or inaccurate noise will be generated. This means that the data manipulation within the software packages will not require time-consuming cleanups.

The physical contact nature of these GRE methods does not require a reflective component surfaces to be covered with a non-reflective coating to ensure accurate data acquisition. Different probe orientations allow the gathering of accurate data from vertical and oblique surfaces as well.

3.3.2 Non-Contact Methods

In comparison to contact (tactile) methods, non-contact methods have several fundamental advantages that contribute to their popularity. Some of the major ones being:

- Data acquisition speed;
- Non-contact methodology;
- Acquiring data from internal profiles.

The main advantage and probably the reason why most data acquisition is done using non-contact methods is the speed at which 3-D positional geometric data is acquired. Several thousand data points can be acquired with a single scan in a relatively short period. Acquiring 3-D positional geometric data without making contact with the component means that no fixturing of the component is required and data from components with soft surfaces can be accurately acquired with ease.

Some non-contact methods are able to acquire accurate data from complex internal profiles of a component without destroying the component in the process. This is a major advantage especially in Non-Destructive Testing (NDT) and engineering applications.

3.4 Limitations of Contact (Tactile) and Non-Contact Methods

3.4.1 Contact (Tactile) Methods

Some limiting factors that influence the decisions of whether a contact (tactile) method should be considered are:

- Slow, labour intensive nature;
- Sparse data leading to difficult surface conversions;
- Limited accuracy in measuring soft components;
- Required skills;
- Acquiring data from internal profiles.

A limiting factor of contact (tactile) data acquisition is the fact that the operator must carefully move the data acquisition machine's probe all over the component, either manually or automatically. This takes a reasonable amount of time, several hours in the case of automation and even days manually for a complex surface geometry, which raises costs since this process ties up a high burden rate machine.

The other significant limitation stems from the type of data they generate. Since the effort of touching each co-ordinate location is so time-consuming, the level of data that is collected can be less than what the designers require. The graphical result of data acquired is a series of sections. Designers must generate NURBs and ultimately 3-D NURBs models from these sections. Although this works well enough with simple components since they can extrude from the lines and curves, it is not effective for complex shapes since the area in between the sections is not a straight line. Therefore, constructing accurate 3-D NURBs models from acquired 3-D positional geometric data can be a very labour-intensive process.

A contact (tactile) method makes it difficult to accurately measure something very soft. Touching this type of surface even very lightly causes it to depress. Since it isn't possible for the operator or machinery to depress each point to the same exact degree, measurements of soft components are prone to inaccuracy. Even with firmer components, accuracy is always a concern because the skill of the operator affects the measurements to such a large extent. With a CMM for example, if the operator loses contact with the part surface for an instant, accuracy suffers. Aside from operator influence, a CMM is capable of achieving a reasonable level of accuracy but is not well suited to the task of acquiring data from complete surfaces. Similarly with the electro-mechanical method, the operator must be highly trained and even when he works carefully there can still be a great deal of variability in the data based on his influence. Due to the construction of contact (tactile) measuring equipment, data acquisition from complex internal profiles is very difficult, and often impossible.

3.4.2 Non-Contact Methods

Some limiting factors that influence the decision whether a non-contact method should be considered are:

- Nature of the raw data;
- Noise generation;
- Surface profile and finish.

Non-contact methods generate unorganised 3-D positional geometric data resulting in elaborate requirements of a singular modelling software package. Initial data manipulation may be achievable with GRE software but a transfer into CAD modelling software may also be required.

The fact that the data acquisition process relies completely on the capabilities of the non-contact method and very little human intervention, the gathering of considerable levels of noise is inevitable. This noise can cause inaccurate measurements and may require tedious manipulation with the possibility of an ill-represented 3-D NURBs model. Some non-contact methods rely on source reflection from the component's surfaces. Strange angles and surface finishes might lead to inaccurate data acquisition and the generation of noise.

3.5 Evaluation of Contact (Tactile) and Non-Contact GRE Methods

With the advantages and limitations of the different GRE methods identified, a well-educated guideline is established to assist in the evaluation and identification of a suitable GRE method to acquire accurate and sufficient 3-D positional geometric data.

By using the advantages, limitations and the supporting literature on contact (tactile) and non-contact methods, a summarised evaluation of the respective GRE method capabilities with regard to general equipment factors is presented in *Table 3.1* and *Table 3.2*.

Table 3.1: *Evaluation of contact (tactile) GRE methods with regard to general equipment factors.*

Equipment Factors	***Contact (Tactile) GRE Methods***			
	Geometrical Inspection and Measurements	Point Triangulation Devices	Electro-Mechanical Point Scanning	Co-ordinate Measuring Machines *(CMM)*
Acquisition Speed	***1***	***2***	***2***	***3***
Accuracy *(Inherent Limitations)*	***3***	***3***	***4***	***4***
Set-up & Calibration	***3***	***3***	***3***	***3***
Accessibility *(Material Composition)*	***5***	***5***	***5***	***5***
Automation Level	***1***	***2***	***3***	***4***
Accessibility *(Fixtures)*	***4***	***3***	***3***	***4***
Affordability	***5***	***4***	***4***	***3***

1 = Pathetic ***2 = Poor*** ***3 = Average*** ***4 = Good*** ***5 = Excellent***

Table 3.2: *Evaluation of non-contact GRE methods with regard to general equipment factors.*

Equipment Factors	***Non-Contact GRE Methods***							
	Magnetic Resonance Imaging *(MRI)*	Optical Methods						Ultrasonic Wave Sound
		Structured Lighting	Radio-graphy	Computed Tomography	Fibre-Optics	Image Analysis	Ranging	
Acquisition Speed	***5***	***4***	***4***	***5***	***3***	***3***	***3***	***5***
Accuracy *(Physical Limitations)*	***3***	***2***	***3***	***2***	***3***	***3***	***3***	***4***
Set-up & Calibration	***4***	***2***	***3***	***4***	***3***	***3***	***3***	***4***
Accessibility *(Material Composition)*	***1***	***5***	***2***	***3***	***5***	***5***	***5***	***2***
Automation Level	***4***	***3***	***4***	***5***	***2***	***3***	***3***	***4***
Accessibility *(Fixtures)*	***5***	***2***	***5***	***5***	***4***	***2***	***2***	***5***
Affordability	***2***	***3***	***3***	***3***	***3***	***3***	***3***	***2***

1 = Pathetic ***2 = Poor*** ***3 = Average*** ***4 = Good*** ***5 = Excellent***

These evaluations may lead to the identification of an inadequate GRE method if the attributes of the component being studied are not taken into account. Evaluation with regard to component attributes are summarised in *Table 3.3* and *Table 3.4*.

Table 3.3: *Evaluation of contact (tactile) GRE methods with regard to component attributes.*

Component Attributes	***Contact (Tactile) GRE Methods***			
	Geometrical Inspection and Measurements	Point Triangulation Devices	Electro-Mechanical Point Scanning	Co-ordinate Measuring Machines *(CMM)*
Large Components	***5***	***3***	***3***	***2***
Non-Rigid Materials	***3***	***2***	***2***	***2***
Vertical Surfaces	***5***	***4***	***4***	***3***
Oblique Surfaces	***5***	***4***	***4***	***4***
Internal Corners	***3***	***2***	***2***	***2***
Internal Geometry	***3***	***2***	***2***	***2***

1 = Pathetic ***2 = Poor*** ***3 = Average*** ***4 = Good*** ***5 = Excellent***

Table 3.4: *Evaluation of non-contact GRE methods with regard to component attributes.*

Component Attributes	***Non-Contact GRE Methods***							
	Magnetic Resonance Imaging *(MRI)*	Optical Methods						Ultrasonic Wave Sound
		Structured Lighting	Radio-graphy	Computed Tomography	Fibre-Optics	Image Analysis	Ranging	
Large Components	***2***	***4***	***4***	***3***	***4***	***5***	***4***	***3***
Non-Rigid Materials	***5***	***5***	***5***	***5***	***4***	***5***	***5***	***5***
Vertical Surfaces	***4***	***2***	***4***	***5***	***3***	***2***	***2***	***4***
Oblique Surfaces	***5***	***2***	***4***	***5***	***3***	***2***	***2***	***5***
Internal Corners	***4***	***1***	***5***	***5***	***2***	***1***	***1***	***4***
Internal Geometry	***5***	***1***	***5***	***5***	***4***	***1***	***1***	***4***

1 = Pathetic ***2 = Poor*** ***3 = Average*** ***4 = Good*** ***5 = Excellent***

Although *Table 3.1* to *Table 3.4* provides a general guideline, the most promising GRE method to reverse engineer the Garret GT 42 turbine housing could at this stage not be identified since the necessary attributes of the turbine housing had not been considered yet.

3.6 Garrett GT 42 Turbine Housing Attributes

Visual internal and external analyses of the Garrett GT 42 turbine housings were therefore conducted to determine the attributes to be considered in the selection process of a suitable GRE method(s).

The external geometry of the turbine housing can be sub-divided into three basic sub-components as displayed in *Figure 3.1*:

- An exhaust gas inlet;
- An exhaust gas outlet, which is the interface with the central housing and eventually the compressor housing;

- A free-form section where the exhaust gases are accelerated onto the turbine impeller to generate the actual work, better known by the engineering industry as the scroll;

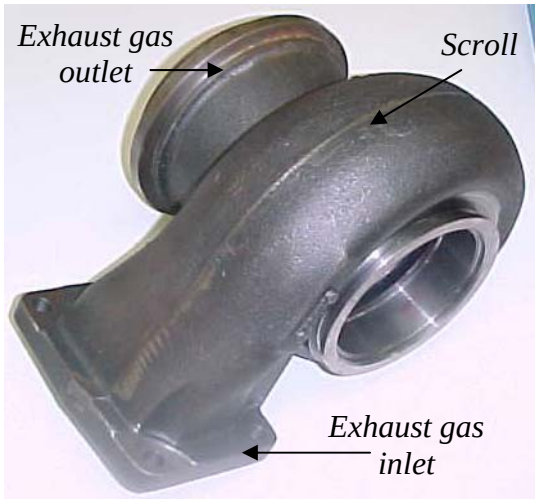

***Figure 3.1**: External photographic view of the Garrett GT 42 turbine housing's sub-components.*

According to Campbell and Flynn (2001), definitions of free-form surfaces and components are often intuitive rather than formal. Synonymous adjectives include sculpted, free flowing, piecewise smooth, for some desired degree of continuity. The presence of vertical and oblique surfaces within a free-form geometry is eminent.

- The exterior surface of both the exhaust gas outlet and the turbine scroll has a sandblasted like finish due to the casting process used to manufacture it. Some parts, such as the exhaust gas inlet have a smoother surface finish as the result of machining after manufacturing;

- Measurements obtained by inspecting additional decommissioned centrifugal turbine housings indicated that the material thickness of the turbine housing in question varies from 2 mm to 25 mm in some sections;

- The turbine housing is 250 mm long and has a width of 220 mm and a height of 250 mm as displayed in *Figure 3.2*, with an approximate weight of 12 kg.

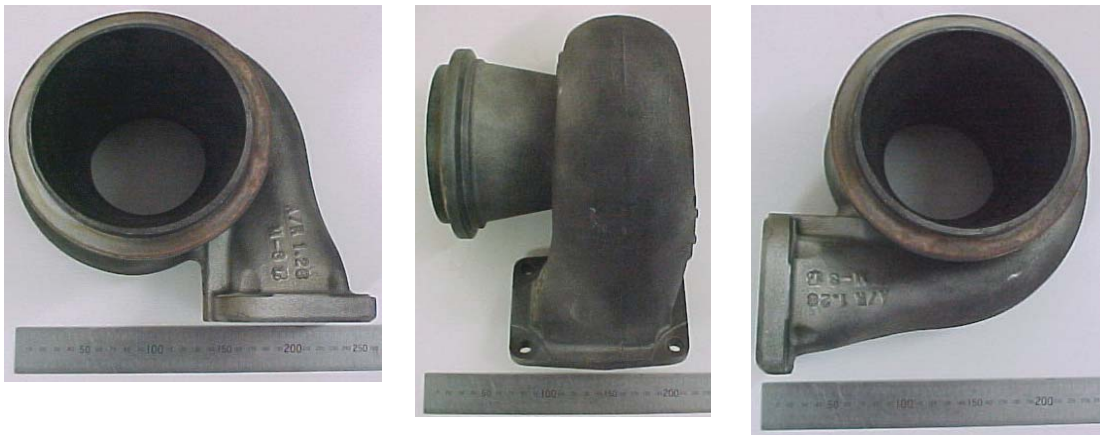

(a) *(b)* *(c)*

Figure 3.2: *Photographic views of Garrett GT 42 turbine housing's physical exterior dimensions.*

Visual internal inspections revealed that the turbine housing has two symmetrical continuous channels running from the turbine exhaust gas inlet all the way through to the turbine exhaust gas outlet. These cavities are better known as volutes. Theoretically, the purpose of these volutes is to guide and accelerate exhaust gases onto the turbine impeller. To accomplish this feat the area through which the gases proceed must decrease, resulting in quite a complex internal profile [*Figure 3.3*].

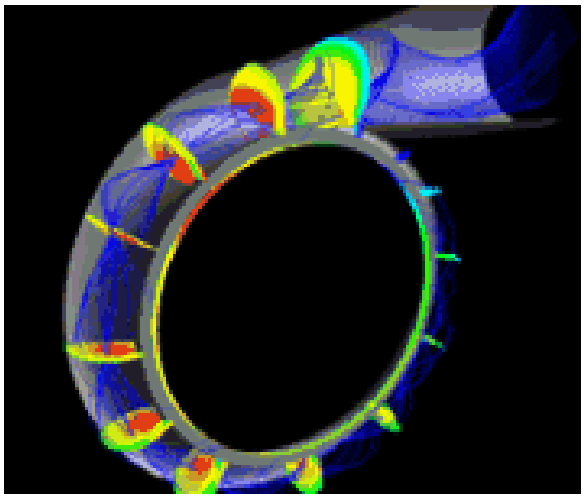

Figure 3.3*: CFD model illustration of the exhaust gas flow through a centrifugal turbine housing volute.*

3.7 Discussion and Conclusions

Visual inspection revealed characteristics and basic attributes that greatly influenced the identification of the most promising GRE method(s) to reverse engineer the Garrett GT 42 turbine housing. Geometrical complexity, physical component size and weight, and surface finish are just some of the major ones.

By combining the evaluation of the different GRE methods presented in *Table 3.1* to *Table 3.4* with the turbine housing's attributes, the general impression was that non-contact GRE methods in a broader sense, were the most favourable. Magnetic Resonance Imaging (MRI), ultrasonic sound waves and Computed Tomography (CT) were pre-eminent.

MRI is generally a good GRE method except for the fact that MRI cannot acquire data from ferrous components, since the fundamental mechanism of the technique depends on magnetic pulses. Ferrous components such as the turbine housing would cause chaos and may even damage the equipment. MRI as a GRE method could therefore not be used within the scope of this project.

Ultrasonic sound waves, exploiting a scanning acoustic microscope (SAM), is a valid GRE method, however, the curvature and the material thickness of the turbine housing posed a problem. The thicker the material becomes, the lower the scanning frequency has to be and the lower the frequency drops, the larger the scanning probe has to be. An additional complexity is the fact that scanning has to be done perpendicular to the component's exterior surface otherwise scanning errors might occur. With the surface curvature of the turbine housing and the size of the scanning probes required, unacceptable inaccuracies were likely to result.

The final GRE method to be discussed is CT. The primary advantages of CT over contact (tactile) as well as the remaining non-contact methods are that objects with internal or hidden features, or components made of different materials can be simultaneously detected during data acquisition. This capability is crucial especially when data is required from components where their destruction in the process is not allowed.

While radiography methods usually produce two-dimensional (2-D) images (projections of 3-D space) of objects, CT produces narrowly spaced 2-D image slices that are used to construct a 3-D image of an object. Modern CT-methods based on X-rays are successfully applied routinely to assist with medical diagnoses, surgical procedures and prosthesis design. Neutron Computed Tomography (NCT) is mainly applied for materials NDT, GRE and quality assurance. Stanley *et al.* (1995), Ma *et al.* (1997) and Yancey *et al.* (1996) did some research on reverse engineering with X-rays while Schillinger *et al.* (1999) presented a paper on reverse engineering with neutrons.

The basic GRE methodologies of the two CT applications are briefly discussed in the following subsections to determine if these methods would satisfy the reverse engineering requirements of the Garrett GT 42 turbine housing.

3.7.1 X-ray Computed Tomography (X-ray CT)

X-ray CT applications can be sub-divided into two main disciplines namely medical and industrial X-ray CT. Current industrial X-ray CT systems have progressed to the point where they can provide dimensional measurements, however, achievable accuracy may be inferior to that of co-ordinate measuring machines (CMM) and laser scanners. The scanning process delivers well-ordered points representing the surface contours of a component organised layer by layer. Each layer has a number of contours depending on the complexity of the geometry being measured.

Waterman (1997) stated that industrial X-ray CT systems are well suited for large parts or thick-walled metal parts that would require high-intensity scanning. ARACOR (Pty) Ltd., an industrial X-ray CT system manufacturer, reports maximum component weight of 450 kg and maximum working volume of 0.5m x 0.5m x 0.6m for one of their systems. Industrial scan costs may be higher than a local hospital and they may not be located close by.

A major consideration when using medical X-ray CT is that the part might not be scanned immediately due to patient load requirements. Medical technicians may also insist that specific scanning protocols are compiled and provided for the scanning of

components. With hospital X-ray CT scanning systems the largest matrix of 512 x 512 pixels versus 1024 x 1024 for an industrial X-ray CT system can typically be expected. The lowest field of view (FOV) would be 9.6 cm which would result in an X-Y pixel dimension of 0.19 mm x 0.19 mm (where Z resolution is 0.5 mm).

Another important consideration with medical CT scanners is that generally the accuracy required and achievable is less than for industrial CT scanners.

3.7.1.1 GRE Methodology

First, the component of interest is fastened to the platen of a suitable X-ray CT system and is scanned. Generally, standard machine tool hardware is available for clamping the part to the platen. In many cases, just positioning the part on top of a low-density substrate, like foam, is sufficient. Occasionally, a special fixture may be necessary to keep it from shifting during a scan. No special pre-programming or indexing is required, and scanning can begin as soon as the part has been secured to the platen. The scan data may consist of a few slices, a stack of planes, or a full volumetric image.

According to the literature, the following information and/or parameters should be determined before the scanning of a component:

- Type of scanner: The model and make of the X-ray CT scan machine should be determined. One should be certain that the image reconstruction software can translate the data;

- Kind of scan: Axial or helical;

- Slice Thickness: 1.0 mm is recommended;

- Scan spacing: 0.5 mm or at least one-half the smallest dimension of interest;

- X-ray intensity;

- Resolution: Options include image dimensions of 256 x 256, 512 x 512, and 1024 x 1024 pixel and 8,16 or (on some machines) 32 bits/pixel;

- Field of View (FOV): Component imaged should fill the field of view without extending beyond it;

- Position: Long axis of the component should be parallel to the bore of the scanner. Generally, scans should start just off the component and finish off the other side of the component (so that the entire component is imaged). Components to be scanned should not be taped down or placed on similarly dense components, since it will be incorporated into the scan data;

- Artifacts: If significant variations in material densities exist within the component to be scanned, distortion can be experienced. In the case of metal artifacts, the distortion can be severe. The scan protocol can and should be adjusted to take into account the presence of artefacts;

- Slice Time: 2 second/slice is recommended. Images reconstructed at 512 x 512 pixels with a 16-bits/pixel resolution should require about 0.5 Mbytes of memory per slice. According to Haystead (1997), the average data sets can be expected to range from 25 to 100 Mbytes. From the image data, the reconstruction software is then used to extract part contours and/or surfaces, as the case may be. Many thousands of internal and external measurements are quickly generated from the data.

Since penetrating radiation is used, there is no inherent difference between inside and outside, optically hidden or visible. All features in the component are present in the image data and can therefore be extracted by the software with no penalty in scan time. Moreover, internal material defects are captured as well. If they are important, they can also be extracted and characterised. If only a geometrical description of the part is important, defect information can be discarded. The end result is a 3-D virtual model that should be exportable, in different file formats, to allow interfacing with other design environments.

3.7.1.2 Accuracy Issues

The literature shows that accurate measurement of X-ray CT absorption values depends on reproducible reconstruction of attenuation values, which in turn, are a function of the density and composition of a component. Accuracy of the X-ray CT study may be reduced by a number of factors, some of which are inherent of the system. All other structures not present in the component under study that appear in the X-ray CT picture are defined as artifacts. Errors in scanning or data processing can produce streaks or areas of altered density that do not correspond to any real structures in the component. Because of their characteristic appearance, these machine-caused artifacts are generally recognised but might still pose reconstruction difficulties in some cases.

Research by Towson and Hill (1996) states that with good technique and data, X-ray CT scan accuracy generally falls within +/- 20% of the slice data. For a 1 mm slice this would equal +/- 0.2 mm. The skill of the image reconstruction operator and the strength of the mathematical algorithms within the reconstruction software can influence accuracy of the reconstruction considerably.

3.7.2 Neutron Computed Tomography (NCT)

The basic principle of NCT is similar to CT with X-rays. However, unlike X-rays, which interact with the electron cloud, the neutron interaction is not characterised by a rational dependence on the atomic number of the sample material. Therefore, the attenuation coefficients of different elements for neutrons and for X-rays are completely different.

Thermal neutrons and X-rays share the common properties that neither is charged and both have wavelengths comparable with the mean separations of atoms in solids. However, their properties contrast rather than compare in other important aspects. While X-rays interact with the electron cloud surrounding the nucleus of an atom, neutrons interact with the nucleus itself, as depicted in *Figure 3.4* (where atomic number is plotted against mass attenuation coefficient).

In general, as the atomic number increases, X-ray attenuation increases for lower X-ray energies and/or higher density materials. There is no such rule, however, for the attenuation of thermal neutrons, as shown by the scattered points in *Figure 3.4*. Some light elements (e.g. hydrogen and boron) have high thermal neutron attenuation coefficients, while some heavier elements (e.g. lead, iron, chromium, etc.) have relatively smaller attenuation coefficients.

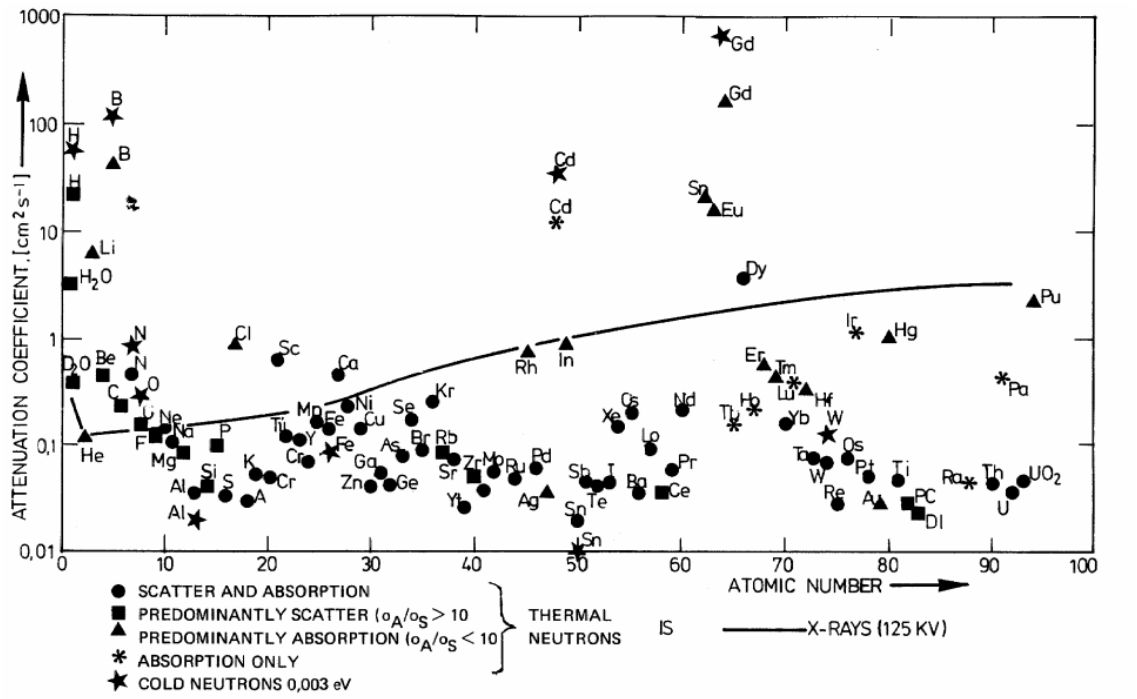

Figure 3.4: *Neutron and X-ray mass attenuation coefficients for the elements [Byrne (1994)].*

This comparison demonstrates that, depending on the materials, which have to be investigated by CT, the proper kind of radiation has to be used, as stated by Byrne (1994). Since neutrons are able to distinguish between different isotopes, NCT in an important tool for the investigation of ferrous materials.

3.7.2.1 GRE Methodology

For a 3-D reconstruction of a component's interior, 2-D transmission images taken from different view angles are required. To obtain these slices, the component is placed between the collimator exit and the detector, all actions being computer-driven, which records a 2-D image. According to the literature, a high-quality 3-D

reconstruction of a sample requires at least 200 2-D transmission images from different view angles of the specimen. This can be realised by putting the sample on a rotary table and by taking images after each rotation step. To accomplish this, the sample to be imaged is placed on a rotating platform, which is rotated using a stepper motor. The stepper motor is controlled using a PC based stepper motor controller card. The image acquisition, processing and sample rotation control programs have been synchronised so that after each image acquisition operation, the sample can be rotated through the desired angle for the next image acquisition. Kak and Slaney (1988) and Russ (1995) stated that good results could be expected by rotating the component in the beam by 180° with 0.9° steps. In this way the entire data acquisition for NCT has been automated.

A typical NCT system set-up consisting of a CCD camera, mirror, neutron screen, rotation and translation stage can be seen in *Figure 3.5*.

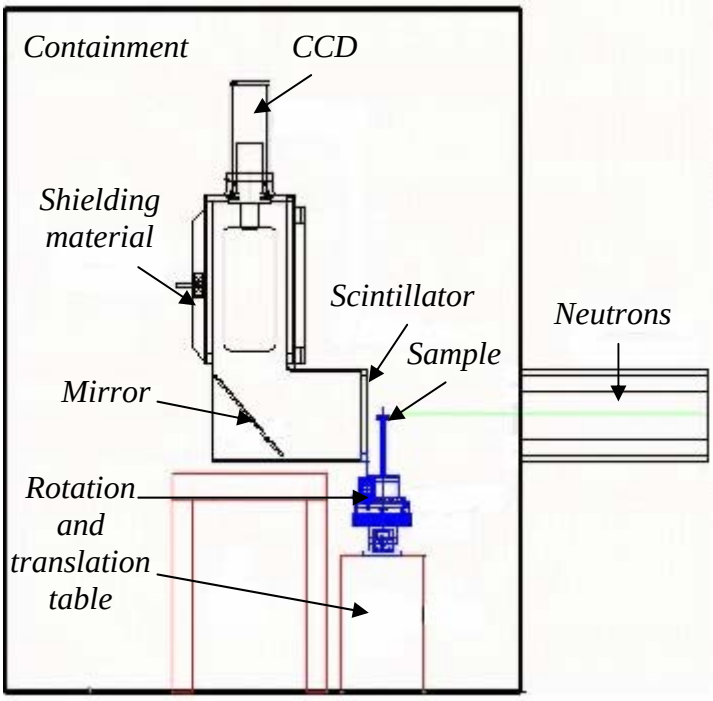

Figure 3.5: *Set-up of the typical NCT system.*

Behind the component is a scintillator screen. The impact of the neutrons on this generates photons (light), which are then reflected by an angled mirror up through a lens to a Peltier CCD device camera, so capturing the images, or radiographs. This image contains information about the composition and structure of the sample

interior, as a result of the interaction of neutrons with matter. The quality of the NCT depends strongly on the number of images from different view angles.

The main advantage of this technique compared to conventional translate-rotate CT is that in the CCD method the only operation required is rotation of the sample and from each projection data set, not only 2-D slice can be constructed but also 3-D information corresponding to different slices can be obtained. This results in considerable saving of data acquisition time.

According to Domanus (1992), NCT provides a very efficient tool in the field of reverse engineering. First results were published by Kobayashi *et al.* (1990), McFarland *et al.* (1991), Rausch *et al.* (1996) and Schillinger *et al.* (1996). However, image processing took so long that routine application was difficult to say the least. Today's standard PC and Unix workstations have become so fast that processing time is not the limiting factor anymore.

Considering the strengths and limitations of the different GRE methods and the attributes of the component to be reverse engineered, the conclusion was made that CT, exploiting the two radiation sources X-rays and neutrons, is the most promising GRE method to reverse engineer the Garrett GT 42 turbine housing.

CHAPTER 4: IMPLEMENTATION OF COMPUTED TOMOGRAPHY (CT)

4.1 Introduction…….p. 38
4.2 X-ray Computed Tomography (X-ray CT)……..p. 38
4.2.1 System Set-up and Characteristics…….....p. 39
4.2.2 Implementation……... p. 39
4.2.3 3-D NURBs Model Generation……...p. 42
4.2.4 Discussion and Conclusions…..…….….p. 44
4.3 Neutron Computed Tomography (NCT)……. p. 45
4.3.1 System Set-up and Characteristics……...……...p. 45
4.3.2 Implementation……...…… p. 48
4.3.3 3-D NURBs Model Generation……...p. 58
4.3.4 Discussion and Conclusions…..……..… p. 61

4.1 Introduction

Based on the evaluation results obtained in *Chapter 3,* Computed Tomography (CT) was implemented as the most promising GRE method to reverse engineer the Garrett GT 42 turbine housing to create a 3-D NURBs model for mould production purposes. An attempt was made to successfully complete the two phases of the GRE process by applying the following radiation sources:

- *X-ray Computed Tomography (X-ray CT)*;
- *Neutron Computed Tomography (NCT).*

4.2 X-ray Computed Tomography (X-ray CT)

Millpark Hospital, located in Johannesburg, had previous experience in the GRE application of medical X-ray technology and offered assistance in applying X-ray CT to this reverse engineering problem.

4.2.1 System Set-up and Characteristics

A *Philips® TomoScan™ AV* spiral scanner regularly does X-ray CT at the hospital with *TomoVision®'s Slice-O-Matic™* 3-D modelling software inspecting and reconstructing the raw CT data into 3-D polygonal models for medical display purposes. Unfortunately, the internal component set-up and characteristics of the *Philips® TomoScan™ AV* spiral scanner are trade secrets and can therefore not be presented and discussed, however, it is known that the scanner in question is equipped with a copper (Cu) anode and operates at an X-ray intensity of 175 kV and 250 mA.

4.2.2 Implementation

The turbine housing was placed in the scanner where a patient's head would normally be situated in a medical application. Before scanning commenced, 2-D radiographs in three different orientations were taken to ensure that optimum CT presentation results could be obtained [*Figure 4.1(a), (b) and (c)*].

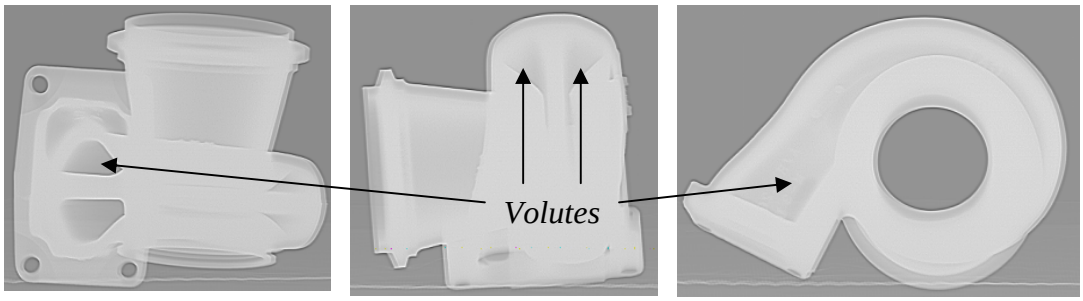

(a) *(b)* *(c)*

Figure 4.1: *2-D X-ray radiographs of the Garrett GT 42 turbine housing in three different orientations.*

The turbine housing's external geometry, which consists of the three aforementioned sub-components, could clearly be identified [*Figure 4.1(a) and (b)*]. However, the integration between the respective sub-components was not distinguishable. In spite of the fact that most of the profile edges were blurred, some internal profiles, including the volutes, were visible to a reasonable extent [*Figure 4.1(c)*].

Three axial scans were performed in the orientations displayed in *Figure 4.2(a)*, *Figure 4.3(a)* and *Figure 4.4(a)*. A slice thickness of 1 mm with a scan spacing of 0.5 mm was selected for all of the scans.

A total of 242 X-ray CT slices were acquired. Some 2-D images were obtained for illustration purposes, which are displayed at 10 slice intervals in *Figure 4.2(b-f)*, *Figure 4.3(b-f)* and *Figure 4.4(b-f)*. This was achieved by importing the raw CT data into the *Osiris 4™* shareware software and manipulating the data to obtain the desired visual effect. Instructions on viewing the different X-ray CT animations, which are available on the Compact Disk (CD) attached, are discussed in *APPENDIX D*.

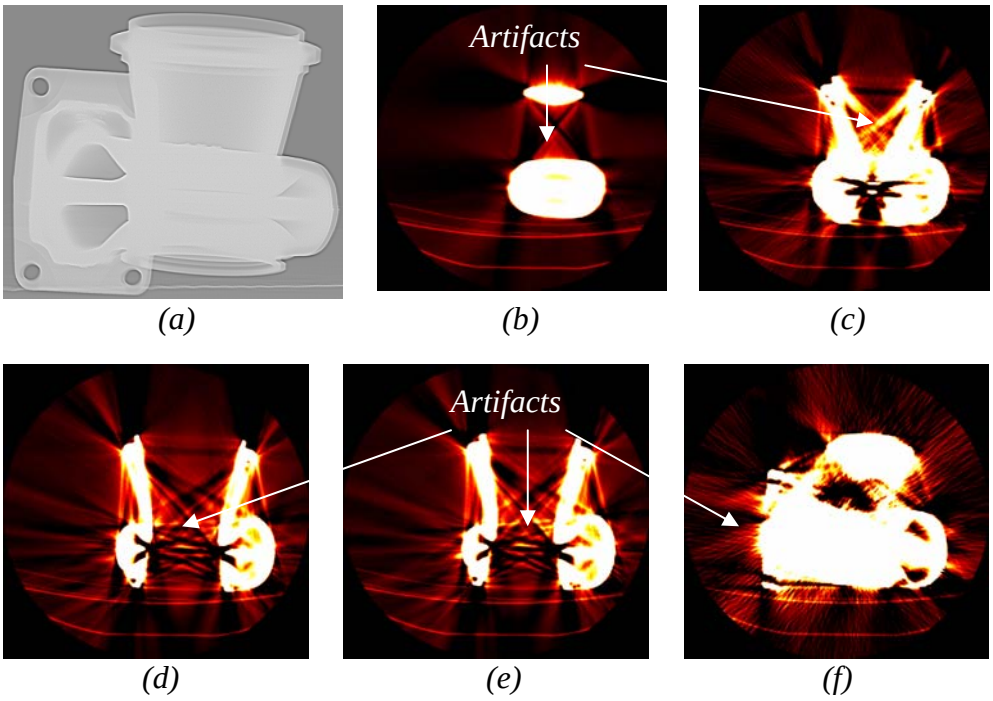

Figure 4.2: *2-D images of the first X-ray CT orientation as displayed by Osiris 4™.*

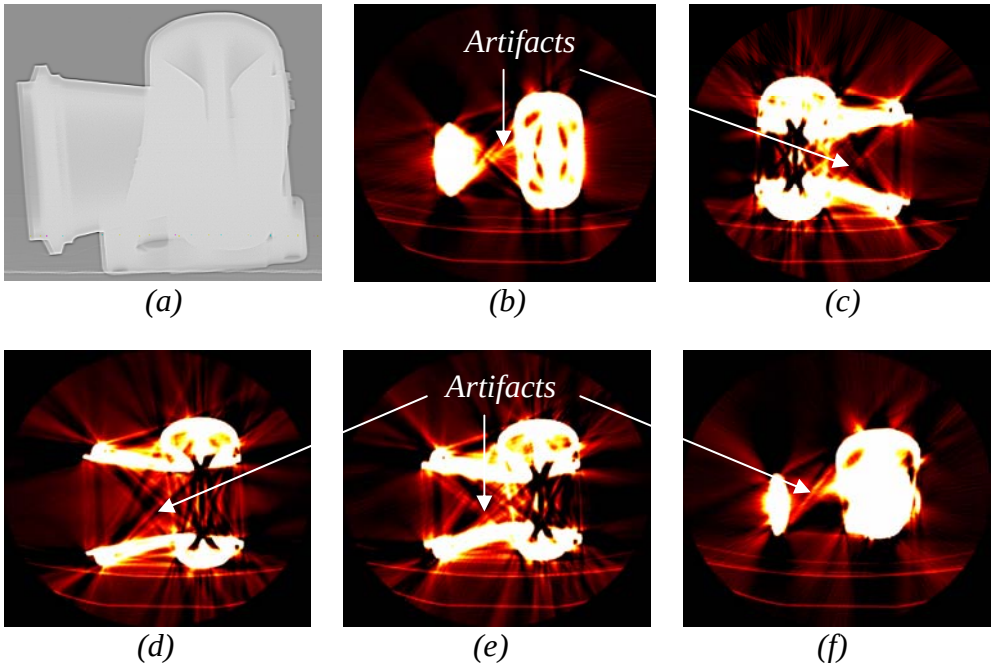

Figure 4.3: *2-D images of the second X-ray CT orientation as displayed by Osiris 4™.*

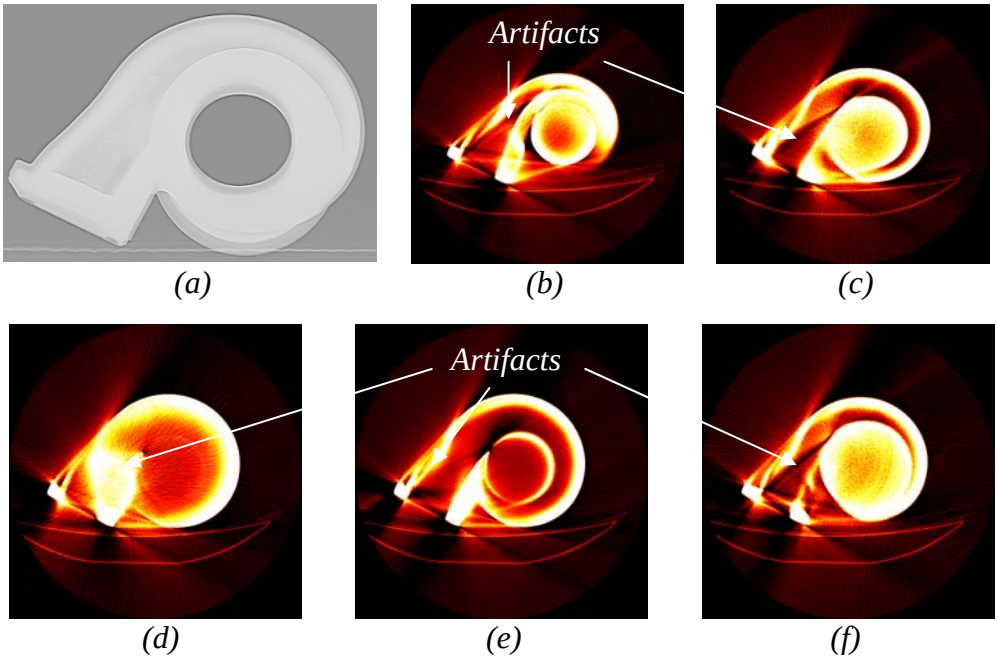

Figure 4.4: *2-D images of the third X-ray CT orientation as displayed by Osiris 4™.*

Although both external and internal profiles of the turbine housing could be identified to a reasonable extent, X-ray CT scanning irregularities, also known as artifacts, were present in all of the images. Originally, the severe density of the spheroidal ductile cast iron was thought to have caused the artifacts. However, the most probable cause was probably due to the fact that Cu-radiation gave rise to secondary florescence, a phenomenon known to take place when samples containing iron are irradiated with Cu, resulting in the scattering of X-rays in space.

Studies by Towson and Hill (1996) showed that in the case of severe artifacts in the area of interest, as with this case, the X-ray intensity must be maximised in order to reduce the effect of the artifacts. They also stated that slice thickness is important when a metal artifact is present. The slice thickness would depend on the amount of signal noise in the slice as opposed to spatial accuracy and to allow for the distortion, the slice thickness may vary from 1 mm to 4 mm depending on the spacing.

Since the internal component set-up and properties of the *Philips® TomoScan™ AV* spiral scanner are trade secrets, they could not be analysed to find a probable cause or solution for the amount of artifacts experienced.

Threshold, filter and window settings also influenced the quality of the CT results but could not be optimised and evaluated, as the scanner had to be made available for medical purposes. Although not always practical, the simplest solution was to remove the object causing the artifacts, which was impossible in this case.

4.2.3 3-D NURBs Model Generation

4.2.3.1 3-D Modelling Software

The raw CT data was imported into the *Slice-O-Matic™* 3-D modelling software, which was used to generate a 3-D polygonal model by manipulating the contour data taken directly from the X-ray CT data sets. Screenshot images of the manipulation process within the *Slice-O-Matic™* software are displayed in different orientations in *Figure 4.5*, with the resulting 3-D polygonal model displayed in *Figure 4.6*.

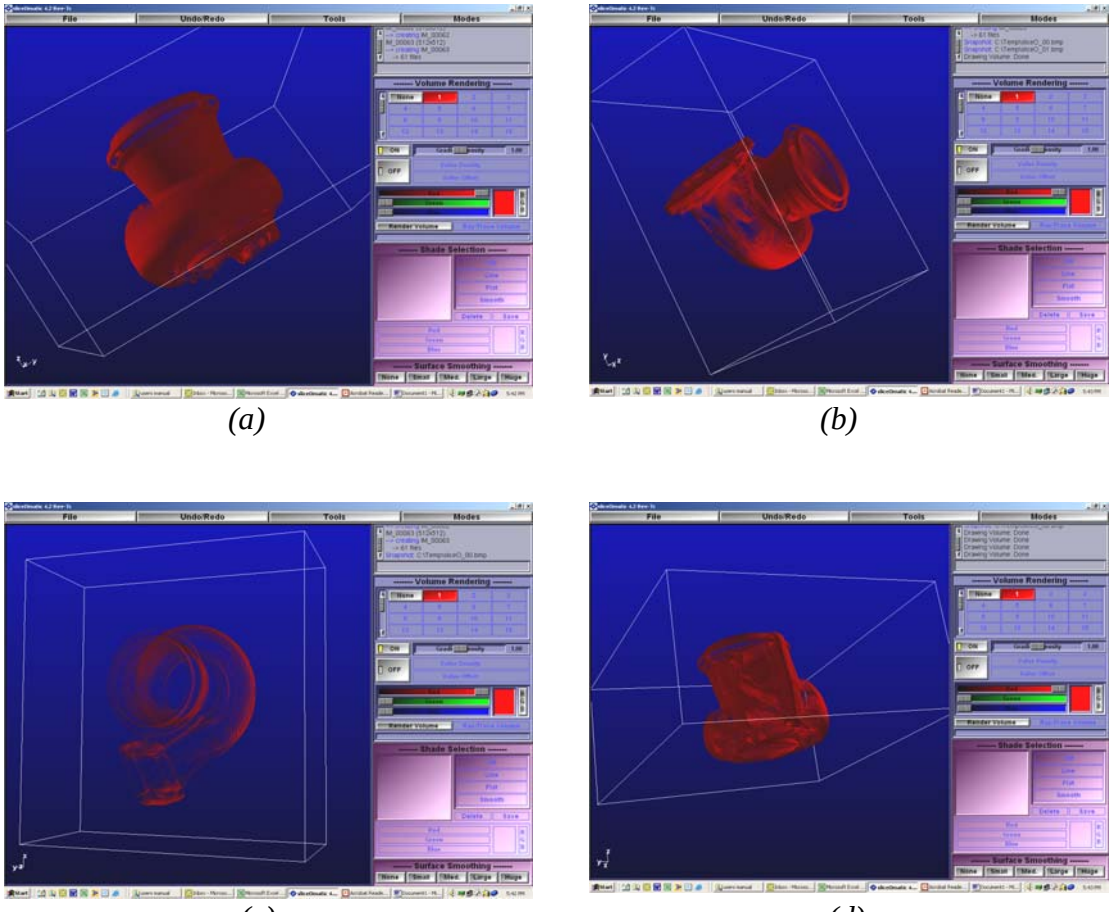

(a) *(b)*

(c) *(d)*

Figure 4.5: *Screenshot images of the 3-D polygonal model in different orientations within the Slice-O-Matic™ software.*

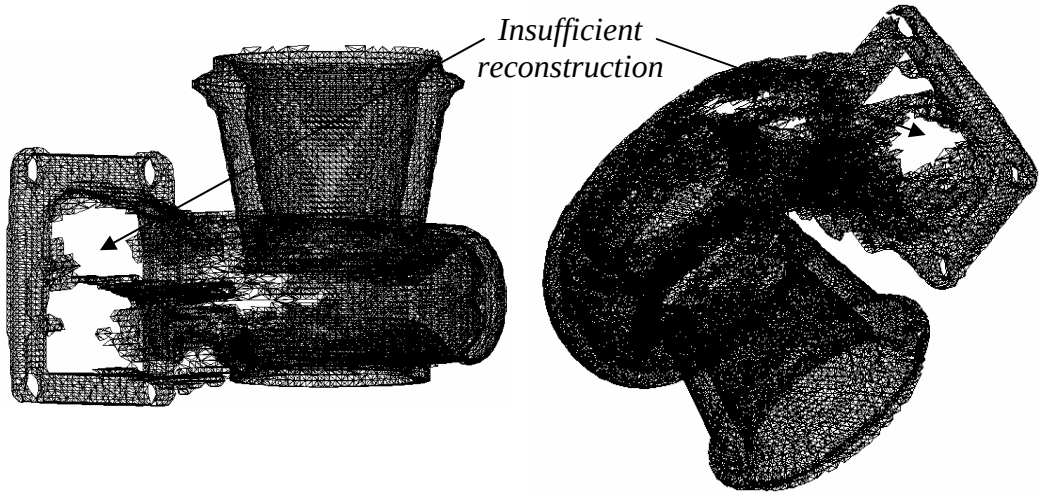

(a) *(b)*

Figure 4.6: *Top (a) and isometric (b) views of the Garrett GT 42 turbine housing's 3-D polygonal model within the Slice-O-Matic™ software.*

Visually, the 3-D polygonal model represented the actual turbine housing quite well, but the amount of artifacts generated proved to be more of a problem than originally anticipated. Although the three aforementioned sub-components could be identified, the data manipulation and reconstruction process was unsuccessful, leaving holes in the 3-D polygonal model. The insufficient reconstruction indicated that the manipulation of data in this fashion was useless, as a direct transfer of this 3-D polygonal model to a GRE and/or CAD software would not be sufficient for mould production purposes. An alternative method was required to salvage and manipulate some of the acquired CT data into a usable 3-D NURBs model.

4.2.3.2 CAD Modelling Software

By using a CAD modelling software package and the 2-D X-ray CT images as contour input data, the generation of a 3-D NURBs model to be used in mould production was attempted. A problem that arose was the fact that the scanning equipment's computer stored the X-ray CT information on an optical disc of up to four gigabytes in size. Few computer workstations could read this optical disc, which meant that the information could not be further evaluated with the available facilities and was therefore transferred from the optical disc to a CD.

The transferred 2-D X-ray CT images were simply a collection of pixels and could therefore not be implemented directly into modern vector based CAD modelling software, requiring enhancement prior to implementation. One solution attempted was to use commercial computer software packages *Adobe's*® *CorelDRAW 9*™, *CorelPHOTO-PAINT 9*™ and *CorelTRACE 9*™ to manipulate the 2-D images.

CorelPHOTO-PAINT 9™ was used on the early processing of image filtering and edge detection. In *CorelDRAW 9*™, a number of operations such as orientating the images, removing unwanted areas from images, sharpening edges, extracting edges from the images, etc. were applied to try to enhance the 2-D images previously obtained [*Figure 4.7(b)*]. Pre-processed bitmap images were converted into 2-D line drawings (i.e. dxf format) by tracing the outlying edges with *CorelTRACE 9*™ [*Figure 4.7(c)*].

(a) *(b)* *(c)*

***Figure 4.7**: Example of the 2-D X-ray CT image conversion process into a 2-D line drawing with Adobe® software.*

Unfortunately, the artifacts in the X-ray CT slices were so severe that the tracing of the 2-D X-ray CT images did not produce accurate 2-D line drawings. Discontinuous outlines representing the internal and external profiles could barely be identified, as displayed in *Figure 4.7(c)*. The next step of importing the 2-D line drawings into CAD modelling software, to be converted into NURBs and ultimately a 3-D NURBs model, could not be completed.

4.2.4 Discussion and Conclusions

Although the presence of metal artifacts (caused by iron in the turbine housing's material matrix) hampered the generation a complete 3-D NURBs model of the

Garrett GT 42 turbine housing, medical X-ray CT is an accurate and valuable GRE method. However, caution should be taken in the selection of the correct threshold, filter and window settings to ensure that the optimum scanning results are obtained.

4.3 Neutron Computed Tomography (NCT)

The South African Nuclear Energy Corporation (NECSA) at Pelindaba, west of Pretoria, offered assistance in applying NCT to this reverse engineering problem, using a neutron source generated within the SAFARI-1 nuclear research reactor.

4.3.1 System Set-up and Characteristics

A portion of the total number of neutrons generated in the SAFARI-1 nuclear reactor's core through the fission of enriched uranium are released through a small hatch, known as a beam port, set into the reactor's containment wall. When the beam port is opened, the neutrons are emitted and passed through a collimator system to direct them to travel in a straight line, which is essential for the effective NCT process. The number of neutrons can be regulated by means of a beam shutter system with different settings, but the maximum neutron flux is usually used as it reduces the time required for a NCT. The maximum neutron flux at SAFARI-1 is 107 neutrons/cm^2/sec for an approximate scanning time of 20 minutes through 180° with a beam diameter of 300 mm.

Exposure time per frame ranges from two seconds to 300 seconds, and in some instances the longer the exposure, the higher the resolution. Depending on the type of sample, the spatial resolution is in the order of 100 µm. Samples of dimensions of up to 250 mm × 250 mm, and a weight of up to 25 kg, can be accommodated.

A schematic of the NCT system set-up for the SAFARI-1 reactor is shown in *Figure 4.8* with the major system component descriptions and characteristics presented in *Table 4.1*.

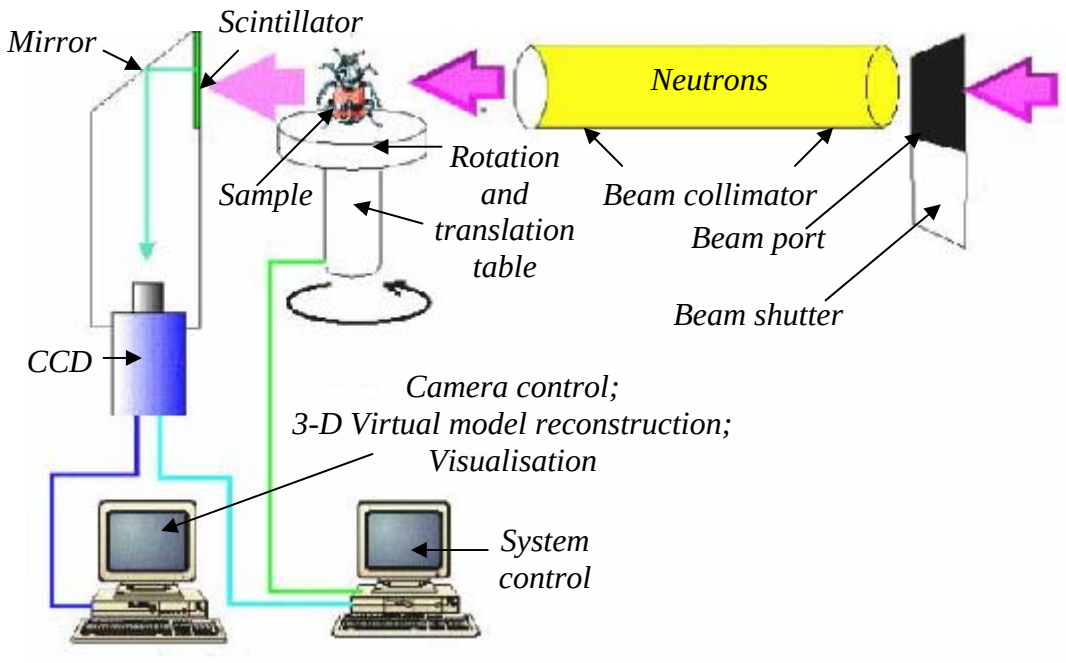

***Figure 4.8**: A simplified layout of the NCT set-up for the SAFARI-1 reactor.*

***Table 4.1:** NCT system component descriptions and characteristics.*

Description	***Characteristics***
Light Tight Box	Manufactured by Swiss Company
Thermal Neutron Scintillator Screen:	
Model	AST *(UK)*
Size	250 mm x 250 mm
Intrinsic Resolution	100 µm
Spatial Resolution	0.4 mm
Peak Wavelength for Thermal Neutrons	450 µm
Camera:	
Model	DV 434 from *ANDOR*® Technology
Pixel Array	1024 x 1024
Pixel Size	13 µm
Cooling	Peltier: Air to ~ -50ºC
Quantum Efficiency at 450 nm	~ 80%
Lenses:	
Types	*PENTAX*™ 50 mm, F 1.2 100 mm, F 2.8 135 mm, F 2.8
Field of View *(FOV)*	90 mm, 130 mm, 250 mm

As for the neutron beam itself, it is stopped by the beam-stop, a rail-mounted multi-layered door more than a meter thick, which also acts as part of the radiological shielding of the NCT chamber [*Figure 4.9*]. The beam port cannot be opened unless the beam-stop door is firmly closed, thus making the process of NCT intrinsically safe.

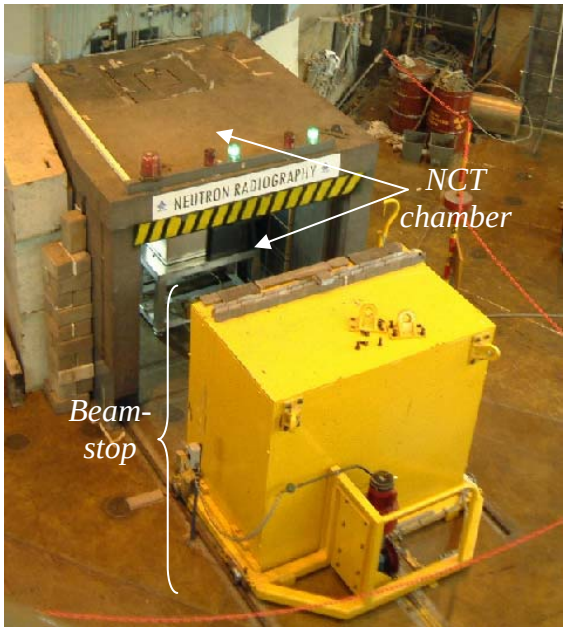

Figure 4.9: *Photographic image of the NCT system's beam-stop at SAFARI-1.*

As with any nuclear operation, actions have to be done remote controlled, with the actions at SAFARI-1 controlled from the hart of the NCT facility, the system control room [*Figure 4.10*].

Figure 4.10: *Photographic image of the NCT system control room at SAFARI-1.*

Several software packages are used to operate and manipulate the NCT system from the control room. Each aspect of the system runs on a different software program i.e.:

(i) *LabView™* computer software: Used for mechanical manipulation of the rotation and translation table;

(ii) *ANDOR®* CCD camera software: Used for image capture;

(iii) *IDL®* 3-D modelling software: Used for 3-D polygonal model reconstruction;

(iv) *VG-Studio® 1.1* 3-D rendering software: Used to display 3-D polygonal models.

4.3.2 Implementation

Before scanning commenced, the NCT system was calibrated and correctly set-up using the following procedure:

- The rotation and translation table was adjusted according to the turbine housing's proposed orientation;
- The neutron source was activated by opening the reactor's beam shutter;
- The complete dynamic reach of the detection system-greyscales was acquired without the turbine housing, to set a reference.

After the calibration and system set-up was completed, the Garret GT 40* turbine housing [*Figure 4.11*] was placed in front of a collimated beam of neutrons and subjected to a neutron flux of 107 neutrons/cm^2/sec in two exposure orientations. This was done to ensure that optimum NCT presentation results of the internal profile could be obtained. Some neutrons were attenuated by the elements in the turbine housing as the beam passed through. The remaining neutrons were collected at the imaging plane. The results were two negative 2-D images of the turbine housing, with the lighter areas indicating the greatest neutron attenuation and the darker areas indicating the least neutron attenuation [*Figure 4.12(a) and (b)*]. The images were

** Due to the tight PBMM plant completion schedule, the Garrett GT 42 turbine housing was unavailable for the implementation of NCT. An alternative test subject in the form of the Garrett GT 40 turbine housing was allocated. The basic GRE attributes of both housings were similar and minor differences in geometry did not influence the methodology required to complete the research adequately.*

created through exposing high-resolution photographic film by means of a gadolinium converter screen.

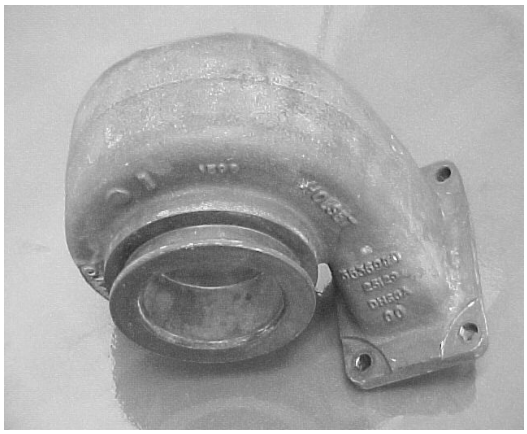

Figure 4.11: *External photographic image of the Garrett GT 40 turbine housing.*

The 2-D neutron radiograph of the turbine housing in an orientation perpendicular to the axial-axis is displayed in *Figure 4.12(a)*, with *Figure 4.12(b)* displaying the 2-D neutron radiograph of the turbine housing in an orientation parallel to the axial-axis.

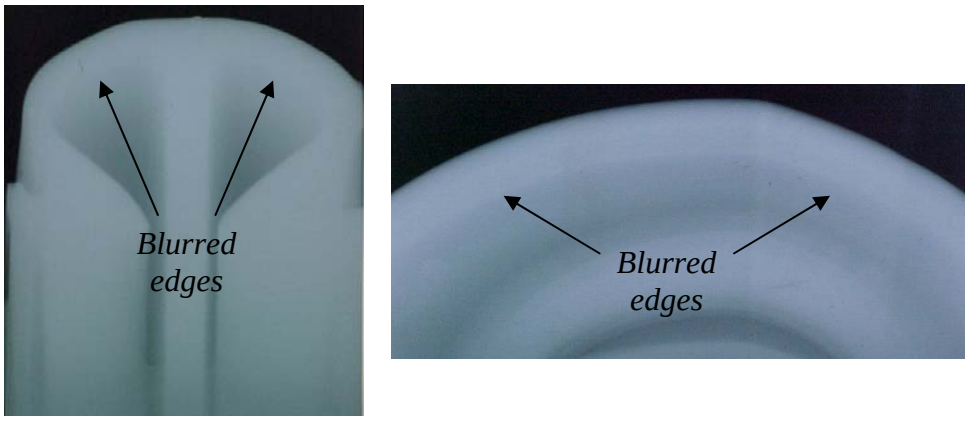

(a) *(b)*

Figure 4.12: *2-D neutron radiographs of the Garrett GT 42 turbine housing's perpendicular (a) and parallel (b) orientations.*

In *Figure 4.12*, the blurred edges of the turbine housing's volutes can be identified. It was thought that the substantial material thickness, density and curvature of the profiles caused the limited visual access. Although the 2-D radiographs were not sufficient to accurately describe the turbine housing's internal profile and the volutes were only visible to a certain extent, further NCT was attempted.

4.3.2.1 NCT at a Rotational Angle of One Degree

The turbine housing was placed on the rotating table in the orientation displayed by the 2-D projection in *Figure 4.13(a)*. The rotating table was set to rotate 1º after each projection using the *LabView™* computer software package. A total number of 180, 2-D radiographic projections were obtained using the *ANDOR®* Charged Couple Device (CCD) camera software. 2-D radiographic projections taken at 60º intervals are presented in *Figure 4.13(b-f)* for illustration purposes. Instructions on viewing the NCT animations at this orientation and settings, which are available on the CD attached, are discussed in *APPENDIX D*.

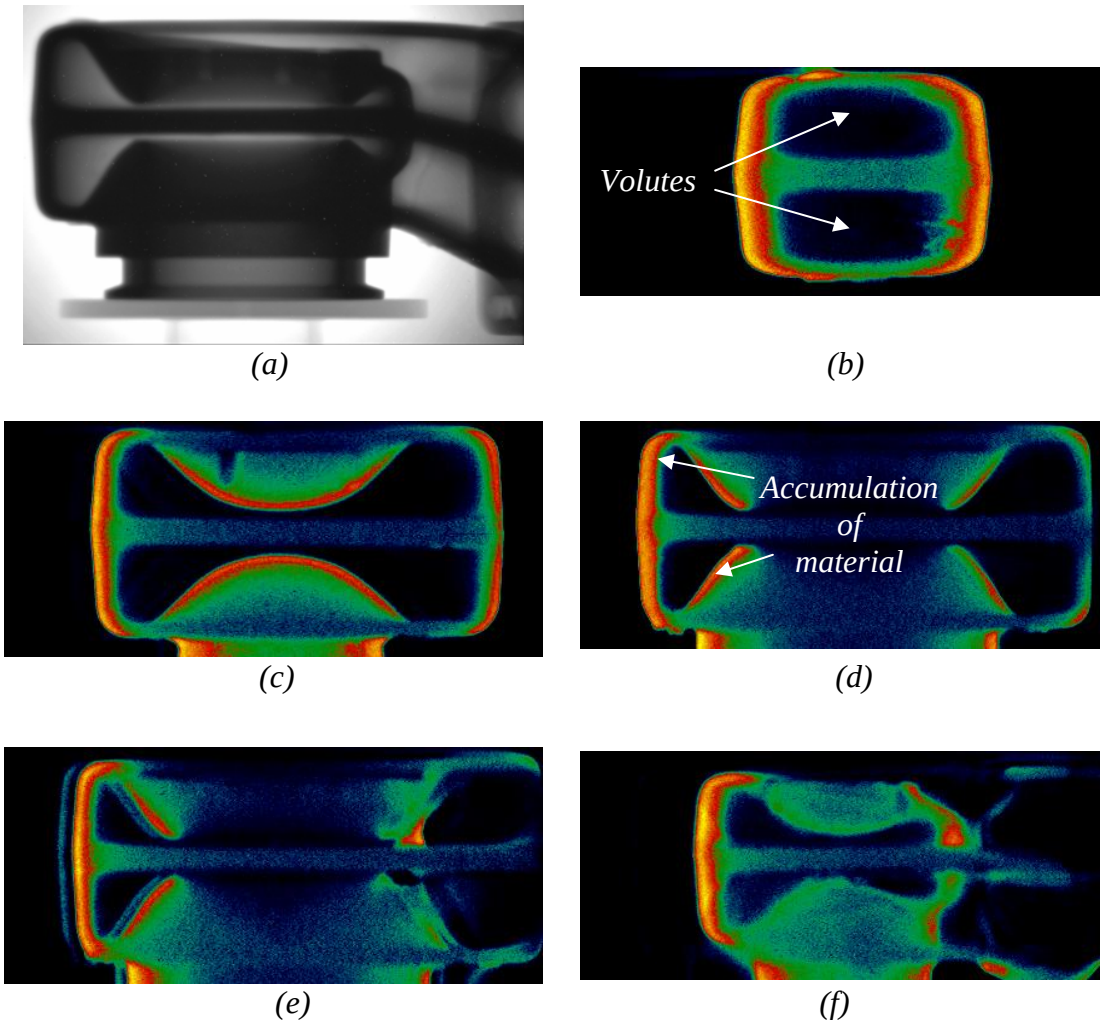

Figure 4.13: *2-D neutron radiographic projections at a 1º rotation angle.*

The internal geometry of the turbine housing, which consists of the two volutes, can be identified to a reasonable extent as displayed in *Figure 4.13(a)*. The integration between the respective sub-components can however not be distinguished clearly due

to the substantial thickness and density of the material as well as the curvature of the free-form profile.

Figure 4.13(b-f) show that the transition from the turbine housing's material to the surrounding air could not easily be distinguished. It should also be noted that the closer the colour within the 2-D neutron radiographic projections images tends towards the red side of the colour spectrum, the greater the projection thickness of the material becomes and visa versa.

The 2-D neutron radiographic projections were imported into *IDL*® 3-D modelling software. The integrated manipulation functions were used to generate a 3-D polygonal model of the turbine housing. The 3-D polygonal model was transferred to *VG-Studio*® *1.1* for display purposes [*Figure 4.14*].

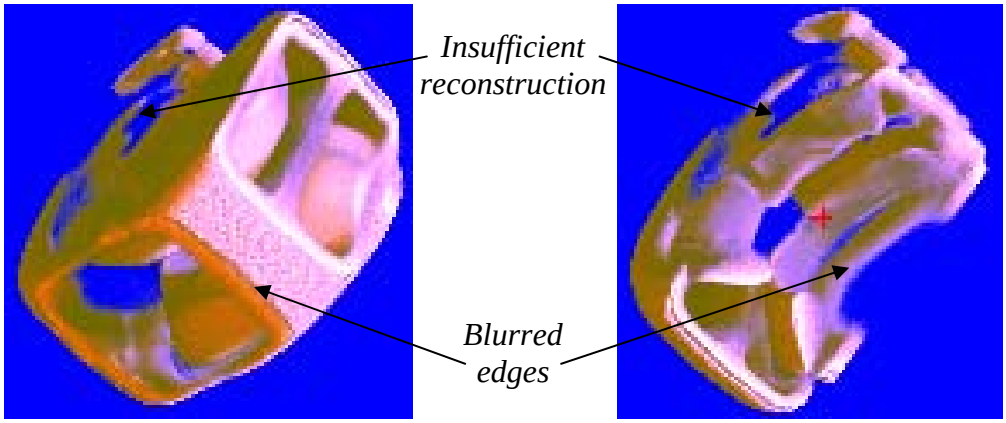

Figure 4.14: *The Garrett GT 40 turbine housing's 3-D polygonal model as visualised by VG-Studio® 1.1 at 1º rotation angle.*

The reconstructed 3-D polygonal model was sliced at arbitrary angles and cross sections to determine the quality of the internal profile reconstruction. The internal profile was reconstructed with relative success. Insufficient reconstruction of the exhaust gas inlet could however be identified by visually comparing the reconstructed 3-D polygonal model with the original turbine housing. Identifying definite edges of the component was almost impossible, as the edges appeared blurred. Alterations to the NCT set-up were made to try to improve the quality of the 2-D radiographic projections and ultimately the 3-D polygonal model reconstruction.

4.3.2.2 NCT at a Rotational Angle of 0.6 Degrees

The same orientation [*Figure 4.15(a)*] was used for the second scanning of the turbine housing. The rotating table, however, was set to rotate 0.6º after each projection using *LabView™* computer software package. A total number of 300, 2-D radiographic projections were obtained using the *ANDOR®* Charged Couple Device (CCD) camera software. 2-D radiographic projections taken at 40º intervals are presented in *Figure 4.15(b-f)* for illustration purposes. Instructions on viewing the NCT animations at this orientation and settings, which are available on the CD attached, are discussed in *APPENDIX D*.

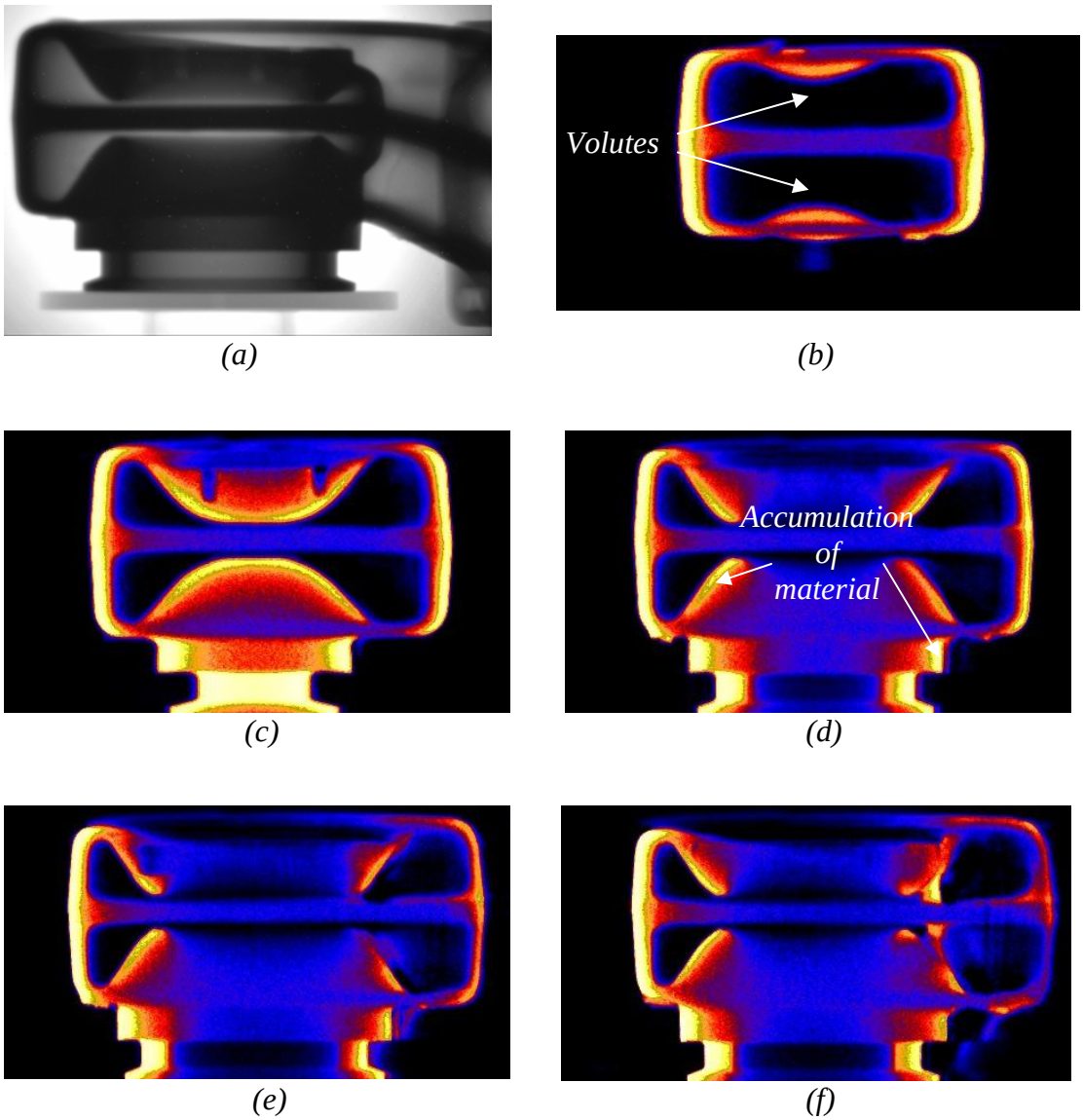

Figure 4.15: *2-D neutron radiographic projections at a 0.6º rotation angle.*

The internal geometry of the turbine housing could be identified to a certain extent, with the integration between the respective sub-components still not distinguishable, as was the case with the previous attempt.

The same colour interpretation with regard to the projection thickness still applied i.e. a red colour indicates an accumulation of material with a bluish colour indicating a lesser projection density. A definite transition from material to surrounding air could still not be identified.

The 2-D neutron radiographic projections were again imported into *IDL*® 3-D modelling software. The integrated manipulation functions were used to generate the 3-D polygonal model of the turbine housing. The 3-D polygonal model was transferred to *VG-Studio*® *1.1* for display purposes [*Figure 4.16*].

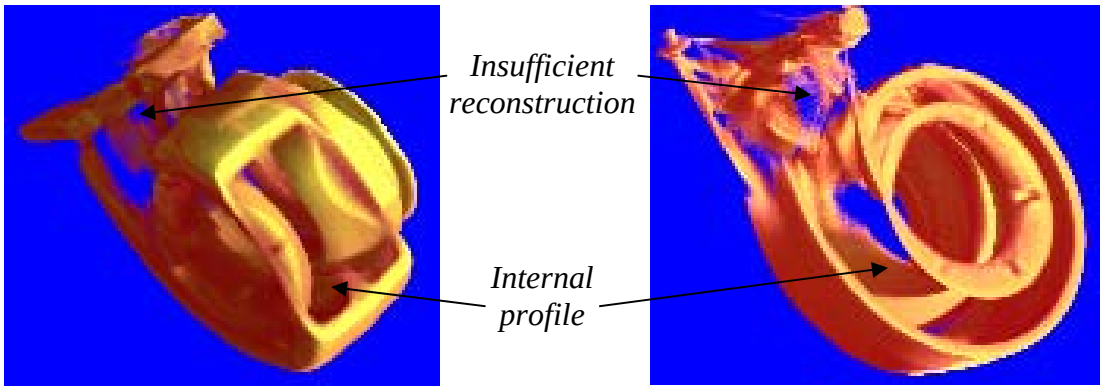

Figure 4.16: *The Garrett GT 40 turbine housing's 3-D polygonal model as visualised by VG-Studio® 1.1 at 0.6º rotation angle.*

The reconstructed 3-D polygonal model was again sliced at arbitrary angles and cross sections to determine the quality of the internal profile reconstruction. The reconstruction of the internal profile was significantly better than the original NCT attempt. The sharpness of the model was better as well. Insufficient reconstruction of the exhaust gas inlet could however still be identified by visually comparing the reconstructed 3-D polygonal model with the original turbine housing. Final alterations were made to the NCT set-up to try to improve the quality of the 2-D radiographic projections and ultimately the 3-D polygonal model.

4.3.2.3 NCT at a Minimum Material Orientation with a Longer Exposure Time

For the third scanning, the turbine housing was placed in an orientation that would result in the minimum material accumulation and moved closer to the sintillator screen [*Figure 4.17*].

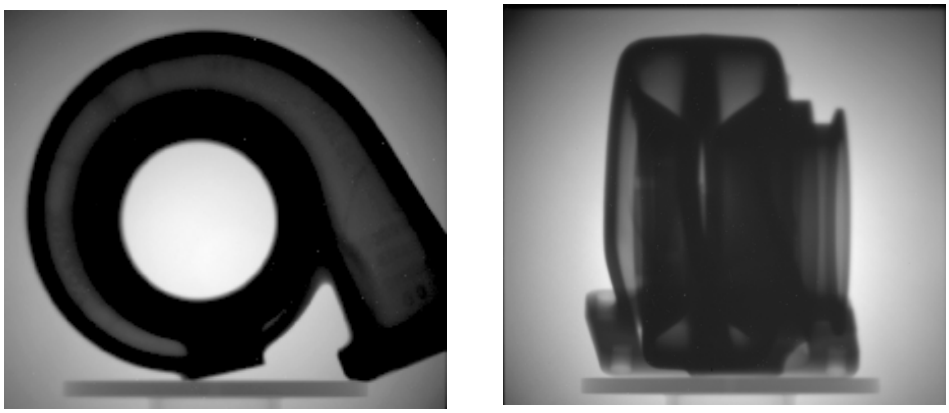

(a) *(b)*

Figure 4.17: *The Garret GT 40 turbine housing at a minimum material orientation.*

The rotating table was set to rotate 0.6º after each projection using the *LabView™* computer software package. A total number of 300, 2-D radiographic projections were obtained using the *ANDOR®* Charged Couple Device (CCD) camera software at a longer exposure time. 2-D radiographic projections taken at 80º intervals are presented in *Figure 4.18* for illustration purposes. Instructions on viewing the NCT animations at this orientation and settings, which are available on the CD attached, are discussed in *APPENDIX D*.

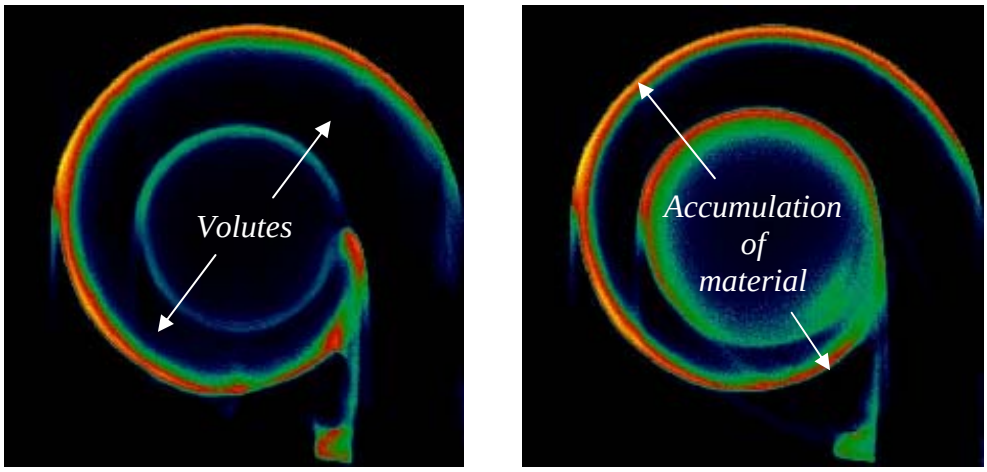

(a) *(b)*

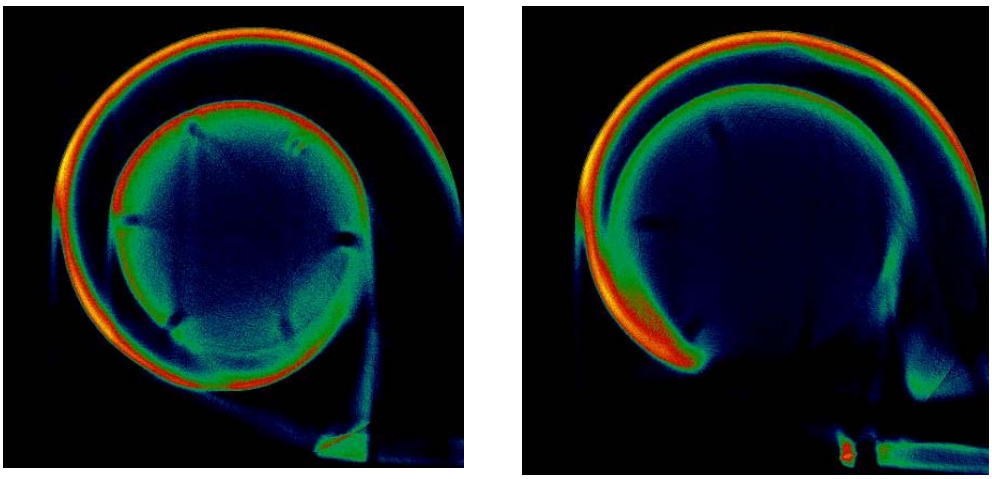

(c) *(d)*

Figure 4.18: *2-D neutron radiographic projections at a 0.6º rotation angle and a minimum material orientation.*

Even with additional adjustments, a definite internal profile could not be identified. A decrease in material accumulation was however noticed, as indicated by the decrease in the amount of red within the 2-D neutron radiographic projections.

The 2-D neutron radiographic projections were again imported into *IDL*® 3-D modelling software. The integrated manipulation functions were used to generate the 3-D polygonal model of the turbine housing. The 3-D polygonal model was transferred to *VG-Studio*® *1.1* for display purposes [*Figure 4.19*].

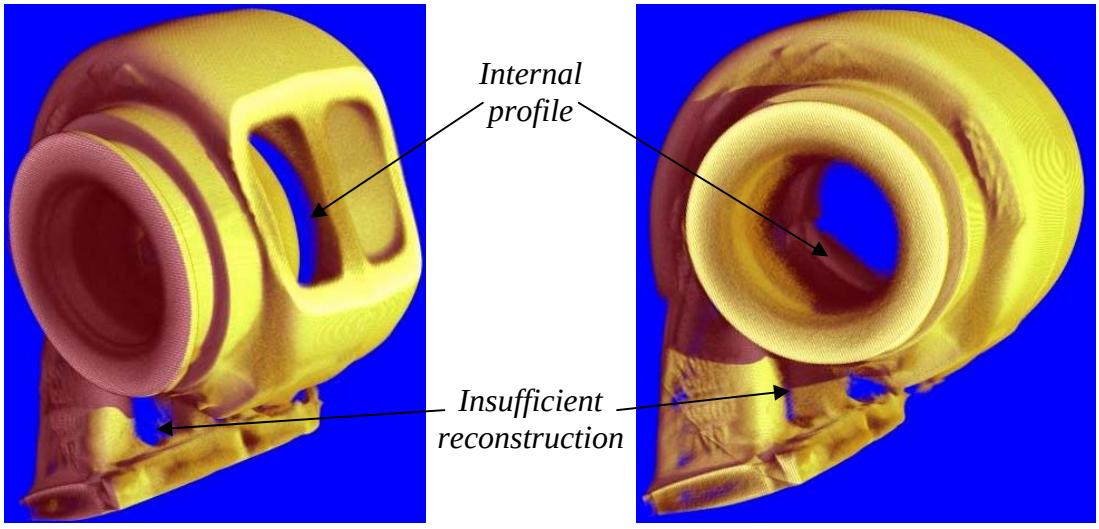

(a) *(b)*

Figure 4.19: *The Garrett GT 40 turbine housing's 3-D polygonal model as visualised by VG-Studio*® *1.1 at a minimum material orientation and a longer exposure time.*

The reconstructed 3-D polygonal model was sliced at arbitrary angles and cross sections for a final time to determine the quality of the internal profile reconstruction. Although not satisfactory, a significant improvement in the reconstruction of the internal profiles and exhaust gas inlet was noticed.

In general, scattered neutrons made up the largest part of the detected signal, so much so that some shapes of e.g. the step wedge were not imaged correctly in all of the attempts. The cloud of scattered neutrons might have lead to missing information in those regions and can be seen in the reconstructed slices as blurred contours [*Figure 4.13, Figure 4.15 and Figure 4.18*].

The reason for the limited success even after three attempts can be attributed to a number of reasons, one being the limited neutron beam diameter of 300 mm. At some rotating angles, the turbine housing moved out of the neutron reach and no data could be acquired. The major reason however was thought to be the material composition of the Garrett GT 40 turbine housing.

- *Irregularities and recommendations regarding the scanning of spheroidal ductile cast iron with NCT.*

De Beer (2003) stated that spheroidal ductile cast iron is by no means very transparent for neutrons and the limit for thermal NCT is usually in the order of a few centimetres (five to six, depending on the alloy) of the total penetration thickness. De Beer (2003) also stated that spheroidal ductile cast iron scattered neutrons quite badly and that there could have been quite an influence mainly in the regions of the component where neutrons had to pass through thick material layers, which mainly depended on the component's dimensions. According to De Beer (2003), for large components made from iron or nickel based alloys, the effect of the scattered neutrons has the most detrimental effect on the NCT results.

A possible solution, according to Schillinger *et al.* (1996), was to reduce the influence of scattered neutrons by increasing the distance between the component and scintillator plane (at the expense of image sharpness) or to use some neutron collimator between sample and detector, which would eliminate the cloud of scattered

neutrons. Schillinger *et al.* (1996) stated that aluminium honeycomb with small channels and the channel walls covered with a thin layer of gadolinium painting, would have been a good choice for the collimator. Unfortunately, this option was not available at SAFARI-1.

He also recommended that for small components, the distance between the component and the scintillator should be no less than five centimetres and preferably more for bigger components in order to keep the scattered neutron part small. This meant that a very well collimated beam was required to be able to increase the component-detector distance while well-defined images were still obtained. A linear neutron accelerator would have to be used if insufficient NCT results were still acquired. However, this was not available at SAFARI-1.

- *Irregularities with the 3-D polygonal model reconstruction from NCT data*

In *VG-Studio® 1.1*, the data obtained were converted to a triangular surface mesh, also called a 3-D polygonal model. The 3-D polygonal model consisted of several million triangles covering the component's surface. Unfortunately, the rendered 3-D polygonal model could only be viewed with *VG-Studio® 1.1* and a usable 3-D NURBs model could not be generated. *VG-Studio® 1.1* did not accommodate a direct transfer of the 3-D polygonal model to GRE or CAD modelling software.

VG-Studio® is available in two different sizes and prices. The version at SAFARI-1 is the standard 3-D rendering package (*VG-Studio® 1.1*) with all necessary functions for the visualisation of 3-D polygonal models. *VG-Studio® MAX*, the updated and more expensive version, is capable of importing and even generating 3-D NURBs models as well as exporting file formats compatible with additional CAD/CAM software. *VG-Studio® MAX* was unfortunately not available.

A similar approach that was used on the manipulation of the X-ray CT data for implementation into CAD modelling software was attempted to generate a 3-D NURBs model from the 2-D NCT slice data.

4.3.3 3-D NURBs Model Generation

The stack of unorganised 2-D line drawings as displayed in *Figure 4.20* clearly illustrates that the *Adobe's® CorelTRACE 9™* option, as with the X-ray attempt, did not provide sufficient input data for implementation into CAD modelling software either.

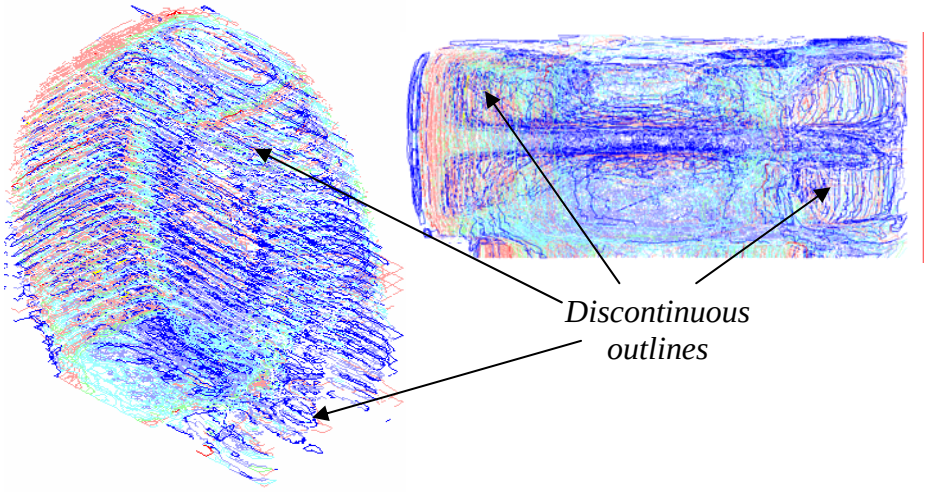

(a) *(b)*

Figure 4.20: *2-D line drawings with CorelTRACE 9™ imported into CAD modelling software, in different display orientations.*

As an alternative, the 2-D NCT slices were traced by hand, estimating the transition between metal and air. This tracing by hand technique was applied to every tenth NCT slice to obtain a series of 2-D line drawings [*Figure 4.21*].

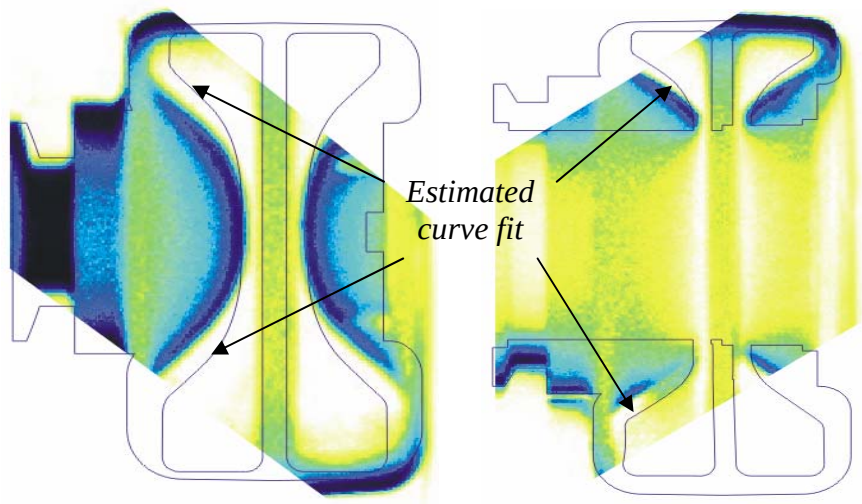

(a) *(b)*

Figure 4.21: *Examples of 2-D bitmap images converted into 2-D line drawings with the tracing by hand approach.*

The accuracy could however not be guaranteed as estimations on curvature fits were made.

The 2-D line drawings were then transferred into the CAD modelling software [*CADKEY® V21*, distributed by *MECAD™*, South Africa] as the input for the 3-D NURBs model reconstruction. *CADKEY® V21*, which uses NURBs to define and create 3-D NURBs models, did not recognise 2-D line drawing as a model generation module. This meant that the 2-D line drawings had to be converted into NURBs within *CADKEY® V21*. The transferring and NURBs fitting of the 2-D line drawings within *CADKEY® V21* are discussed in *APPENDIX E*.

The resulting stacking of these NURBs contours is presented in *Figure 4.22*.

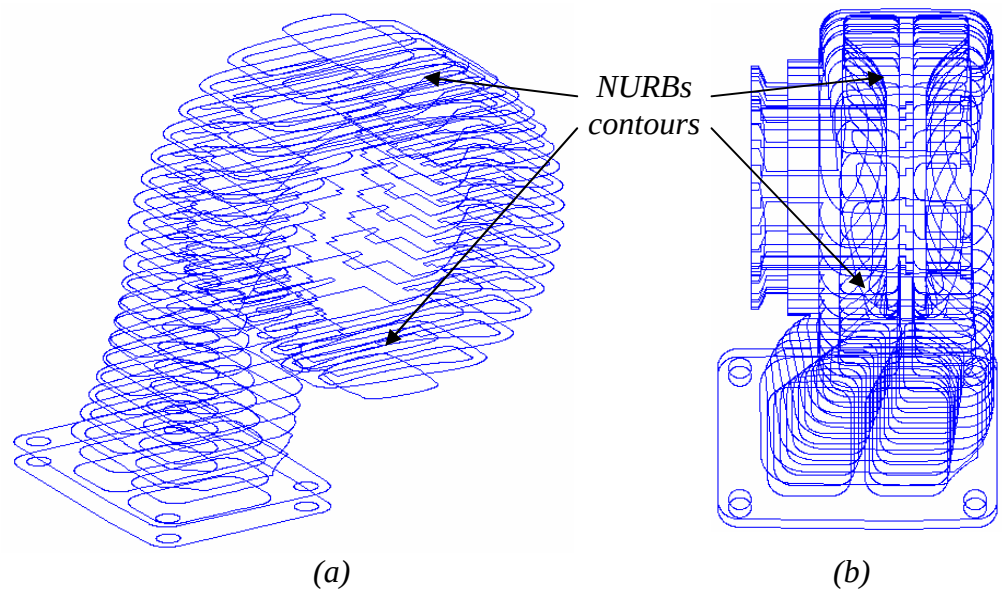

Figure 4.22: *Stacking of the hand traced NURBs contours within CADKEY® V21, in different display orientations.*

An approximated turbine housing, represented by the NURBs contours, could somewhat be seen [*Figure 4.22*]. Even some internal profiles were visible.

A 3-D NURBs model of the Garrett GT 40 turbine housing [*Figure 4.23*] was created by lofting through the stack of NURBs, using the integrated "Create-Loft NURBs" function within *CADKEY® V21*, as discussed in the latter part of *APPENDIX E*.

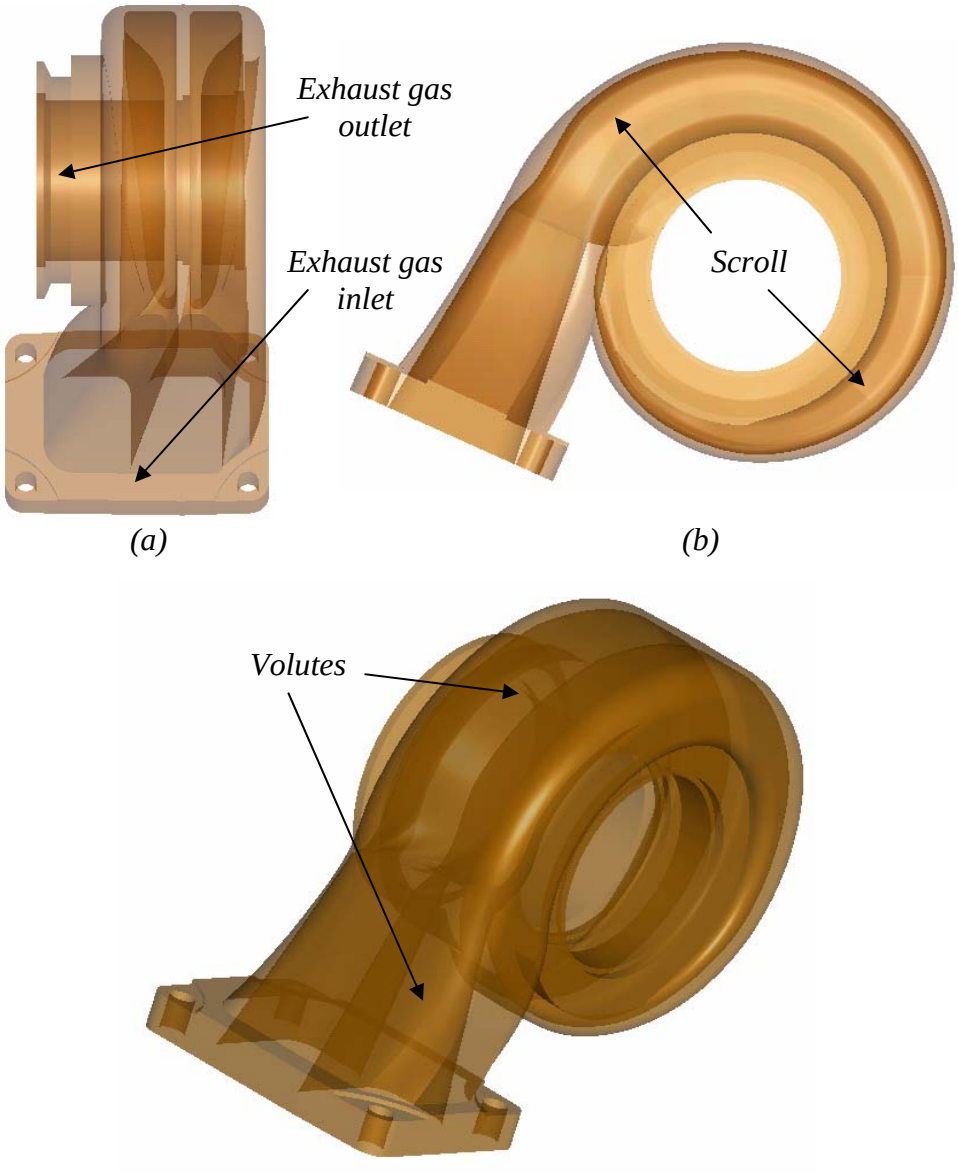

Figure 4.23: *The Garrett GT 40 turbine housing's 3-D NURBs model, generated from the NCT slices, in different display orientations.*

Visually, the reconstructed 3-D NURBs model of the Garrett GT 40 turbine housing resembled the existing turbine housing satisfactorily. In *Figure 4.23(a)*, the reconstruction of the exhaust gas in- and outlets are clearly visible. *Figure 4.23(b)* illustrates the scroll reconstruction with the two symmetrical volutes displayed in *Figure 4.23(c)*. However, the geometrical accuracy of the 3-D NURBs model had not been determined yet.

Due to the physical inaccessible nature of the turbine housing's interior, the geometrical accuracy had to be determined by sub-dividing the accuracy into geometrical external and volumetric internal approaches. At first the geometrical external accuracy was determined by comparing distinctive external measurements of the 3-D NURBs model obtained by using the integrated "Data-Verify Distance" function within *CADKEY® V21*, with the corresponding external measurements of the existing turbine housing obtained with hand held measuring equipment. An overwhelming majority of the respective measurements concurred within 0.5 millimetres, resulting in a geometrical external accuracy of 95%.

A volumetric internal accuracy of 94% was calculated by comparing the existing turbine housing's volume, determined by filling the volutes with water, with the 3-D NURBs model's volume obtained by using *CADKEY® V21*'s integrated volume calculation function.

With a geometrical external accuracy of 95% and a volumetric internal accuracy of 94%, a tolerable geometrical internal accuracy of the 3-D NURBs model was eminent.

4.3.4 Discussion and Conclusions

By using the aforementioned NCT methodology and the resulting 3-D NURBs model, an acceptable mould could be created using CAM technologies to recast the Garrett GT 42 turbine housing in the desired material to satisfy the PBMM plant's design requirements. However, the geometrical accuracy obtained raised concerns, motivating the necessity for a further independent GRE method to calibrate the NCT results against.

CHAPTER 5: VERIFICATION OF RESULTS

5.1 Introduction…….p. 62
5.2 Geometrical Inspection and Measurements…….……...p. 62
5.2.1 External 3-D NURBs Model…….……...p. 63
5.2.2 Internal 3-D NURBs Model…..…….…. p. 65
5.2.3 Complete 3-D NURBs Model……..p. 68
5.3 Discussion and Conclusions……... p. 69

5.1 Introduction

In the previous chapter, Computed Tomography (CT) was implemented as the most promising GRE method to reverse engineer the centrifugal turbine housings. In this chapter, a 3-D NURBs model of the Garrett GT 40 turbine housing, generated by implementing an alternative contact GRE method in the form of geometrical inspection and measurements, will be compared with the 3-D NURBs model obtained with CT to determine if CT is the better of the two GRE methods. It is necessary to verify that sufficiently accurate 3-D NURBs models of the centrifugal turbine housings were obtained to ensure that acceptable accurate moulds could be created to recast the turbine housings in suitable materials, if it was required.

5.2 Geometrical Inspection and Measurements

The contact nature of this GRE method did not allow the simultaneous acquisition of data from both the complex volutes and the external profile of the turbine housing without destroying it in the process. One solution attempted to solve this problem was to sub-divide the geometry of the turbine housing into separate external and internal GRE problems. These two GRE problems were dealt with separately, resulting in the generation of external and internal 3-D NURBs models using CAD modelling software. A complete 3-D NURBs model of the Garrett GT 40 turbine housing was generated by subtracting the internal 3-D NURBs model form the external 3-D NURBs model within the CAD modelling software.

5.2.1 External 3-D NURBs Model

The Garrett GT 40 turbine housing was rotated along the centre axis of the exhaust gas outlet with the exterior surface divided into 15º radial segments and marked with a permanent marker [*Figure 5.1*].

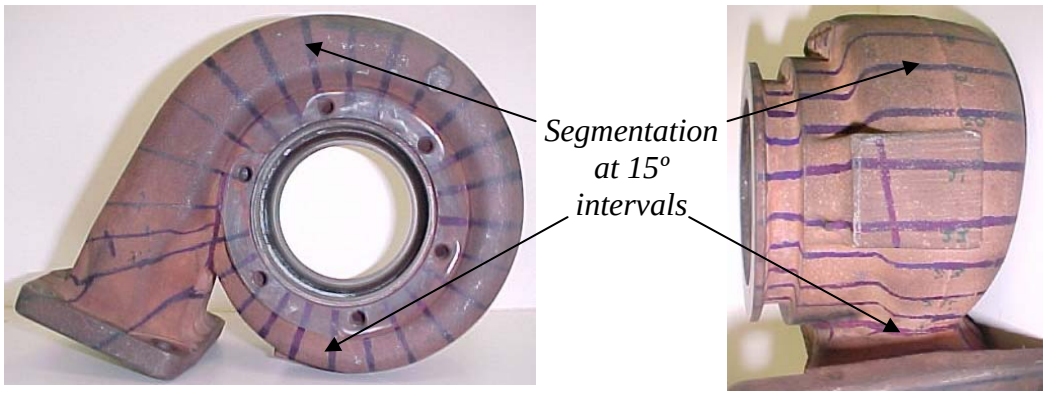

(a) *(b)*

***Figure 5.1**: Photographic images of the Garrett GT 40 turbine housing's exterior surface, segmented and marked at 15º intervals.*

By measuring the segmented exterior surface profiles at 15º intervals with standard hand-held verniers and micrometers, large numbers of contour measurements describing the exterior surface of the turbine housing relative to a reference plane, were acquired.

By using the contour measurements as input data, NURBs at 15º intervals were created within CAD modelling software [*CADKEY® V21*]. The NURBs were orientated relative to reference planes (parallel with the axial-axis) as displayed in *Figure 5.2*.

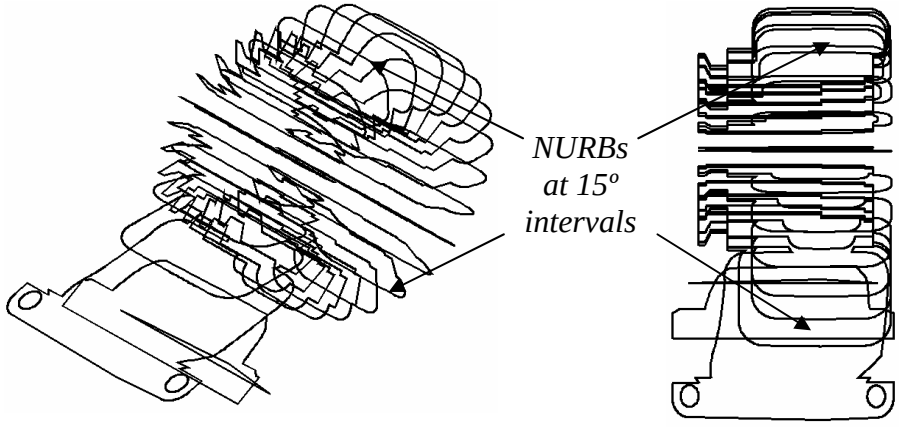

(a) *(b)*

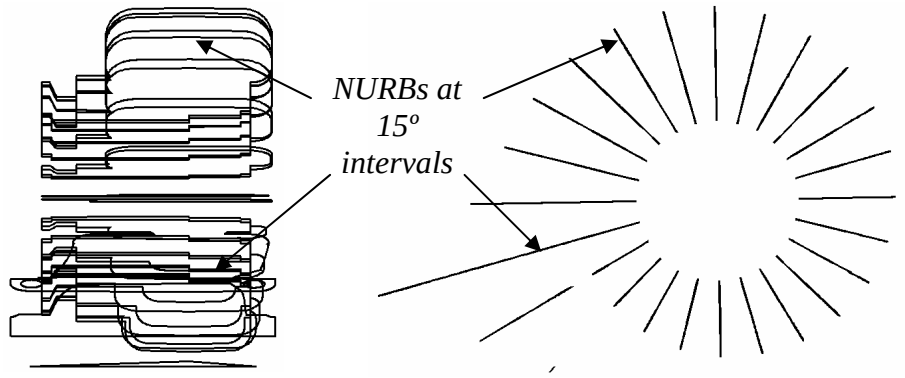

(c) *(d)*

Figure 5.2: *NURBs at 15º segments in CADKEY® V21 in different display orientations.*

By using the "Create-Loft NURBs" function within *CADKEY® V21*, as discussed in the latter part of *APPENDIX E*, the 15º segmented NURBs were lofted to generate the 3-D NURBs model of the Garrett GT 40 turbine housing's exterior as displayed in *Figure 5.3*.

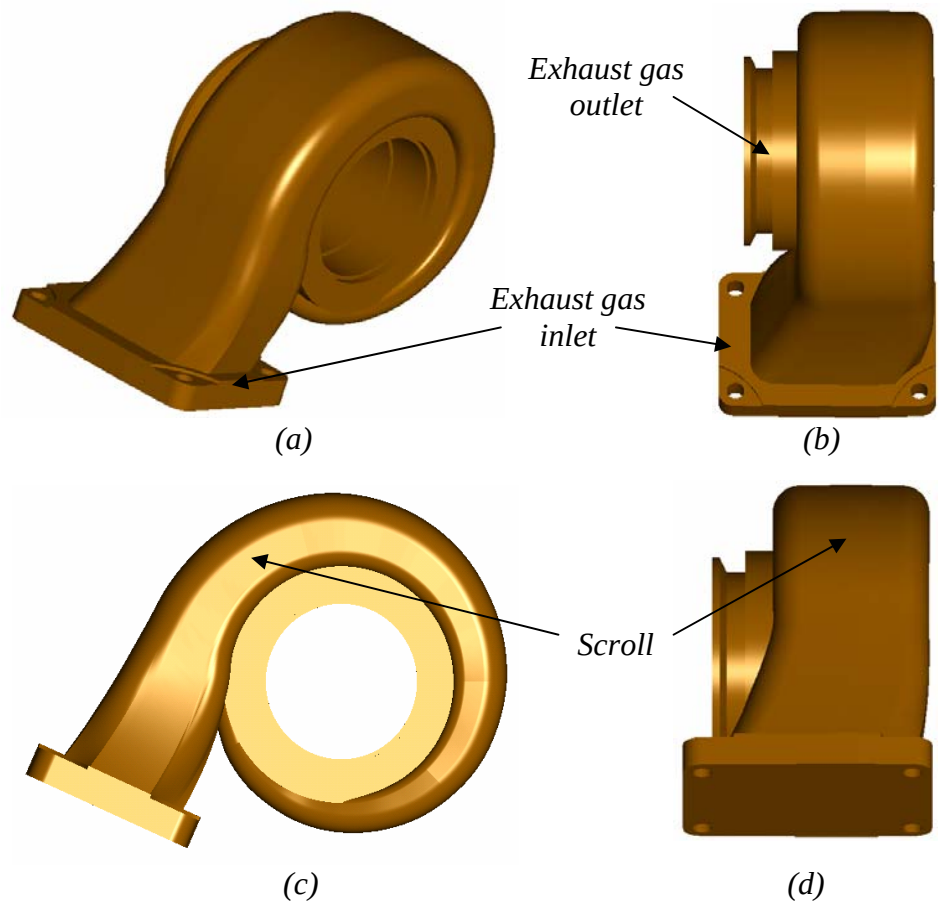

(a) *(b)*

(c) *(d)*

Figure 5.3: *The Garrett GT 40 turbine housing's exterior 3-D NURBs model, displayed at different orientations.*

The reconstructed exhaust gas inlet, outlet and scroll are clearly visible in *Figure 5.3*. Visually the reconstructed 3-D NURBs model of the Garrett GT 40 turbine housing's exterior represented the existing turbine housing satisfactorily, suggesting that a relative accurate reconstruction method was applied. This was again verified by comparing distinctive measurements of the 3-D NURBs model obtained by using *CADKEY® V21'*s integrated "Data-Verify Distance" function, with distinctive measurements from the existing turbine housing obtained with hand held measuring equipment. A geometrical accuracy of 87% was achieved. This geometrical accuracy illustrated that geometrical inspection and measurements provided a possible alternative to GRE the exterior of the Garrett GT 40 turbine housing.

5.2.2 Internal 3-D NURBs Model

A method attempted to acquire internal profile data using geometrical inspection and measurements was to cast a dimensionally stable polymer into a cavity that could easily be extracted once it has set. This was followed by measuring the polymer casting to obtain information of the cavity's internal profile. *Silastic J™ (250202)* also referred to as engineering rubber was selected and cast into the turbine housing's volute. *Silastic J™ (250202)* was chosen due to the following characteristics:

Shore Hardness:	A 55
Tensile Strength:	5.5 Mpa
Elongation at Breakage:	250 %
Tearing Strength:	15 kN/m
Density at 25ºC:	1.29 kg/m^3
Linear Shrinkage:	0,1 %

Unfortunately the internal surface finish of the Garrett GT 40 turbine housing has a sand paper like finish due to the casting process used to manufacture it. This posed a problem as the internal polymer acquired the same roughness, almost like a negative impression of the surface finish, interlocking with the volute and preventing problem free extraction.

A thin wax layer was cast into the volute that filled the rough sand paper internal volute surface, providing a smoother internal surface finish. Although thin, the additional wax layer compromised the accuracy of the internal polymer casting. The wax layer was covered with a releasing agent in the form of talk powder to ensure that no further problems with extraction were encountered.

The *Silastic J™* polymer was cast and given 72 hours to set. Extraction was no problem but the polymer did not fill the Garrett GT 40 turbine housing's volute completely and internal profile information at the smallest end of the volute was lost [*Figure 5.4*].

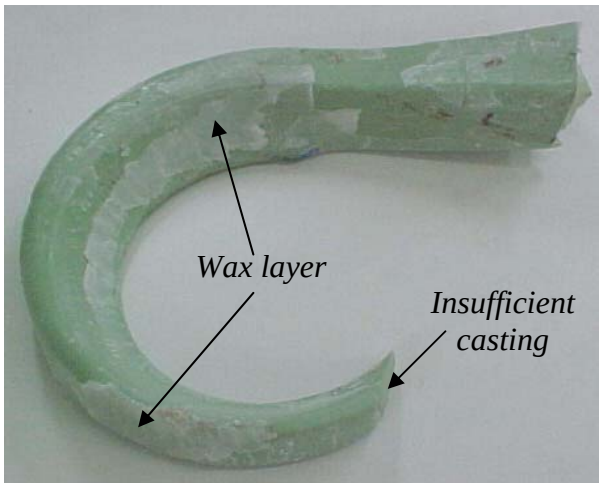

Figure 5.4: *Photographic image of the Silastic J™ internal polymer casting.*

This insufficient cast occurred due to the accumulation of wax where the volute area narrows to such an extent that it formed an obstruction prohibiting the polymer to flow freely. Although incomplete, the polymer casting provided vital information, attempting to describe the profile of the turbine housing's volute adequately.

Similar to the exterior of the turbine housing, the internal polymer casting was divided into 15º sections, marked and measured with verniers and micrometers along the profile contours and transferred into *CADKEY® V21*, converting the data to NURBs.

The incomplete internal polymer casting did not supply sufficient information for the generation of an internal 3-D NURBs model of the turbine housing's volute. To rectify this, the flow of the polymer within the volute was predicted by extrapolating

the NURBs within *CADKEY® V21*. The extrapolated NURBs describing the internal volute profile are presented in *Figure 5.5*.

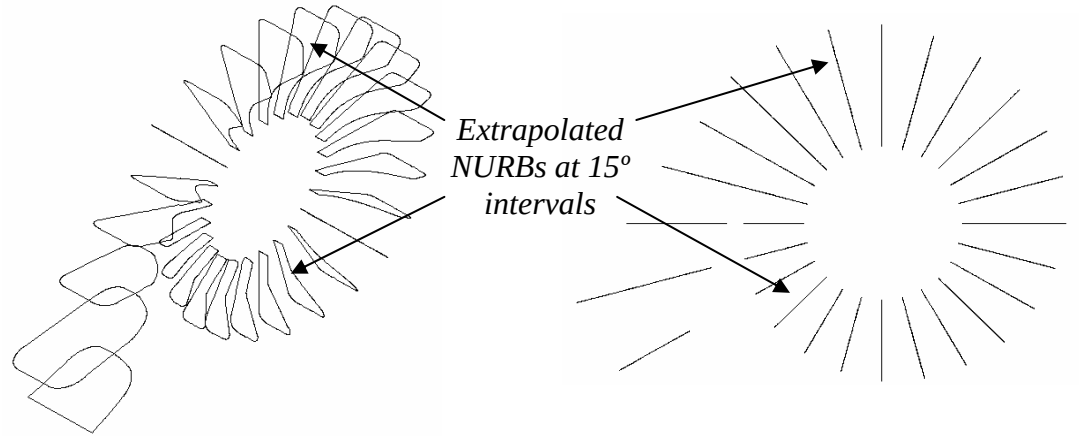

(a) *(b)*

Figure 5.5: *Respective views of the volute profile's extrapolated NURBs.*

Lofting through these NURBs in the manner described in the latter part of *APPENDIX E* created the complete internal 3-D NURBs model [*Figure 5.6*] to be subtracted from the external 3-D NURBs model of the Garrett GT 40 turbine housing.

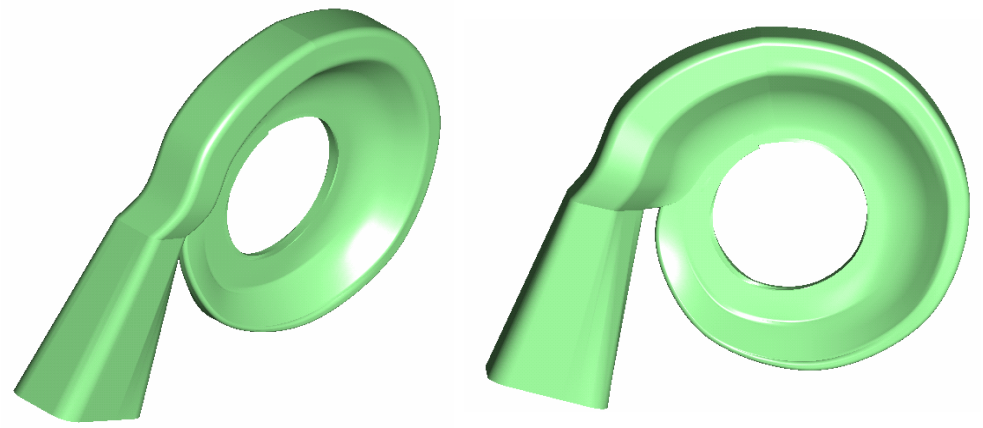

(a) *(b)*

Figure 5.6: *Respective views of the internal volute profile's 3-D NURBs model within CADKEY® V21.*

Visually, the reconstructed 3-D NURBs model of the internal profile resembled the theoretical volute of a centrifugal turbine housing satisfactorily [*Figure 3.3*]. However, the accuracy of the 3-D NURBs model had not been determined yet.

Accuracy was determined by comparing distinctive measurements of the 3-D NURBs model obtained by using the integrated "Data-Verify Distance" function within

CADKEY® V21, with the corresponding measurements of the internal polymer obtained with hand held measuring equipment. The majority of the measurements concurred within a few millimetres with the exception of a few, resulting in a geometrical accuracy of 85%.

5.2.3 Complete 3-D NURBs Model

To create the complete Garrett GT 40 turbine housing's 3-D NURBs model, the internal 3-D NURBs model was subtracted from the exterior 3-D NURBs model using the "Modify-Difference" module in *CADKEY® V21* with the resulting 3-D NURBs model of the Garrett GT 40 turbine housing as displayed in *Figure 5.7*.

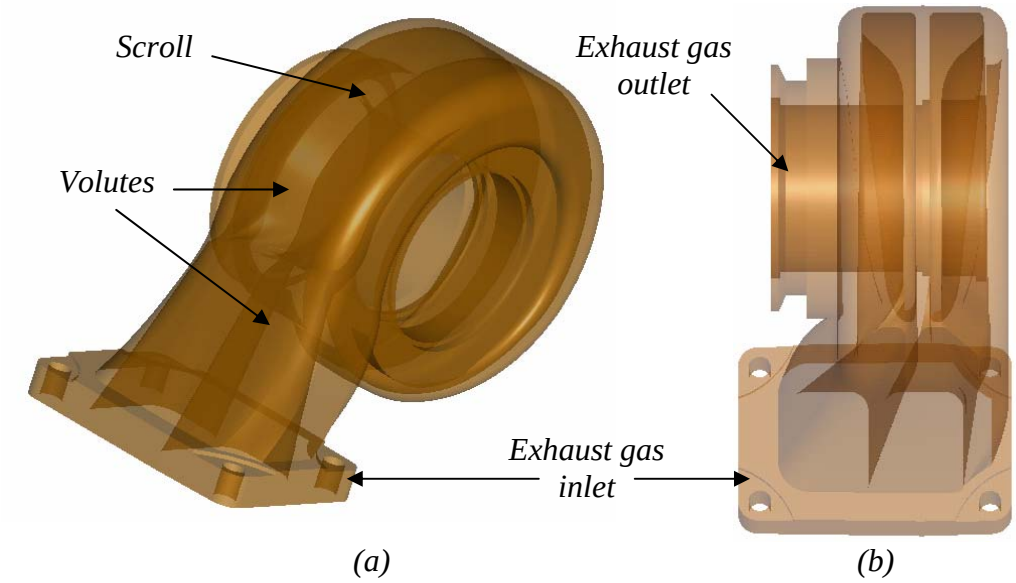

Figure 5.7: *Respective views of the complete Garrett GT 40 turbine housing's 3-D NURBs model.*

Visually, the reconstructed 3-D NURBs model of the Garrett GT 40 turbine housing resembled the existing turbine housing satisfactorily. In *Figure 5.7* the reconstruction of the exhaust gas in and outlets and the scroll, with the two symmetrical volutes, are clearly visible.

A similar approach to determine the geometrical accuracy of the 3-D NURBs model obtained with NCT was applied in this instance. At first the geometrical external accuracy was determined by comparing distinctive external measurements of the 3-D NURBs model obtained by using the integrated "Data-Verify Distance" function

within *CADKEY® V21*, with the corresponding external measurements of the existing turbine housing obtained with hand held measuring equipment. An overwhelming majority of the respective measurements concurred within 0.8 millimetres, resulting in a geometrical external accuracy of 87%.

A volumetric internal accuracy of 85% was achieved by comparing the existing turbine housing's volume, calculated by filling it with water, with the 3-D NURBs model's volume obtained by using *CADKEY® V21*'s integrated volume calculation function.

With a geometrical external accuracy of 87% and a volumetric internal accuracy of 85%, a tolerable geometrical internal accuracy of the 3-D NURBs model was eminent.

5.3 Discussion and Conclusions

The 3-D NURBs model's geometrical external accuracy of 87% and volumetric internal accuracy of 85% achieved illustrated the an alternative methodology for reconstructing 3-D NURBs models by subtracting a separately constructed internal 3-D NURBs model from an external 3-D NURBs model using geometrical inspection and measurements, is a valuable GRE method to reverse engineer the Garrett GT 42 turbine housing. By using the aforementioned methodology and the resulting 3-D NURBs model, a mould could be created using CAM technologies to recast the turbine housing in the desired material to satisfy the PBMM plant's design requirements. However, the lesser accuracies illustrates that NCT using CAD modelling software provided superior results to reverse engineer the Garrett GT 42 turbine housing.

CHAPTER 6: CONCLUSION

6.1 Introduction…….p. 70
6.2 Summary……..…….…… p. 70
6.3 Conclusions…..…….……..p. 73

6.1 Introduction

In this chapter, a summary of the most important findings and results obtained during the course of this research, as discussed in the previous chapters, are provided. Conclusions, supported by these findings and results will be presented as well.

6.2 Summary

The Pebble Bed Micro Model (PBMM), a simulation model for the Pebble Bed Modular Reactor (PBMR), required that the spheroidal ductile cast iron turbine housing of the Garrett GT 42 turbocharger unit withstand a pressure of 896 kPa at a temperature of 700 °C. According to the ASME B31.3 (1996) Code for Pressure Piping, which the PBMM had to comply with, spheroidal ductile cast iron cannot withstand such high pressures at high temperatures. A solution considered was to have the turbine housing recast in an acceptable material that could withstand the PBMM plant's design pressures at high temperatures. For this purpose, a mould produced through Computer Aided Manufacturing (CAM) technologies, using a 3-D Non-Uniform Rational B-spline (NURBs) model obtained by reverse engineering methods, was required.

Therefore, the purpose of this research was to study and evaluate reverse engineering methods and techniques in order to identify and implement the most promising method(s) to reverse engineer the existing Garrett GT 42 turbine housing. It was required that non-destructive reverse engineering methods and techniques are implemented to produce a 3-D NURBs model, as the housing was required for future use.

A literature survey was conducted during which it was found that no previous work on the reverse engineering of a centrifugal turbine housing was available. The emphasis was therefore placed on the most applicable approach to create a 3-D NURBs model of the turbine housing (Geometrical Reverse Engineering (GRE)).

Different contact (tactile) and non-contact GRE methods were evaluated using the advantages and limitations of each method influenced by practical data acquisition problem areas as guidelines. **Computed Tomography (CT)**, a non-contact GRE method, was identified as the most promising method to reverse engineer the turbine housing. The primary advantages of CT over contact (tactile) as well as the remaining non-contact methods are that objects with internal or hidden features, or components made of different materials can be simultaneously detected during data acquisition. This was considered a necessity to acquire data from a component without destroying it in the process.

X-ray Computed Tomography (X-ray CT) and Neutron Computed Tomography (NCT) were implemented.

Three sets of axial X-ray CT scans, in different orientations, were performed on the turbine housing with a *Philips® TomoScan™ AV* medical spiral scanner at Millpark Hospital, Johannesburg. Although the internal profile of the turbine housing was identifiable to a certain extent, metal induced artifacts were present in all the scanning results. These metal induced artifacts were caused by secondary fluorescence, a phenomenon known to take place when samples containing iron are irradiated with copper (Cu). The internal component set-up and properties of the *Philips® TomoScan™ AV* spiral scanner are trade secrets and could not be analysed to find a probable cause or solution for the amount of artifacts experienced. Threshold, filter and window settings also influenced the quality of the CT results but could not be optimised and evaluated, as the scanner had to be made available for medical purposes. The artifacts experienced proved so severe that only a partially constructed 3-D polygonal model of the turbine housing could be generated with the integrated rendering software. The generation of a complete 3-D NURBs model was attempted with additional CAD modelling software, with no success.

Neutron Computed Tomography (NCT) at three different settings and two orientations were performed on the turbine housing. Neutrons generated within the SAFARI-1 nuclear research reactor at the South African Nuclear Energy Corporation (NECSA) were used as radiation medium. 3-D modelling software was used to reconstruct 3-D polygonal models for display purposes.

Insufficient reconstruction of the 3-D polygonal models was observed in all of the attempts. Blurred contours were visible as well. The limited reconstruction success could be attributed to a number of reasons, one being the limited neutron beam diameter. At some rotating angles, the turbine housing moved out of the neutron reach and no data could be acquired, resulting in insufficient reconstruction. The major reason however was thought to be the material composition of the turbine housing. A cloud of scattered neutrons, caused by the high density of the material might have lead to missing information in those regions displayed as blurred contours.

A possible solution to improve the results was to reduce the influence of scattered neutrons by increasing the distance between the component and scintillator plane (at the expense of image sharpness) or to use some neutron collimator between sample and detector, which would eliminate the cloud of scattered neutrons. Aluminium honeycomb with small channels, with the channel walls covered in a thin layer of gadolinium painting, would have been a good choice. Unfortunately, this option was not available at SAFARI-1.

Due to financial restrictions resulting in the lack of access to the correct data manipulation software, additional manipulation was performed using accessible CAD manipulation software [*CADKEY® V21*]. A 3-D NURBs model was created by lofting through NURBs created with the manipulation of 2-D NCT slice data, resulting in a geometrical external accuracy of 95% and a volumetric internal accuracy of 94%.

A 3-D NURBs model of the turbine housing, generated by applying an additional contact GRE method in the form of geometrical inspection and measurements, was used to compare with the 3-D NURBs model obtained with CT to determine if CT was the better of the two GRE methods. It was necessary to verify that sufficiently accurate 3-D NURBs models of the centrifugal turbine housings were obtained to

ensure that sufficient moulds of acceptable accuracy could be created to recast the turbine housings in suitable materials, if it was required.

The contact nature of geometrical inspection and measurements did not allow the simultaneous acquisition of data from both the internal and external profile of the turbine housing without destroying it in the process. To solve this problem, the geometry of the turbine housing was sub-divided into separate external and internal GRE problems. These two GRE problems were dealt with separately, resulting in the generation of external and internal 3-D NURBs models using *CADKEY® V21*. A complete 3-D NURBs model of the turbine housing was generated by subtracting the internal 3-D NURBs model from the external 3-D NURBs model within *CADKEY® V21*. A complete 3-D NURBs model of the turbine housing with a geometrical external accuracy of 87% and a volumetric internal accuracy of 85% was achieved.

6.3 Conclusions

The geometrical external accuracy of 87% and the volumetric internal accuracy of 85% of the 3-D NURBs model achieved with geometrical inspection and measurements illustrates that an alternative methodology for reconstructing 3-D NURBs models is possible, however, a geometrical external accuracy of 95% and a volumetric internal accuracy of 94% concludes that NCT provides superior results when reverse engineering centrifugal turbine housings.

The NCT facility at SAFARI-1, NECSA, is now operating successfully. The higher neutron flux, improved motion control and implementation of additional CAD modelling software have considerably reduced the time from exposure to 3-D NURBs models. By using the aforementioned NCT methodology and the resulting 3-D NURBs model, a mould could be created using CAM technologies to recast the Garrett GT 42 turbine housing in the desired material to satisfy the PBMM plant's design requirements.

REFERENCES

Aloimonos J., Shulman D., (1992), *Integration of visual models-An extension of the Mar Paradigm*. ISBN0-12-053020-1, pp. 289-371.

ASME B31.3 (1996), *ASME B31.3 Code for Pressure Piping*. American Society of Mechanical Engineers national standard.

Ballard D. H., Brown C. M., (1982), *Computer vision*. Prentice-Hall, Englewood Cliffs, N.J.

Besl P., (1989), *Active optical range imaging sensors*. Advances in Machines Vision. Cht1, Soringer Verlag, pp. 1-63.

Bidanda B., Hosni Y. A., (1994), *Reverse engineering and its relevance to industrial engineering: a critical review*. Computers Ind. Eng. Vol. 26, No. 2, pp. 343-348.

Bradly C., (1998), *Computer vision techniques in reverse engineering*. Engineering design & Automation 4(2), 101-112.

Briggs A., (1992), *Acoustic microscopy*. Oxford: Clarendon Press, pp. 73.

Brocha R., Young M., (1995), *Getting from points to products*. Computer-Aided Engineering.

Butler C., Shams I., (1990), *Precision co-ordinate measurement using a fibre optic touch probe*. Proceedings of 28th International MATADOR Conference, Manchester, pp. 477-480.

Byrne J., (1994), *Neutrons, nuclei and matter*. An exploration of the Physics of Slow Neutrons, Institute of Physics Publishing.

Campbell R. J., Flynn P. J., (2001), *A survey of free-form object representation and recognition techniques*. Computer Vision and Image Understanding 81, pp. 166-210.

Cauchick-Miguel P.A., Kings T.G., (1998) *Factors which influence CMM touch trigger probe performance*. Inter. J. of Machine Tools and Manufacture 38, pp. 363-374.

Chang M., Wan D. S., (1991), *On-line automated phase-measuring profilometry*. Opt. & Lasers in Eng. 15, pp. 127-139.

Chen L. C., Lin G. C. I., (1997), *An integrated reverse engineering approach to reconstructing free-form surfaces*. Journal of Computer Integrated Manufacturing Systems, Vol. 10, N 1, pp. 49-60.

Commen P. K., Smith K. E., Bhatia G., Vannier M. W., (1994), *Geometric design of a multi-sensor structured light range digitiser*. Optical Engineering. 33(6), pp.1349-1358.

Curless B. L., (1997), *New methods for surface reconstruction from range images*. Ph.D. thesis, Stanford University.

Curless B., Levoy M., (1995), *Better optical triangulation through space-time analysis*. Int. Conf. Om Computer Vsion, pp. 23-32.

Dalton G., (1998), *Reverse engineering using laser metrology*. Sensor Review, Vol. 18, Issue 2, pp. 92-96.

De Beer F., (2003), (fdebeer@necsa.co.za) *Discussion on NCT*. [Email to:] Rossouw M.C. (mgimcr@puknet.puk.as.za) Jul. 30.

Domanus J. C., (1992), *Practical neutron radiography*. Kluwer Academic Publishers, Dordrecht.

Duncan J. P., Mair S., (1983), *Sculptured surfaces in engineering and medicine*. Cambridge University Press, New York.

Eck M., Hoppe H., (1996), *Automatic reconstruction of B-spline surfaces of arbitrary topological type*, Computer Graphics (SIGGRAPH 96), Vol 30.

EI-Hakim S. F., Pizzi N. J., (1993), *Multi-camera vision-based approach to flexible feature measurement for inspection and reverse engineering*. Optical Engineering. 32: No 9, pp. 2201-2215.

Fan K. C., (1994), *Precision positioning detection technique using CCD*. Proc. Of the 3rd Conf. of Chinese Metrology Society, Part B, pp. 43-50.

Fan K. C., (1997), *A non-contact automatic measurement for free-form surface profiles*. Computer Integrated Manufacturing Systems, Vol. 10, No. 4, pp. 277-285.

Fan K. C., Chen M. J., Huang W. M., (1998), *A six-degree-of-freedom measurement system for the motion accuracy of linear stages*. International Journal of Machine Tools and Manufacture, Vol. 38, No. 3, pp. 155-164.

Fan K. C., Lee J. C., (1999), *Range image segmentation of mechanical parts by locating critical points of one-dimensional curves*. J. of the CSME, Vol. 20, pp. 21-27.

Fua P., (1997), *From multiple stereo views to multiple 3-D surfaces*. International Journal of Computer Vision, Vol. 24, Issue 1, pp. 19-35.

Gadhwani A., Bhatia G., Vannier M. W., (1994*), Calibration of a multi-sensor structured light range scanner*. Optical Engineering. 33(4), pp. 1359-1367.

Greiner G., Hormann K., (1997), *Interpolating and approximating scattered 3-D data with hierarchical tensor product B-splines*. In: Surface Fitting and Multi-resolution Methods, Eds: A. Le M´ ehaut´ e, C. Rabut and L. L. Schumaker, Vanderbilt University Press, pp. 163-172.

Hall E., Tio J., McPherson C., Sadiadi M., (1982), *Measuring curved surfaces for robot vision*. Computer. V15, pp. 42-54.

Harthong J., Sahli H., (1992), *Theory of moiré sensing means of contour functions*. App. Opt. 31(10), pp. 1436-1443.

Haystead J., (1997), *Computed-tomography-based medical imaging*. Visions Systems, Volume 2, No. 7. pp. 14-19.

Hoppe H., DeRose T., Duchamp T., McDonald J., Stuetzle W., (1993), *Mesh optimisation*. In Computer Graphics, SIGGRAPH ’93, volume 27.

Hoppe H., De Rose T., Duchamp T., McDonald J., Stuetzle W., (1994), *Piecewise smooth surface reconstruction*. In Computer Graphcis, SIGGRAPH ’94, vol. 28.

Hoschek J., Dietz U., Wilke W., (1998), *A geometric concept of reverse engineering of shape: approximation and feature line*. In: Mathematical Methods for Curves and Surfaces II, Eds: M. Dæhlen, T. Lyche and L. L. Schumaker, Vanderbilt University Press, pp. 253-262.

Hu G., Jain A. K., Stockman G., (1986), *Shape from light stripe texture*. CVPR (86), pp. 412-414.

Hutchins D. A., Wright W., M., D., Hayward G., Gachagan A., (1994), *Air-coupled piezoelectric detection of laser-generated ultrasound*. IEEE Trans. Ultrason. Ferroelec. Freq. Contr., Vol. UFFC-41, No. 6, pp. 796-805.

Jarvis R. A., (1983), *A perspective on range finding techniques for computer vision*. IEEE PAMI, Vol. 5, No. 2, pp 122-139.

Jin G. C., Tang S., (1989), *Automated moiré contouring of diffuse surfaces*. Opt. Eng., 28 (11), pp. 11-1215.

Kak A. C, Slaney M., (1988), *Principles of computerised tomographic imaging*. IEEE Press, New York.

Kim S. W., Choi Y. B., Oh J. T., (1999), *Reverse engineering: high-speed digitisation of free-form surfaces by phase shifting grating projection moiré topography*. International Journal of Machine Tools & Manufacture, Vol. 39, pp. 389-401.

Knopf G. K., Al-Naji R., (2001), *Adaptive reconstruction of bone geometry from serial cross-sections*. Artificial Inelegance in Engineering, Vol. 15, pp. 227-239.

Kobayashi H., Tomura K., Harasawa S., Hattori M., (1990) in: Proc. 3rd World Conf. On Neutron Radiography, pp. 421-428.

Koivunen V., Bajcsy R., (1992), *Rapid prototyping using 3-D computer vision*. Technical Report, MS-CIS-92-70, University of Pennsylvania.

Kruth J. P., Ma W., (1994), *CAD/CAM integration for reverse engineering*. 26th CIRP International Seminar on Laser Assisted Net shape Engineering, LANE '94, Erlangen, Germany.

Labuschagne J. T., (2002), *PBMR Micro Model M400 steady state results report*. Document Number: PBMM-0053.

Lai J. Y., Doong L. J., Yao C. Y., (1999), *3-D CAD model reconstruction from image data of computer tomography*. International Journal of Imaging Systems and Technology, Vol. 19, Issue 4, pp. 328-338.

Lin A. C., Lin S. Y., (1998), *Computer-aided mould engraving: from point-data smoothing NC machining, to accuracy checking*. Journal of Materials Processing Technology, Vol 86, Issues 1-3, pp. 101-114.

Lounsbery M., Mann S., Loop C., Meyers D., Painter J., De Rosa T., Sloan K., (1992), *A survey of triangular scattered data fitting in curve and surface design*. H. Hagen (ed.), SLAM.

Ma W, Swaelens B., Vancraen W., (1997), *Surface modelling from CT- images*. Proceedings of the International Conference on Manufacturing Automation, Hong Kong, pp. 1021-1026.

Maev R. G., (1988), *Einsatz der akustomicroskopie in den materialwissenschaften*. Review of the BRD-USSR bilateral seminar. Microscopy in Material Sciences, Moscow: Science Publishing, pp. 35.

Maev R. G., Shao H, Maeva E. Y., (1992), *Thickness measurement of a curve multi-layered polymer system using an ultrasonic pulse-echo thickness method*. Mater Charact 41, pp. 97-105.

Magee M., Weniger R., (1992), *Isolation of 3-D features of known height using a light-striped stereopic system*. SPIE, V1822, pp. 175-187.

Manthey D. W., Knappll K. N., (1994), *Calibration of a laser range-finding co-ordinate-measuring machine*. Optical Engineering. 33(10), pp. 3372-3380.

Mauvoisin G., Bremeand F., Lagarde A., (1994), *3-D shape reconstruction by phase-shifting shadow moiré*. App. Opt. 33(11), pp. 163-2169.

McFarland E. W., Lanza R. C., Poulos G. W., (1991), IEEE Trans. Nucl. Sci. 38 (2).

Modjarrad A., (1988), *Non-contact measurement using a laser scanning probe*. SPIE, Vol. 1012 In-Process Optical Measurements pp 229-239.

Moring I., Heikkinen T., Myllyla R., (1989), *Acquisition of three-dimensional image data by a scanning laser range finder*. Journal of Optical Engineering. Vol. 28, No. 8, pp.897-902.

Moss J. P., Linney A. D., Grindrod S. R., Mosse C. A., (1989), *A laser scanning system for the measurement of facial surface morphology*. Journal of Optics and Lasers in Engineering, Vol. 10, pp 179-190.

Motavalli S., Bidanda B., (1991), *A part image reconstruction system for reverse engineering of design modifications*. Journal of Manufacturing Systems. Vol. 10, No. 5, pp 383-395.

Nishihara H. K., (1984), *Practical real-time imaging stereo matcher*. Journal of Optical Engineering. Vol. 23, No. 5, pp 536-545.

Okutomi M., Kanade T., (1993), *A multiple-baseline stereo*. IEEE Transactions on Pattern Analysis and Machine Intelligent. 15: No. 4, pp. 353-363.

Oster R., Munich D., (1999), *Computed tomography as a non-destructive test method for fibre main rotor-blades in development, series and maintenance*. International Symposium on Computerised Tomography for Industrial Applications and Image Processing in Radiology, Berlin, Germany.

Posdamer J. L., Altschuler M. D., (1982), *Surface measurement by space-encoded projected beam systems*. Journal of Computer Graphics and Image Processing, Vol. 18, pp 1-17.

Rausch C., Bücherl T., Hofmann J., Schillinger B., v Seggern H., (1996), in: Proc. 5th World Conf. Neutron Radiography Berlin, pp. 113-117.

Rious M., (1984), *Laser range finder based on synchronised scanners*. Applied Optics, V23, pp. 3837-3844.

Rockwood A., Winget J., (1996), *3-D object reconstruction from two- dimensional images*. This special issue, Computer-Aided Design, Vol. 28, pp 153-158.

Rosenfeld J. P., Tsiko C. J., (1986), *High-speed space encoding projector for 3-D imaging*. SPIE, V728, pp. 146-151.

Rousseau P. G., Greyvenstein G. P., (2001), *Conceptual thermo-hydraulic design of the PBMR Micro Model*. Document Number: PBMM-0001.

Russ J. C., (1995), *The image processing handbook*. CRC Press, Boca Raton, FL.

Saoudi A., Nivat M., (1994), *Parallel algorithms for multidimensional image template matching*. IJPRAI(8), 1994, pp. 457-464.

Sapidis N. S., Besl P. J, (1995), *Direct construction of polynomial surfaces from dense range images through region growing*. ACM TOG, Vol 14, No 2, pp. 171-200.

Sasajima K., Tsukada T., (1998), *Development of 3-D surface measurement on cylinder*. Inter. J. of Machine Tools and Manufacture 38, pp. 445-450.

Satio Y., (1990), *Range finding system for 3-D object recognition*. Information science and engineering, pp. 285-310.

Satio Y., Otsuki M., (1993), *3-D shape reconstruction by active range finder*. CVPR93, New York, NY, pp. 142-147.

Schillinger B., Blümlhuber W., Fent A., Wegner M., (1999), *3-D-neutron tomography: recent developments and first steps towards reverse engineering*. Nuclear Instruments and Methods in Physics Research A 424, pp. 58-65.

Schillinger B., Gebhard R., Haas B., Ludwig W., Rausch C., Wagner U., (1996), *3-D neutron tomography in material testing and archaeology*. Proc. 5th World Conf. On Neutron Radiography, Berlin, pp. 688-693.

Schreiber R. R., (1992), *The dynamics*. Manufacturing Engineering. pp. 58-63.

Sobh T. M., Owen J. C., (1995), *A sensing strategy for the reverse engineering of machined parts*. Journal of Intelligent and Robotic Systems, pp. 1-18.

Sokolowski J. H., Maev R. G., Lee H. T., Maeva E. Y., Maslov K. I., (1998), *Analysis of casting subsurface structure using acoustic microscopy*. Proc. QNDE, Snowbird, Utah. New York: Plenum. pp. 1665-1670.

Song C. K., Kim S. W., (1997), *Reverse engineering: Autonomous digitisation of free-formed surfaces on a CNC co-ordinate measuring*. International Journal of Machine Tools and Manufacture, Vol. 37, No. 7, pp. 1041-1051.

Stanley J. H. *et al.*(1995), *CT-assisted solid free-form fabrication*. Proceedings of the sixth International Conference on Rapid Prototyping, Dayton, OH, pp. 267-274.

Stanley J. H., Yancey R. N., (1998), CT-assisted rapid tooling. Internal report, Advanced Research and Applications Corporation (ARACOR), CA 94086.

Stevenson W., (1992), *The use of triangulation probes in co-ordinate measuring machines for part tolerance inspection and reverse engineering*. SPIE Vol. 1821, pp. 406-414.

Strand T. C., (1985), *Optical 3-D sensing for machine vision*. Optical Engineering, V24, N1, pp. 33-40.

Thompson W. B., Owen J. C., Germain de St., James H., Stark S. R., Herderson T. C., (1999), *Feature-based reverse engineering of mechanical parts*. Vol. 15, Issue 1, pp. 57-66.

Towson W., Hill T. R., (1996), *Marketing literature*. Cyber-form International Inc. Richardson Texas. Howmet Corporation, Hampton, Virginia.

Tsai R. Y., (1987), *A versatile camera calibration technique for high-accuracy 3-D machine vision metrology using off-the-shelf TV camera and lenses*. IEEE Trans. Robot Automation. 3: No. 4, 323-344.

Tsujimura T., Yabuta T., Morimitsu T., (1989), *Shape-reconstruction system for 3-D objects using an ultrasonic distance sensor mounted on a manipulator*. Transactions of ASME, Vol. 111, pp 180-186.

Varady T., Martin R. R., Cox J., (1997), *Reverse engineering of geometric models-an introduction*. Computer-Aided Design 29 (4), pp. 255-268.

Wackenhut G., (1999), *Computer tomography-image enhancement*. Http://www. Informatik.unistuttgart.de/ipvr/bv/projekte/CTB/CTB_engl.html.

Wang Y F., Aggarwal J. K., (1987), *3-D object description from stripe coding and multiple views*. Proceedings of the 5th Scandinavian Conference on Image Analysis, Vol. 60, No. 6, pp 669-680.

Watanabe S., Yoneyama M., (1992), *An ultrasonic visual sensor for 3-D object recognition using neural networks*. IEEE Transactions on Robotics and Automation, Vol. 8, No. 2, pp 240-249.

Waterman P., (1997), *3-D digitising*. In Desktop Engineering, Volume 2, Issue 12. pp. 51-57.

Will P. W., Pennington K. S., (1972), *Grid coding: A novel technique for image processing*. Proceedings of the IEEE, Vol. 60, No. 6, pp 669-680.

Woodham R. J., (1978), *Photometric stereo: A reflectance map technique for determining surface orientation from a single view, image understanding systems and industrial applications*. Proc. SPIE 22nd Annual Technical Symposium, San Diego, California, Vol. 155, pp 136-143.

Wright W., M., D., Hutchins D., A., Hayward G., Gachagan A., (1996), *Ultrasonic imaging using laser generation and piezoelectric air-coupled detection.* Ultrasonics, Vol. 34, No. 2-5, pp. 405-409.

Yancey R. *et al.* (1996), *Integration of reverse engineering, solidification modelling, and rapid prototyping technologies for the production of net-shape investment cast tooling*. Advanced Research and Applications Corporation (ARACOR) Dayton, OH 45431.

Yee S. R., Griffin P. M., (1994), *3-D imaging system*. Optical Engineering, 33(6), pp. 2070-2075.

Zhao Y., Li P., Pu Z., (2001), *Shape measurement based on fibre-optic technique for complex internal surface*. Measurement 30 pp. 289-295.

APPENDIX A: CONTACT (TACTILE) GRE METHODS AND TECHNIQUES

A.1 Geometrical Inspection and Measurements……p. 85
A.2 Point Triangulation Devices……p. 85
A.3 Electro-Mechanical Point Scanning……p. 86
A.3.1 Touch-Trigger Probes (TTP)……..……..…p. 86
A.4 Co-ordinate Measuring Machines (CMM)……..p. 87
A.4.1 Mechanical Analogue Probes (MAP)…….p. 88

A.1 Geometrical Inspection and Measurements

Probably the most traditional and obvious method of acquiring data from a component's geometry is by means of geometrical inspection and measurements. This method is not usually used by the manufacturing and engineering industry mainly because the success depends on the component's geometry and the operators approach and skill level, however it is worth mentioning for the purpose of this research.

The technique comprises of visually inspecting a component and manually measuring the component's geometry with hand held measuring equipment e.g., verniers, micrometers, measuring tapes etc. The acquired data comprises of several measurement sets describing the component's profiles in the applicable measurement unit, which can be imported into CAD modelling software to generate a 3-D NURBs model of the original component.

A.2 Point Triangulation Devices

Point triangulated devices can be described as alternative, non-conventional contact (tactile) data acquisition devices. These are relatively low cost or home made devices that use two separately located measuring tapes or calibrated wires that are connected to a pointing wand.

The pointing wand is extended, pulling the tapes or wires and placed on the component's surface. For non-electronic measuring tapes, the lengths of the two tapes are written down. Using triangulation, the *(x, y, z)* location of the measurement points can be determined. These calculations may be done using a computer program. For electronic versions, the extended lengths of the tapes or wires are determined electronically and the triangulation is done automatically without having to write down numbers. These devices are often used on components that are too large for other 3-D data acquisition devices.

A.3 Electro-Mechanical Point Scanning

This device consists of a multi-jointed mechanical arm with a measuring point (Touch-Trigger Probe (TTP)) where the fingers would be. It is essentially a 3-D data acquisition stylus or pen.

The arm is pulled and the measuring point tip positioned on the component of interest followed by a click of a button to input the *(x, y, z)* point position of the measurement tip. Then the arm and tip is repositioned to another spot with the next 3-D geometry point entered. This method generates relative small data sets, typically around 1-120 points per minute. The advantage is that the component to be measured does not always have to be moved to acquire full 3-D positional geometric data. Additionally, by acquiring data from only corners and edges, it is easier to recover the topography of the 3-D component. Internal openings pose less of a problem. This method is labour intensive and time consuming. Although these devices are very accurate, input can be tedious and the range of the mechanical arms limits the size of the component that can be reverse engineered.

A.3.1 Touch-Trigger Probes (TTP)

TTP have a slow data acquisition rate since manual operations are applied to acquire data acquisition from sculptured surfaces. A major advantage is that TTP can pick up geometric data accurately and accommodate components with sharp angles and corners. TTP provide high measuring accuracy and repeatability. A disadvantage

however is that TTP cannot be used to measure soft or untouchable components and the measured result of a TTP requires corrections using stylus radius compensation.

A.4 Co-ordinate Measuring Machines (CMM)

According to Cauchick-Miguel and Kings (1998), Sasajima and Tsukada (1998) and Fan (1997), the Cartesian manipulator capable of acquiring a vast amount of data within a single manual or automatic attempt is better known as a Co-ordinate Measurement Machine (CMM). The CMM is the most commonly used contact device for extracting 3-D positional geometric data from part surfaces by touching a component's surface using mechanical arms. A sensing device at the end of the CMM's arm, better known as a Mechanical Analogue Probe (MAP), determines the relative co-ordinate locations and sends information back to a computer software package which stores the data to be used in further applications.

Data acquisition can be accomplished in an automatic or a manual mode. Automatic data acquisition enables the operator to allocate a path for the CMM off-line, saving valuable machine time and providing a more efficient use of the CMM system. Different surfaces can be pre-determined before data acquisition commences, thus allowing the use of specialised data acquisition routines. Although manual data acquisition is very labour-intensive, it is often applied to improve accuracies achieved with pre-programmed scanning. It uses the same basic measurement tools to produce the 3-D data set with the only difference being the CMM manual guidance to acquire data that are more specific. It is mainly used for one-off scans when none of the other methods or techniques are available or when a specific methodology of data acquisition is required.

A complicated free-form surface may require several scans to generate a 3-D cloud of data points, but the data accuracy is not fully guaranteed. Fan (1997), Butler and Shams (1990), Song and Kim (1997) determined that this variation in accuracy depends upon the direction of approach, speed of approach, length of stylus, and other factors. According to studies by Kruth and Ma (1994), Chen and Lin (1997), a universal intelligent data acquisition strategy with a high degree of automation that

overcomes the disadvantages of a MAP is required to improve the performance of CMM and to scan geometric data more effectively.

A.4.1 Mechanical Analogue Probes (MAP)

MAP can detect 3-D positional geometric data at a speed of up to 2000 points per second, with accuracy as good as a TTP. The data acquisition patterns can also be programmed to move along certain data acquisition paths and obtain a fixed data density. When the MAP touches the surface, a signal is sent back to the machine, which records the *(x, y, z)* co-ordinates of the probe's head.

APPENDIX B: NON-CONTACT GRE METHODS AND TECHNIQUES

B.1 Magnetic Resonance Imaging (MRI)……..p. 89
B.2 Optical Methods……..p. 90
B.2.1 Structured Lighting……p. 90
B.2.2 Radiography……p. 93
B.2.3 Computed Tomography (CT)……..p. 94
B.2.4 Fibre-Optic Shape Measurement……p. 95
B.2.5 Image Analysis……p. 95
B.2.6 Ranging……...p. 96
B.3 Ultrasonic Sound Waves……p. 97
B.3.1 Scanning Acoustic Microscope (SAM)……p. 98

B.1 Magnetic Resonance Imaging (MRI)

MRI involves sensing the strength of a magnetic field source by activating atoms in the material to be measured, and then measuring the response.

In MRI, the device acquires a number of cross-sectional planes of data through the component being studied. MRI technology is most commonly associated with mapping of the human anatomy and is based on the oscillation of hydrogen nuclei contained in soft body parts, such as in muscles, blood and brain tissue. However, industrial uses of MRI exist. In some cases, a component can be submersed in water and the inverse of the component can be created. MRI also requires reconstruction and visualisation since all of these planes are used to obtain a complete 3-D virtual model of what the original component was like. GRE methodologies using MRI can mainly be found in biomedical and bio-mechanical applications [Knopf and Al-Naji (2001)].

Magnetic probes are used as well. This method usually senses the location and orientation of a stylus within the field. A trigger allows the operator to record specific point data once the stylus is positioned at a point of interest. MRI probes are used in

similar applications to ultra-sound when internal profiles of components are to be measured.

B.2 Optical Methods

Optical methods are probably the broadest and most popular with relatively fast acquisition rates. There are six important categories of optical GRE methods discussed here: structured lighting, radiography, Computed Tomography (CT), fibre-optic shape measurement, ranging and image analysis.

B.2.1 Structured Lighting

The general methodology of structured lighting is to reflect a laser beam (either a laser spot [Satio (1990)], slit rays [Satio and Otsuki (1993), Magee and Weniger (1992) and Commen *et al.* (1994)], a pattern disk [Gadhwani *et al.* (1994)], a light grid [Hu *et al.* (1986)], or a binary pattern [Rosenfeld and Tsiko (1986), Yee and Griffin (1994)]) onto the surface of the workpiece and then detect the position of the reflected beam using a Charged Couple Device (CCD). The received image reveals 2-D co-ordinates of the surface point. Since this point is located at the intersection of the line of the laser beam and the line of the CCD axis, triangulation procedures are used to calculate the depth of the point [Bidanda and Hosni (1994)].

Triangulation is a method that uses location and angles between light sources and photo sensing devices to deduce position. A high-energy light source is focused and projected at a pre-specified angle at the surface of interest. A photosensitive device, usually a video camera or a CCD senses the reflection of the surface and then by using geometric triangulation from the known angle and distances, the position of a surface point relative to a reference plane can be calculated. The light source and the camera/CCD can be mounted on a travelling platform, which then produces multiple scans of the surface. These scans are therefore relative measurements of the surface of interest.

Various different high-energy light sources are used, but laser probes are the most common.

B.2.1.1 Laser Triangulation Probes

A number of studies proved that the primary benefits of laser data acquisition devices are their fast scanning rate and non-contact operation [Schreiber (1992), Fan *et al.* (1998), Bradly (1998), Strand (1985), Hall *et al.* (1982), Besl (1989), Manthey and Knappll (1994) and Dalton (1998)]. This means that this type of probe can scan 3-D positional geometric data from materials such as soft clay, plastic, and softwood. With a small laser beam spot, the probes can measure the finely detailed geometric data from complex surfaces. Butler and Shams (1990) states that the accuracy of laser triangulation probes is highly dependent upon probe orientation relative to the surface, and on the surface characteristics. Stevenson (1992) studied the performance of triangulation probes. He evaluated error sources in triangulation probe measurements and proposed strategies to avoid and minimise unexpected errors in improving performance. The disadvantages in applying laser probes to acquire data from workpieces include: failure to detect correct peak and valley positions on rough surfaces, centroid shift at an edge, ghost images from asperities on an edge face, image distortion at large surface angles and reflectance variations on the surface.

Some researchers [Lin and Lin (1998), Fan and Lee (1999), Rious (1984), Curless and Levoy (1995)] have designed a dual-detection laser probe to enhance accuracy while measuring a surface with a sharp reflectance boundary.

Another problem in using laser triangulation probes is that they produce unacceptable errors when scanning shiny or transparent surfaces. Laser probes under such conditions tend to read into the material and not collect true surface data, or collect no data at all. The usual way to avoid this problem is to paint or apply powder to the surface to be inspected, which helps to diffuse the reflectivity characteristics, the transparency, or the inherent colour of the surface. However, this method is not suitable when the application requires strict measurement accuracy.

It is important to note that the range-resolution trade-off is common to all triangulation sensors. According to Gadhwani *et al.* (1994), Rosenfeld and Tsiko (1986), Yee and Griffin (1994), if the measurement is narrowed to a small inspection area, the measurement accuracy can be enhanced by a few microns, or alternatively an accuracy of several millimetres over depths of field of several metres can be achieved. Some researchers have investigated effective solutions to resolve the problems which cause measurement inaccuracy, such as surface reflectance variances, surface geometric deviation from planarity, partial occlusion of light paths to the sensors, and laser speckle due to surface roughness [Curless (1997)]. This kind of measurement has much potential in the near future, and can be utilised in co-operative sensing approaches.

Laser triangulation probes can also acquire data at very fast rates. The accuracy is determined by the resolution of the photosensitive device and the distance between the surface and the probe. Motavalli and Bidanda (1991) presented a reverse engineering strategy using laser triangulation. Moss *et al.* (1989) presented a detailed discussion of a classic laser triangulation system used to capture shape data from complex surfaces. A discussion of accuracy and applications is also included. The use of laser triangulation probes on a CMM is presented by Modjarrad (1988). These references give a broad survey of methods, approaches to and limitations of laser triangulation.

Another popular method of structured lighting is shadow Moiré interferometry.

B.2.1.2 Moiré Interferometry

Interferometry methods measure distances in terms of wavelengths using interference patterns, which are projected onto a surface producing lighted contour lines. These contour lines are captured in an image and are analysed to determine distances between the lines. This distance is proportional to the height of the surface at the point of interest and so the co-ordinates of surface points can be deduced. Interferometry can acquire large amounts of data with a single image frame, but the analysis to determine positions of data can be rather complex. This can be a very accurate method of measurement since visible light has a wavelength of the order of hundreds

of nano-meters, while most GRE applications distances are in the centimetre to meter range. In principle, other parts of the electromagnetic spectrum could also be used. In practice, a high-energy light source is used to provide both a beam of monochromatic light to probe the component and a reference beam for comparison with the reflected light.

Moiré interferometry techniques researched by Manthey and Knappll, (1994), Mauvoisin *et al.* (1994), Harthong and Sahli (1992), Chang and Wan (1991), Jin and Tang (1989), Kim *et al.* (1999) are based on the generation and recording of spatial beating, or moiré fringes between two regular patterns of similar frequencies. This method illuminates a surface with the patterns of light obtained by passing light through an optical grate. When the image is viewed through another grate, the resulting fringe patterns are analysed to calculate the depth. The accuracy can be regulated by refining the grating scale and increasing the resolution of the CCD camera. The moiré fringes can rapidly and automatically be interpreted into 3-D component information. Components with sizes from a few square centimetres to several square metres can be measured using the Moiré technique, with a resolution varying between 0.01 millimetre and 1 centimetre. This method is limited to less depth of measurement field and measurement resolution when compared to other laser triangulation techniques.

Will and Pennington (1972) uses grids projected onto the surface of components to determine point locations. Wang and Aggarwal (1987) use a similar approach but use stripes of light and multiple images. In general, using a planar light or a light stripe instead of a light point the speed of data acquisition can be enhanced. Although the data acquisition speed is very fast, and the measuring process is non-contact, the measurement accuracy is low compared with contact (tactile) methods and techniques.

B.2.2 Radiography

Radiography provides a very efficient tool in the field of Non-Destructive Testing (NDT), GRE as well as many applications in fundamental research such as internal profile inspection.

A radiation beam, gamma rays, x-rays or neutrons, penetrating a specimen is attenuated by the sample material and detected by a 2-D imaging device. The image gathered by this device contains information about materials and structure inside the sample because particles are attenuated according to the basic law of radiation attenuation. X-ray radiography is currently the most popular method and is more widely used than gamma rays or neutrons. Gamma rays, X-rays and neutron radiography can reveal important internal structure information not obtainable by more traditional methods.

B.2.3 Computed Tomography (CT)

CT is a technique that produces images representing 2-D slices through a component. Oster and Munich (1999) and Lai *et al.* (1999) determined that measurements of a component result in a set of attenuation profiles of an intersection plane, that can be used to numerically reconstruct a cross-section image of the plane. The radiographs are back-projected into a tomographic image set that maps the locations of specific material densities. These slices can be stacked to produce a 3-D image, which represents the internal and external features of the component. Recent advances in sophisticated reconstruction algorithms have produced the ability to utilise CT data to generate a 3-D point cloud, representing all internal and external surfaces and/or boundaries of a component [Stanley and Yancey (1998) and Bidanda and Hosni (1994)]. Once the point cloud is produced, 3-D virtual models from the point data can be generated by surface/solid modelling techniques.

The primary advantage of CT over other conventional methods is that data from components with internal or hidden features, or components made of different materials, can simultaneously and rapidly be acquired with the same scanning procedure. However, this kind of technique also faces problems. These include difficulties in achieving the mono-energetic radiation required by the reconstruction assumption and measurement inaccuracy (about 1 millimetre) due to the significant width of the source beam. The generation of artifacts in the reconstructed image when the beam is parallel or almost parallel to an edge of the component, and noisy reconstructed images due to the non-availability of high energy densities of radiation beams. Therefore, efforts have been made to enhance scanning resolution and

accuracy in advanced image processing and in the selection of scanning radiation [Wackenhut (1999)].

B.2.4 Fibre-Optic Shape Measurement

Internal shape measurement based on fibre-optic technique is a very new topic in GRE fields. A novel single-mode fibre-optic sensor to acquire data of complex surface shapes, based on the principle of beam reflection, is presented by Zhao *et al.* (2001). The fibres in the sensor probe are arranged like the spokes of a wheel with eight symmetrically cross-arranged receiving fibres and one centred emitting fibre. Thus, the sensor can compensate for the offsets caused by fluctuations of surface reflectivity and light power and is fit for application under rough and formidable conditions with non-contact, fast shape measurement. This technology could be modified and eventually applied as a GRE method.

B.2.5 Image Analysis

Image analysis is similar to structured lighting methods in that frames are analysed to determine co-ordinate data. However, the analysis does not rely on projected patterns. Instead, typically, stereo pairs are used to provide enough information to determine height and co-ordinate position. The *(z)* co-ordinate can be found using two cameras to view the part from two different views. Triangulation is used to find the range information. This method is often referred to as a passive method since no structured lighting is used. Active methods are distinguished from passive methods in that artificial light is used in the acquisition of data. Correlation of image pairs and landmarks within the images are big difficulties with this method and this is why active methods are preferred. Another image analysis approach deals with lighting models, where an image is compared to a 3-D virtual model. The 3-D virtual model is modified until the shaded images match the real images of the component of interest.

There is a vast amount of literature on stereo imaging. Nishihara (1984) uses a real-time binocular stereo matching algorithm for making rapid range measurements. Posdamer and Altschuler (1982) describe a method for real-time measurement of surface data using stereo methods. Also, see Woodham's (1978) work on shape from shading. Finally, a contribution by Rockwood and Winget (1996) describes an energy

minimisation approach of a mesh to match a collection of 2-D images. A common application of this technology is photometry.

B.2.5.1 CCD Triangulation Stereo Matching Photometry

Fan (1994), EI-Hakim and Pizzi (1993) and Tsai (1987) found that stereo disparity-based approaches for data acquisition are passive compared to laser triangulation methods. Viewing the component from different positions, two or more images are captured. After this, the baseline distance is formed by the disparity between the same feature in two separate images. A triangulation procedure is then used to find the depth of the point that is normally located on the surface boundary or at the discontinuity area. This method has been applied to different applications, such as a 3-D virtual model reconstruction of complex shapes [Duncan and Mair (1983)] or of machined parts [Sobh and Owen (1995) and Thompson *et al.* (1999)].

The difficulty in using this kind of data acquisition method lies in the identification of the matching image pixels that correspond to the same point on the component. However, other researchers have effectively solved this problem in recent years [Okutomi and Kanade (1993), Ballard and Brown (1982), Aloimonos and Shulman (1992), Saoudi and Nivat (1994), EI-Hakim and Pizzi (1993) and Tsai (1987)].

Chen and Lin (1997), Sobh and Owen, (1995), EI-Hakim and Pizzi (1993) and Fua (1997) found that stereo vision techniques have the potential to be used in combination with contact (tactile) probes or laser probes in order to obtain a high degree of automation.

B.2.6 Ranging

Ranging methods measure distances by sensing time-of-flight of light beams; practical methods are usually based on lasers and pulsed beams. Moring *et al.* (1989) describes a range finder based on time-of-flight calculations. The article presents some information on accuracy and performance. Jarvis (1983) presents an in-depth article on time-of-flight range finders giving detailed results and analysis.

B.3 Ultrasonic Sound Waves

Utilising ultrasonic sound waves is an acoustic GRE method. This is where sound is reflected from a surface and recorded. Kim *et al.* (1999) stated that sound waves are mechanical vibrations or stress waves and therefore have varying wavelengths and velocities, depending upon the frequency of the wave and the material in which it propagates. There are many different types of waves, which may be used for NDT and GRE purposes. The most commonly used are longitudinal (compression) waves, shear (transverse) waves, Rayleigh (surface) waves and Lamb (guided or plate) waves.

Ultrasonic measurement generally utilises the generation of ultrasonic pulses, which can be used to detect the differences in sound impedance between the workpiece material and the air. The time-of-flight difference between the transmitted pulse and the reflected pulse can then be used to calculate the depth of the surface. The accuracy of this type of measurement mainly depends upon two factors, the size of the ultrasonic wavelength and the signal processing used to filter noise. Recent advances in air-coupled ultrasonic transducers have made it possible to measure 3-D components [Wright *et al.* (1996) and Hutchins *et al.* (1994)]. These electrostatic (capacitive) ultrasonic transducers operate in air at frequencies of up to and over 1 MHz, and consist of a thin metallic (dielectric) membrane and a rigid conducting back-plate which form two electrodes of a capacitor. Until now, however, ultrasonic techniques have not been widely applied in GRE due to accuracy limitations. Watanabe (1992) uses an ultrasonic sensor for component recognition and Tsujimura *et al.* (1989) place the ultrasonic device on a manipulator.

Acoustic methods have been used for decades for distance measuring. Sonar is used extensively for this purpose. Automatic focus cameras often use acoustic methods to determine range. The method is essentially the same as time-of-flight, where a sound source is reflected off a surface and then distance between the source and surface is determined knowing the speed of sound. Acoustic interference or noise is often a problem as well as determining focused point locations. Dynamic imaging is used extensively in ultra-sound devices where a transducer can sweep a cross-section through a component to capture internal data of a component.

Ultrasonic imaging could also be regarded as a semi-contact technique. Here, a "gun" whose tip emits an ultrasonic signal contacts a point on the part. A series of sensors that form a reference co-ordinate system can identify the location of the tip of the gun and thus the co-ordinate of the point on the part surface. The acquired 3-D data can be used to generate the 3-D virtual model with the appropriate software.

B.3.1 Scanning Acoustic Microscope (SAM)

The scanning acoustic microscopy (SAM) technique uses ultrasonic pulses for near-surface and bulk structure examination/scanning. A single narrow pulse generated by the transducer travels towards the sample surface where it is partially reflected back while the remainder propagates through the specimen interacting with internal structure. The reflected signal, which is received by the transducer generally, contains a peak corresponding to the surface reflection succeeded by echoes reflected from the internal structure. These echoes reach a transducer after a time delay that depends on the ultrasound velocity in a particular area of the sample. The amplitudes of the reflected and transmitted waves are a function of the acoustic properties of the material at each scanning point. Echo reflection can be caused by different kinds of non-homogeneity or discontinuity (for example: phase and grain boundaries, voids, inclusions and cracks). Applications and results in the GRE aspects are given in papers by Maev (1988), Maev *et al.* (1992), Briggs (1992), and Sokolowski *et al.* (1998).

APPENDIX C: NURBs SOLIDS

Non-Uniform Rational B-spline (NURBs) solids appeared early and remains the primary solid format used throughout the GRE and CAD modelling industry. To create a NURBs solid, the user is required to interactively select a region from the set of acquired 3-D positional geometric data to create a network of NURBs. The NURBs should be fairly evenly spaced and should cover the entire proposed NURBs solid region. The NURBs then are used as the basis for skinning or lofting operations whereby the solid is then created. The quality of the NURBs solid is also dependent on the skill level of the user or the operator.

The NURBs solid, generated by a GRE or CAD system, are represented in a computer by polynomial equations and onscreen through the location and shape of curves. For example, the equation of a line, a first-degree polynomial, has this form

$$Y = a\,(x) + b \qquad (1)$$

The equation for a parabola, a second-degree polynomial, has the form

$$Y = a\,(x)^{2} + b\,(x) + c \qquad (2)$$

And the equation of a cubic spline, a third-degree polynomial, looks like

$$Y = a\,(x)^{3} + b\,(x)^{2} + c\,(x) + d \qquad (3)$$

The more terms in the polynomial equation, the more shape the NURBs solid has.

The data structure of a NURBs solid is comprised of points, weights, and parameter values that define a control net, which is tangent to the solid. The control net on a NURBs solid is a rectangular grid of connected straight-line elements. The points in the database that describe the control net are not actually on the surface of the NURBs solid but rather the vertices of the control net. Weights in the NURBs solid's data structure determine the amount of solid deflection toward or away from its control point. Therefore, the NURBs control net is an abstraction of the underlying solid.

Some users have become adept at defining solids using a NURBs control net. But there is a downside. Points on the net are not on the underlying solid, so the net will not create a solid that goes through discrete points, which is sometimes necessary. This is not to say that NURBs solids cannot be forced to obey precise constraints, it's just that the NURBs net modelling technique is not constrained to do so. However, a NURBs control net is an effective editing tool for smoothing and refining the interior region of a NURBs solid. Users do not modify points on the NURBs solids directly. Instead, they modify the control net, which, in turn, forces surface smoothness on the solid during the edit.

Another problem with NURBs control nets is that they are rather fussy mathematical tools. They are rectangular in nature and behave badly if they are stretched into very odd shapes. This means that the operator must look at the component to be scanned and determine how to break it into one or more rectangular-like shapes. The scanning surfaces do not have to be perfectly rectangular. They can even be triangular in shape by making one side of the rectangular surface zero. The result is always an approximation of the operator's interpretation of the data, but is not necessarily what the engineer originally had in mind. The process requires a lot of time, effort and skills and becomes less and less feasible with increased complexity of the original part.

After defining the foundation NURBs solids, they can be trimmed and filleted. Trimming is performed after defining the initial NURBs solid and can be as important to modelling the finished part as defining the initial solids. Trimming alters the shape of the part, e.g. edge fillets around the part are more than aesthetic considerations because they add to the ergonomic design of the part.

Ultimately, a good GRE or CAD system shields users from having to know too much about the mathematics that represents the underlying NURBs solids. In addition, solid modellers should:

- Provide enough tools to completely define any feature on the part using solids;

- Have many functions for defining the different shapes of solids including ruled, revolved, lofted, extruded, swept, offset, filleted, blended, planar boundary, and drafted. Each of these functions has further variations;

- Support functions such as solid trimming, extending, intersecting, projecting, polygonal tessellation, IGES translation, co-ordinate system transformations, and editing;

- Allow extracting solid data such as flow curves, vectors, and planes, among other functions;

- Have a set of tools for defining points, planes, vectors, and splines used with solid modelling.

NURBs solids are supported by IGES (Initial Graphics Exchange Specification), a neutral file format for exchanging data between GRE and CAD systems. If a NURBs solid is created from the raw point data, it ensures that almost any design, analysis or CAD/CAM program can use the NURBs solid created.

APPENDIX D: INSTRUCTIONS FOR VIEWING X-RAY CT AND NCT ANIMATION VIDEO CLIPS

D.1 Windows - System Requirements…….p.102
D.2 Instructions for Viewing Animation Video Clips…… p.102

D.1 Windows - System Requirements

System requirements needed to view the animation video clips are as follows:

- Pentium 2 Personal Computer (PC) or a later model is recommended.
- Windows 95/98 operating system or an updated version is required;
- A minimum of 16 MB Random Access Memory (RAM) is required;
- 25 speed Compact Disc Read Only Memory (CD-ROM) drive or faster;
- 1024 x 768 16-bit colour SVGA monitor or better;
- Standard mouse and keyboard.

D.2 Instructions for Viewing Animation Video Clips

The following instructions will provide the reader with the necessary information to view the animations illustration the X-ray CT as well as NCT scanning operations:

- Insert the Compact Disk (CD) attached at the back of this dissertation into the CD-ROM drive;
- "Double click" on the "My Computer" icon followed by a "double click" of the CD-ROM icon displayed in the pop-up window;
- Two file folders will appear. "Double click" on the file folder named Computed Tomography (CT) Video Clips;
- Two file folders aptly named "X-ray CT" and "Neutron CT" containing the applicable video clips will appear.

The following sequence of steps applies for the viewing of the video clips in both of the aforementioned file folders:

- "Double click" in the file folder of interest;
- A number of video clip icons, labelled according to the appropriate figure numbers in the dissertation, will appear;
- "Click" once on the video clip of interest. The icon will display with a blue background. Keep the "Shift" button on the keyboard pressed in and "right click" with the mouse on the blue icon. Select the "open with" function. An "open with" window will appear;
- View the video clip of interest by selecting the "Window's Media-player" operation.

APPENDIX E: 3-D NURBs MODEL GENERATION WITHIN CADKEY® V21

E.1 NURBs Fitting of the 2-D Line Drawings……...p.104
E.2 3-D NURBs Model Generation……..……..p.104

E.1 NURBs Fitting of the 2-D Line Drawings

2-D line drawings (in a dxf. format) should be imported into *CADKEY® V21* using the integrated "File-Import DXF" command. Each 2-D line drawing should be fitted with NURBs using the "Modify-Fit NURBs" command. If the NURBs-fit is bad, the shape can be adjusted using the NURBs editing tools to create a better fit. The original 2-D line drawings can be used as guides to make sure that the corrections do not stray too far from the actual shape. The creation of a 3-D NURBs model from the NURBs can now commence.

E.2 3-D NURBs Model Generation

The "Create-Loft NURBs" command should be used to loft a 3-D NURBs model through all of the fitted NURBs. When this command is selected, the program will prompt the user to pick each cross-sectional NURBs, in sequence, across the proposed model surface. Note that the two edge NURBs that are parallel to the cross-sectional NURBs should be included. When picking each NURBs, the NURBs should be picked near the same end. The reason for this is that *CADKEY® V21* has no logic and needs to be told which ends of the NURBs should be connected together. This may seem obvious to a human, but there are some cases that could be quite confusing to figure out automatically. After all of the cross-sectional NURBs (and the two parallel edge NURBs) have been selected, *CADKEY® V21* will show a dialog box with a number of options. The important option is the one to define how many rows should be fitted through the NURBs. The more rows entered, the more accurate the fit will be, but more rows will make it more difficult to edit or smooth the 3-D NURBs model.

Smoother or simpler 3-D NURBs models require fewer rows (perhaps five), but 3-D NURBs models with more curvature require a higher number. The accuracy of this lofting process depends on how the surface on the model is defined and orientated and how evenly spaced the NURBs are.

Once the model has been created, a comparison of the 3-D NURBs model with the original NURBs is required. Zooming in on the rows and columns of the NURBs and checking on how far they are from the 3-D NURBs model can do this. If any corrections are required, any of the solid model editing commands can be used to create a better fit of the 3-D NURBs model to the NURBs. If the 3-D NURBs model was not created according to the required standards, then the "Undo" command can be used and a second attempt can be made.

It should be noted that fitting a 3-D NURBs model to a collection of NURBs is a difficult task, especially if accuracy is a concern. At this point a definition of accuracy is required for the 3-D NURBs model. Otherwise, hours, even days could be wasted to try to fix an accuracy that is not required.